Regional Mechanical Properties and Regeneration of the Mandibular Condylar Cartilage

by

Adam Richard Chin

BS, Florida State University, 2013

Submitted to the Graduate Faculty of the

Swanson School of Engineering in partial fulfillment

of the requirements for the degree of

Doctor of Philosophy

University of Pittsburgh

2019

UNIVERSITY OF PITTSBURGH

SWANSON SCHOOL OF ENGINEERING

This dissertation was presented

by

Adam Chin

It was defended on

November 13, 2019

and approved by

Harvey S. Borovetz, PhD, Distinguished Professor, Department of Bioengineering

Charles S. Sfeir, PhD, DMD, Associate Professor,Department of Periodontics and Preventive Dentistry

Juan M. Taboas, MS, PhD, Associate Professor, Department of Oral Biology

Dissertation Director: Alejandro J. Almarza, PhD, Associate Professor, Department of Bioengineering

Copyright © by Adam Richard Chin

2019

Regional Mechanical Properties and Regeneration of the Mandibular Condylar Cartilage

Adam Chin, PhD

University of Pittsburgh, 2019

The temporomandibular joint (TMJ) is one of the most complex articulating joints in the body. In addition, the surface of the condyle is mandibular condylar cartilage (MCC), which consists of different populations of cells within each of its layers. Damage or displacement to the disc and other abnormalities of the jaw can lead to eventual degeneration of the MCC. If downstream degeneration of the cartilage continues to progress, the avascular nature of the joint renders the tissue unable to regenerate on its own.

Prior studies have attempted regeneration of the mandibular condyle with limited success. Regional viscoelastic properties of the MCC are also not well characterized, making the target of regeneration therapies unclear for this tissue. This dissertation aims to elucidate the regional mechanical properties, and providing a tissue engineering alternative through the use of soft biomaterials for the MCC.

First, the regional compressive properties of the porcine TMJ disc and MCC were evaluated through the use of the transversely isotropic biphasic theory. Mechanical and viscoelastic properties of the five different regions of these tissues were evaluated and compared with one another. The results demonstrated higher compressive properties in the posterior region of the disc and also estimated the moduli in different planes, the Poisson's ratio, and permeability of the MCC. Next, the focus shifted to determining the efficacy of using various soft biomaterials for the mandibular condyle regeneration of an osteochondral defect in the goat model. Acellular polyglycol sebacate and gelatin sponge scaffolds demonstrated cartilage regeneration with

presence of collagen II and glycosaminoglycans after 3 months of healing. In hopes of using a cell-laden therapy, *in vitro* studies with BMSCs and also native cells of the mandibular condyle were conducted. Gelatin hydrogels supported differentiation of BMSCs towards a cartilage lineage, and a gelatin hydrogel composite supported chondrogenesis, and inhibited both mineralization and chondrocyte hypertrophy. Compressive properties of the *in vitro* scaffolds were also comparable to the measured values of the native MCC. The results of this dissertation give rise to an understanding of the viscoelastic properties of the MCC and give insight on promising soft biomaterials.

Table of Contents

List of Tables

List of Figures

Preface

I would first like to thank the funding sources that made this endeavor possible. The initial part of graduate school was funding by the NSF ERC RMB, with the rest coming from the NIH grants BiRM. Next I would like to thank the faculty within the CCR for answering any questions I had as well as letting me use their equipment knowing very well there may be a chance that I might break it.; thank you Dr. Dobrawa Napierala, Dr. Fatima Seyed-Picard, Dr. Alexandre Viera, Dr. Heather Szabo-Rogers, and Dr. Eliah Beniash,. With that said I want to give a huge thanks to all the friends I made within the CCR and helping me with many aspects of my projects, leaving things on my desk, and being truly outstanding people to work with and call my colleagues.

I also owe a lot to my thesis committee for being able to mentor me through this process and provide value feedback to make dissertation possible. Thank you Dr. Charles Sfeir for starting the CCR and gathering the most talented, dedicated, and selfless people to pursue their research in this center. I would also like to show my appreciation to Dr. Harvey Borovetz who has provided me guidance, and continues to make the Bioengineering department at the University of Pittsburgh better every day with his commitment to student excellence. Many thanks to Dr. Juan Taboas who has, by technicality, been my second PI; his knowledge on many subjects and humor have made this experience great. Last, but not least, thanks to Dr. Alejandro Almarza for taking in a fellow Seminole and being not just an incredible committee chair, but an incredible leader to our laboratory. I will attribute my growth as a scientist and a person to the incredible amount of time he has invested in my research and me. Your teachings to me and the rest of the lab will not be forgotten. On that note, thank you to the Almarza Lab: Jesse Lowe, John Li, Vera Liu, Annie Litrenta, Rohan Bansal, Jake Hirschi, Mauro Tudares, Catherine Hagandora, Sarah Henderson,

and Robert Mortimer for making every day at work more enjoyable. Although they are not part of our lab, we have collaborated enough to be “lab siblings”, so I would also like to show my gratitude to Jingming Chen who has helped me on many projects, spearheaded entrepreneurial endeavors, and has always been there to share laughs with. In addition, thank you to Tyler Swenson who has made a ton of biomaterials for me and has been a great source of entertainment

I could write another dissertation on all the encouragement and friendships I’ve made at Pitt, but I’ll try and keep it to a minimum. Thank you to George Hung, who has been one of my best friends in the CCR from Year 1, as well as: Dandan Hong, Rong Chong, Brandi Lantz, Hajime Yamazaki, Daisy Monier, Andrew Brown, and Amy Chaya. My friends back at home have also given me plenty of support during my time in Pittsburgh. Despite me being nearly 1,000 miles away, our chat group has remained strong these past 6 years since we have all departed and have gone our own ways; I want to show my appreciation to Barry Ellis, Brandon Calhoun, Bao Ton, Jason Chang, Lucas Daniels, Kwan Lun, Zachary Lore, Johnny Hansana, and Rodrigo Gil.

Finally I have received a ton of love and support from my family who made me the person I am today. Thank you to all my aunts, uncles, and cousins that are spread out within the country, but have always made time to see and accommodate me whether I have traveled 2 miles down the road to see them, or 2,000 miles. Last but not least, are my parents and sister. Thank you Alison Chin for being my best friend for the last 24 years. Finally, thank you to Teresa and Richard Chin. Both continue to be a beacon of inspiration and reinforcing the importance of family. From immigrating to the U.S., to growing up in a laundry store to help the family, they are the epitome of selflessness and I am eternally grateful for their guidance and love.

1.0 Introduction

The objective of thesis is to a) determine the viscoelastic parameters of the native porcine temporomandibular joint disc and mandibular condylar cartilage, b) provide insight on the different healing potentials of various soft biomaterials for an osteochondral defect *in vivo*, and c) further investigate our choice of using hydrogels to meet our criteria for mandibular condylar cartilage regeneration. The first phase of the dissertation focuses on characterizing the viscoelastic parameters of both the TMJ disc and MCC in the porcine model. A stress relaxation test was performed on samples from the different regions for both the TMJ and MCC. The second phase of this work then moves onto observing the *in vivo* regenerative effects of soft biomaterials in osteochondral defects. From the results of this study, the third portion of the dissertation chose gelatin hydrogel scaffolds to study in-depth. Both *in vitro* and *in vivo* assays were done to assess the efficacy of the hydrogel. The central hypothesis of this dissertation is *gelatin sponges, and composite hydrogels, in combination, can serve as regenerative alternatives due to their ability to regenerate the discrete layers of the mandibular condylar cartilage.* The following aims were used to test this hypothesis:

1) To characterize the viscoelastic parameters of the different regions in the temporomandibular joint disc and the mandibular condylar cartilage. These structures are extracted from porcine from the local abattoir for unconfined compression testing. Using the biphasic theory, MATLAB was used to construct a fit curve to fit the constitutive equation to the obtained stress relaxation data. The hypothesis of this is that *the loading and viscoelastic parameters for the disc and the cartilage will have regional dependency and be larger in the anteroposterior regions compared to their*

mediolateral counterparts. Statistical analysis was used to detect differences within the regions for the loading and viscoelastic parameters.

2) To assess the regenerative potential of various biomaterials *in vivo*. PGS scaffolds and gelatin sponges were tested in a goat model to observe their healing potential of osteochondral defects. Empty controls were also incorporated in the bilateral surgery. 3 months were allowed for healing and the condyles were extracted for histology. Samples were processed followed by paraffin sectioning. The hypothesis of this is section is that *the soft biomaterials will provide a regenerative response in the form of GAG and collagen production compared to the empty osteochondral defects.* Safranin-O, Masson's Trichrome, hematoxylin & eosin, and a collagen II immunostains were done to assess tissue regeneration.

3) Finally, to determine a gelatin hydrogel composite's ability to foster regeneration and to recapitulate the discrete layers of the mandibular condylar cartilage. In addition to gelatin scaffolds, a new composite hydrogel comprised of gelatin, polyethylene glycol, and heparin was test *in vivo* and *in vitro*. There were two parts to this aim: the first half aimed to test the efficacy of the composite hydrogel and its ability to foster the differentiation of bone marrow stem cells *in vitro.* The second part's purpose was to elucidate the efficacy of long-term culture of primary cells seeded in the two different types of hydrogels with mechanics, biochemistry, and histology. The hypothesis of this two-part aim is that *the primary osteoblasts will continue to mineralize inside of the gelatin scaffolds and the primary chondrocytes will continue to produce GAG in both the gelatin and PGH hydrogel scaffolds.*

1.1 Temporomandibular Joint

The temporomandibular joint (TMJ) is an articulating joint that consists of the glenoid fossa, from the skull, the mandibular condyle, and the temporomandibular joint disc. The anatomy of the joint is much different from other joints inside of the body. During daily physical activities like chewing and talking, the condyle of the mandible rotates and translates out of the glenoid fossa before returning back to its original position. Facial muscles also surround the joint to initiate and stabilize movement; their presence also adds to the complexity of the joint.

With many moving parts, common problems with the joint include: disc displacement, clicking of the jaw, migraines, and downstream degeneration. It is approximated that 10 million Americans are affected by TMJ disorders. With the potential of disc displacement and an abnormal loading environment within the joint, these untreated symptoms have the potential to develop more serious side effects such as degeneration of the disc, fibrocartilage in the joint, or the subchondral bone of the mandible.

As of now, there very limited treatments for temporomandibular joint disorders as the symptoms are difficult to diagnose and treat. For more mild symptoms, pain management is one of the most common treatments. If downstream degeneration occurs, there are limited treatments available to the patient. As of now, there are no regenerative alternatives for the TMJ. Patients who develop severe symptoms need arthroscopies, and those who cannot return to their quality of life opt for TMJ replacement surgery.

1.2 Mandibular Condylar Cartilage

Both the glenoid fossa and the mandibular condyle are lined with fibrocartilage, which creates a supportive environment and facilitates the complex movements of the jaw. The mandibular condylar cartilage (MCC) has multiple layers, similar to articulating cartilage found in the knee. The different layers of this fibrocartilage include: 1) fibrous, 2) proliferative, 3) mature cartilage, 4) hypertrophic and 5) subchondral bone (Figure 1). The biochemical contents of the cartilage include collagen type I, II, VI, IX, and XII. Glycosaminoglycans are also present but quantities of around 5% dry weight in the disc (Almarza & Athanasiou, 2004; Almarza, Bean, Baggett, & Athanasiou, 2006; Detamore et al., 2005; Nakano and Scott (1989a); Nakano & Scott, 1989b) and 10-20% dry weight in the articular cartilage (Almarza & Athanasiou, 2004).

There have been regenerative efforts using PLA and PCL scaffolds. A study by Wang et al. designed an experiment to assess porcine MCC cell growth in poly (lactic acid) (PLA) scaffolds *in vitro*. In addition, a similar study by Bailey et al. seeded umbilical mesenchymal stromal cells in poly glycolic acid (PGA) scaffolds. Both methods showed limited cellular attachment to the materials and moderate proliferation and extracellular matrix production. The brittleness of the materials may also be a concern when implanting it into a loadbearing region.

1.3 Regenerative Biomaterials

1.3.1 Polyglycerol Sebacate

Poly (glycerol sebacate) is a soft biomaterial that has shown promise in regenerating different tissues. The polymer its prominence in cardiovascular regeneration and bone regeneration demonstrates its biocompatibility and efficacy. Past studies from our research group have also investigated the potential of PGS being used as a biomaterial for the temporomandibular joint. Hangadora et al. seeded cylindrical PGS scaffolds with fibrochondrocytes, at different densities, via injection followed by in vitro culture with chemically-defined media. Histological and biochemical assays were peformed after 24h, 2 weeks and 4 weeks of culture. The results showed that the amount of GAG produced from the safranin-O stains and the compressive parameters of the seeded scaffold increased with the seeding density. As such, the middle seeding density provides an ideal amount for future considerations of in vitro experiments using these types of cells and this biomaterial. The production of GAG and ability to recapitulate the peak compressive properties and the modulus of the mandibular cartilage demonstrates the efficacy of using PGS for regenerative efforts of the TMJ.

1.3.2 Hydrogels

Gelatin hydrogels are another viable biomaterial option for soft tissue regeneration due to their biocompatibility and biodegradability. These structures have been shown to provide a microenvironment that supports cellular attachment (Nichol et al., 2010). Nichols et al. have

investigated methacrylated gelatin hydrogels as a tunable material that could be used for creating cell-responsive micro tissues. Because of the hydrogel's ability to change its physical properties via cross-linking different concentrations of gelatin this provides value in tuning the material to the intended area of application. The versatility of hydrogels lends itself to different applications relating to cartilage applications as it can be injected and formed to the contour of different articulating surfaces. Various studies have experimented with seeding the hydrogels with mesenchymal stem cells as well as primary cells (Conrad, Han, & Yang, 2018; X. M. Li et al., 2016).

1.4 Magnesium

Magnesium is an abundant metal ion found inside the body and an important cofactor in many biological processes. In terms of dental-orthopedic applications, magnesium also shows promise as a biomaterial for devices, as it has more similar mechanical properties to bone than the current metals used for prosthetics, such as cobalt chromium molybdenum and titanium. In addition, its ability to degrade inside the body circumvents secondary infections resulting from surgeries. Stress-shielding is also prevented as the amount of load the bone sees from the implantation device is slowly transferred as it degrades. This review encompasses the cellular effects of magnesium ions on osteoblasts and chondrocytes, along with in vivo results of Magnesium plates and pins. After searching the literature, there were no adverse effects associated with moderate concentrations of magnesium ions in vitro. Furthermore, there was an upregulation of osteogenic markers as well as chondrogenic markers. From in vivo experiments, magnesium's osteoconductivity was shown, as both pin and plate implants induced bone overgrowth in some

studies. Although gas formation is a concern when it comes to the biodegradation process of magnesium, there was not enough to be of concern for the duration of the implant throughout the duration of the experiments. The reviewed literature shows promising results for the use of magnesium in future orthopedic applications.

In orthopedic surgery, plates and pins often are the best option to stabilize fractures; however, these present other complications such as the possible need for recurrent surgeries and stress shielding due to the dissimilar properties of the implant and the surrounding native tissue. Titanium has been a widely used metal for prosthetics in the past couple of decades, especially in load-bearing environments. Once the site has been fully healed, another surgery is required to remove the implant, which can lead to more complications (Cordero, Munuera, & Folgueira, 1994). However, in terms of these non-resorbable implants, stress shielding is still a concern. Since most of the forces are loaded on the implant and not the bone, the bones begins to resorb from lack of mechanostimulation. As a result, this unloading affects the osteoblast and osteoclast balance (Frost, 1994). This is the challenge that titanium device users face when deciding whether or not to remove pins, screws, or plates when the bone has completely healed.

Having magnesium (Mg) as a possible material for orthopedic applications would be beneficial as it has the ability to degrade in side of the body and eliminates the need for another surgery. As the bone heals, the magnesium will degrade and eventually allow the regenerated bone to take on the burden on the joint load in a controlled manner. Degradable magnesium alloys also have the ability to be tailored to control their degradation rate by changing the amount of magnesium inside the alloy; if an implant needs to be situated for a long time, less magnesium could be introduced into the alloy to allow slower degradation. Vice versa, more magnesium can be introduced to induce faster degradation. Furthermore, magnesium is an important cofactor in

over 300 biochemical reactions of the body (NIH, 2016). It is also the second most abundant element inside human cells, which attests to its importance of its involvement in biological functions.

This review investigates literature that delves into the cytotoxicity and benefits of magnesium ions on both osteoblasts and chondrocytes in vitro and as implants in vivo. For osteoblasts, the papers chosen for this review were limited to those using MC3T3 cells. After these two in vitro sections, the review shifts focus to implanted magnesium devices to determine the in vivo benefits as well as the cellular interactions within the environment.

1.4.1 In Vitro Studies

Scopus was used to conduct the literature search for the in vitro portion in October of 2018. Articles from the last decade were considered. Different searches terms were used for the osteoblast and the chondrocyte sections. The search terms used for the osteoblast section were in vitro AND magnesium alloy AND osteoblasts. Articles were chosen from the last 10 years, and regions from which the articles were published were limited to: United States, Germany, and China. We then searched within the list of manuscripts for studies that included MC3T3 mouse cells. Studies that had cements and polymer blends were excluded. 10 of the 35 articles found from the Scopus search were chosen for their relevance. For the *Chondrocytes* section, the search terms input into Scopus were: in vitro AND magnesium AND chondrocytes. The same time range and regions were applied to this search as the previous one. 5 of the 20 articles were chosen from this search.

1.4.1.1 Osteoblasts

The following studies have cultured MC3T3 mouse osteoblasts with magnesium ions close to physiological concentrations (Table 1). These studies were also chosen because they reported similar methods to evaluate cytotoxicity. The first four papers tested different types of magnesium alloys containing zirconium (Zr). The next papers incorporated zinc (Zn), strontium (Sr), and aluminum in the alloys. Finally, the rest of the papers use a variety of Mg alloys and ions. Overall, the following studies attempt to elucidate these aspects of magnesium alloys on bone-depositing osteoblasts.

Chou et al. explored the possibility of introducing other elements into a magnesium alloy to improve strength as well as corrosion resistance (Chou et al., 2013) (Table 1). Mg-Y-Ca-Zr (1 wt% and 4 wt% Y: WX11 and WX14, respectively) alloys were created and tested in vitro and in vivo in a mouse model. An indirect cytotoxicity test was performed where varying diluted amounts of WX11, WX11 as-cast, WX14, WX14 as-cast and pure magnesium extract were placed in MC3T3-31 cell culture for 1 and 3 days. In the 1 day cytotoxicity test, all of the groups at extracts of 25% and 10% had higher MC3T3-E1 viability than the control except for pure magnesium. This was a good first study for the new magnesium alloy; in the future, Alkaline Phosphatase (ALP) activity tests can be performed to assess the effects of this alloy on osteoblasts differentiation.

Hong et al. also experimented with the use of zinc (Zn) and zirconium (Zr) in producing a magnesium alloy (Hong et al., 2013) (Table 1). Mg-4 wt.% Zn - 0.5wt% Zr (ZK40) was tested in vitro using an indirect cytotoxicity test. Heat-treated ZK40 and as-cast ZK40 were machined into a 10mm x 10mm x 1mm square and incubated in media for 72 hours. Varying diluted amounts of the media extract were then tested with MC3T3 culture. From the results, a 2x

dilution of as-cast ZK40 resulted in ~80% viability which shows its promise as a cytocompatible alloy. Again, the effect of this alloy on osteoblast differentiation is unknown and warrants a need for further investigation.

Wang Y et al. experimented with JDBM (Mg-Nd-Zn-Zr) and its effects on osteoblasts; specifically a proliferation test was performed (Y. Wang et al., 2012) (Table 1). Discs made of the magnesium alloy and pure magnesium were machined; MC3T3-E1 cells were cultured on them for 1, 4 and 7 days of cultivation. From the results, JDBM showed a higher amount of cell proliferation than pure Mg after the first day of culture. The effects of this alloy on osteogenic markers could have also been assessed for this experiment. Likewise, even though this study was meant as a comparison for pure magnesium, a negative control group could have been included.

Xiaozhe Song et al. studied a similar alloy in Mg-Zn-Y-Nd-Zr. Short term cell viability tests were conducted as well as a long term viability test (Song et al., 2018) (Table 1). Extracts of the alloy were included in the culture media of MC3T3 cells. This alloy was compared to a similar alloy extract without Zr (Mg-Zn-Y-Nd), a positive control (0% extract) and a negative control (10% DMSO). From 24 hour cell viability results, the Mg-Zn-Y-Nd-Zr extracts (20% to 100%) increased cell viability compared to both controls and the Mg-Zn-Y-Nd alloy. When lengthening the amount of time at which they were collected, there was no cytotoxicity observed for extracts taken at 48, 72, 120, and 240 hours. However, when extracts were taken at 1440 hours, any percentage of extract over 1% was significantly lower than the control. This was insightful as it does aid the future design of biocompatible magnesium implants that include these alloys as their degradation products appear to be cytotoxic. In vivo tests would have to

clarify the extent of cytotoxicity because cellular interactions in an in vivo environment could aid in mitigating it.

From these aforementioned studies, the inclusion of Zr has demonstrated its cytocompatibility, but Zr's osteogenic benefits have to be further studied. As such, in an experiment performed by Guan et al., RT-PCR was performed on cultured hBMSCs after 12 and 18 days (Guan et al., 2014). The result was an increased ALP expression from culturing the mesenchymal cells with extracts of a JDBM alloy after 18 weeks when compared to a negative control group.

Berglund et al. studied Mg-Ca-Sr alloys for orthopedic applications (Berglund et al., 2012) (Table 1). The amount of calcium and strontium in the alloy was varied to characterize the material; one assessment measured cytotoxicity using inductively coupled plasma atomic emission spectroscopy (ICP-AES). The alloy was incubated in media for 72 hours before 10% and 50% of the extract was tested in the culture media of MC3T3-E1 mouse cells. These cells were then cultured for 5 days. Three different alloys were used: Mg-0.5Ca-0.5Sr, Mg-1.0Ca-0.5Sr and Mg-1.0Ca-1.0Sr. From ICP-AES, Mg-1.0Ca-0.5Sr had the lowest overall cytotoxicity. This study shows promise for including Strontium in a magnesium alloy, as moderate amounts of it shows minimal cytotoxicity. Incorporation of this metal into future Mg alloys would be beneficial, as similar to Zr, is has also been shown to increase osteogenic differentiation of BMSCs in vitro (Peng et al., 2010).

Liu et al. tested the biocompatibility of Mg17Al12 against pure magnesium (Liu et al., 2015) (Table 1). Bone marrow derived stem cells (BMSCs) and MC3T3-E1 cells were cultured separately with extracts from both Mg17Al12 and pure magnesium (leaching time of 24 hours, no dilution) for 1, 3 and 5 days. After their respective time points, an MTT assay was performed

to count the number of viable cells left in the culture; a relative cell growth rate was then calculated (viable number of cells in experimental extract divided by the viable cell count in the control media). The results of the MTT assay showed that after the first day there was a negligible difference in cell growth between Mg17Al12, pure magnesium and the control media; however, there appeared to be a 30% increase in cell growth from both the magnesium alloy and pure magnesium compared to the control at 3 days. A more pronounced increase was seen in the culture of BMSCs with a ~45% increase in cell growth at 3 days with pure magnesium and the Mg-Al alloy. Gene expression for osteogenic markers could have also been performed to further assess this second phase alloy.

The introduction of Al into a Mg alloy is intriguing as it does offer the benefits of a more controlled degradation and better mechanical properties, but its known cytotoxicity should not be overlooked. The cell viability test was conducted over a few days, but a longer study is warranted as the investigators saw significantly more extracellular matrix production by the cells cultured with pure Mg compared to Mg17Al12. This suggests that Al may give rise to adverse effects *in vitro* over a longer period of time.

Chen et al. tested the biocompatibility of a Mg-Zn (5.6%) alloy in vivo as well as in vitro (D. Chen et al., 2011) (Table 1). For the in vitro portion of the study, MC3T3-E1 cells were seeded onto a disc-shaped structure made of the Mg alloy as well as poly (lactic acid) (PLLA). After 3 days, it was found that the cells cultured on the magnesium alloy had roughly 270% more gene expression for collagen I (COL1α1) than the GAPDH control compared to the 185% seen by cells culture on the PLLA construct. The information on gene expression helps support the notion that osteoprogenitor markers are upregulated with Mg in the culture media; however, quantification of the number of cells attached to the structure or a viability assay would be

informative as well. Rad et al. evaluated the toxicity of Pure Mg, Mg2Ag alloy, and extreme pure Mg (XHP Mg) via direct cell culture for 2, 6 and 12 days (Rad et al., 2017) (Table 1). From quantification, cell death at 12 days for both the Pure Mg and Mg2Ag groups were significantly higher than the XHP Mg group. In vitro, this study has shown the benefit of a higher content of Mg within an alloy, but feasibility studies of XHP in vivo would prove to be useful, as the higher content of Mg would increase both the degradation rate and the possibility of gas bubbles forming near the material.

Tamimi et al. tested the cytotoxicity and biocompatibility of aqueous magnesium phosphate formed under in vivo conditions as a function of pH, temperature and ion concentration (Tamimi et al., 2011). Magnesium phosphate concentrations were made by mixing different amounts of MgCl2 and HPO4 ions together. Measurements of lactate dehydrogenase (LDH) were taken after 24h of culture to test for cytotoxicity (not included in Table 1). Expression of osteoblast differentiation markers were measured using RT-qPCR. It was found that the magnesium phosphates, cattite and newberyite did not significantly increase the amount of LDH released from the cells during culture, signifying their low cytotoxicity. The RT-qPCR results yielded an overall lower gene expression in ALP, collagen type II (Coll1A1), osteocalcin (OCN), and osteopontin (OPN) in the magnesium phosphates compared to hydroxyapatite and brushite. Comparing newberyite and cattite, newberyite consistently had higher expression of osteogenic markers. The results from this study show the potential of magnesium phosphates

Gu et al. conducted biocompatibility tests on a large range of binary Mg alloys (Mg-1x, wt%) (X. N. Gu, Zheng, Cheng, Zhong, & Xi, 2009) (Table 1). Osteoblasts were cultured for 2, 4, and 7 days with non-diluted eluates of the different Mg alloys. The viability assays revealed

that Mg-1Al, Mg-1Sn, Mg-1Zn did not exhibit reduced viability as opposed to the other alloys, suggesting their viability as an alloy for orthopedic applications. This expansive study included a wide spectrum of possible Mg alloys to provide preliminary information on their cytocompatibility, which in turn helps in the decision on whether or not to pursue further in vitro studies on that alloy. However, as mentioned before, this warrants a longer period of study as Liu et al. found that functions of the cells, such as extracellular matrix production, begin to see adverse effects after 14 days of culture with Mg alloy eluates.

The results from the aforementioned studies have shown promise for the future use of magnesium in vivo for bone healing from their in vitro experiments; there was an increase in osteoblast proliferation from the Liu and Wang studies when the cells were treated with the Mg alloy eluates. In addition, all of the proposed alloys have shown to be non-toxic to pre-osteoblasts at a certain concentration range. Measurements of magnesium release would need to be done to determine the actual extent of biocompatibility that these alloys have. However, of these studies, two demonstrated an increase in osteogenic markers (COL1a1) when their respective Mg alloy was used. Most of the other cited research seemed to only validate the safety of using certain Mg alloys. More in depth *in vitro* research such as PCR for characterization could be performed to assess how beneficial the magnesium may be for the cells.

Table 1. In vitro cytotoxicity results for different magnesium alloys tested on MC3T3 pre-osteoblast cells.

Author	Mg Type	Preparation	Cell Line	Cytotoxicity Results
Chou et al.	Mg-Y-Ca-Zr	Eluate	MC3T3-E1	Leaching Time: 72 hours Dilution: 10%, 25% Culture Time: 72 hours Viability: >75%
Hong et al.	Mg-Zn-Zr (ZK40)	Eluate	MC3T3-E1	Leaching Time: 72 hours Dilution: 10%, 25% Culture Time: 72 hours Viability: > 80%
Wang et al.	Mg-Nd-Zn-Zr	Direct culture onto alloy	MC3T3-E1	N/A
Song et al.	Mg-Nd-Y-Zn-Zr	Eluate	MC3T3-E1	Leaching time: 24, 48, 72, 120, 240, 1440 hours Dilution: 20, 40, 60, 80, 100% Culture time: 24 h Viability: > 80%
Berglund et al.	Mg-1.0Ca-0.5Sr	Eluate	MC3T3-E1	Mg-1.0Ca-0.5Sr had 5% cell death at either days 3 and 5 Leaching Time: 72 hours Dilution: 10%, 50% Culture Time: 3 days Viability: > 95%
Liu et al.	Mg17Al12	Eluate	MC3T3-E1	Cells consistently above 100% relative cell growth after 3 days for both alloys Leaching Time: 24 hours Culture Time: 3 days Viability: 100%
Chen et al.	Mg-Zn	Direct culture onto alloy	MC3T3-E1	After 4 hours, there was a greater amount of cells attached to Mg alloy (256.04±4.03) than to PLLA (177.40±5.24)
Rad et al.	Mg2Ag, XHP Mg	Direct culture onto alloy	MC3T3-E1	Mg2Ag and Pure Mg had significantly higher cell death after 12 days of culture than XHP Mg
Gu et al.	Mg-Al Mg-Zn Mg-Sn			Dilution: None Culture Time: 2, 4, 7 days Viability: > 90% for 2, 4 time points

1.4.1.2 Chondrocytes

There is currently more attention has been paid to on the effects of magnesium on bone, as it has been shown to be osteoconductive. However, there are not as many studies on the effects of the metal on chondrocytes. As orthopedic devices are in close proximity to cartilage, the effect on increased magnesium concentrations must be established. The following studies observed the effects of magnesium on chondrocytes as well as fibrochondrocytes, the native cell of the temporomandibular joint and costal cartilage (Table 2).

From the work published by Feyerabend et al., the group decided to use a 3-step tissue engineering model to determine the effects of physiologically higher amounts of chronological sulfate on human articular chondrocytes during: (a) chondrocyte proliferation, (b) redifferentiation of chondrocytes, and (c) chondrogenesis in high-density pellets (Feyerabend, Witte, Kammal, & Willumeit, 2006) (Table 2). During each phase, cells were treated with varying amounts of magnesium sulfate, growth factors, or a combination of both. The authors measured proliferation of the chondrocytes by performing a cell count. The effects of redifferentiation were measured for the different magnesium concentrations using a Western blot analysis. Chondrogenesis was assessed by measuring DNA and glycosaminoglycan (GAG) production per cell (G/D ratio) in addition to a Western blot analysis. From the proliferation results, the authors found the lower Mg concentrations (5, 10 mM) to enhance proliferation, while high Mg concentrations (15, 20 mM) did the opposite. During redifferentiation, they also found that the addition of magnesium enhanced chondrogenic markers. Finally, in the third phase, they saw that supplementing magnesium inhibits extracellular (ECM) formation during chondrogenesis. The authors provided a well-designed experiment as it not only drew conclusions from individual steps, but they also determined effects from consecutive steps;

hence, the 3 phase model. In addition, they took into consideration other variables such as including and excluding treatments simultaneously during the study.

Hagandora et al. studied the effects of increased concentrations of magnesium on fibrochondrocytes, the native cells of costal cartilage and the temporomandibular joint (C. K. Hagandora, Tudares, & Almarza, 2012) (Table 2). Specifically, high concentrations of MgSO4 and MgCl2 at 20, 50, and 100 mM on scaffoldless fibrochondrocyte constructs were observed; these were compared to basal media with 0.8 mM Mg^{2+} concentration. Once the constructs were cultured for 4 weeks, biochemistry and mechanical test were performed. From the biochemistry results, the constructs cultured in 50 mM or above of either MgCl2 or MgSO4 showed a decrease in GAG, collagen, and the collagen type II/type I ratio. The mechanical results demonstrated similar findings; in general, the tangent modulus, peak stress and equilibrium stress all showed a decrease with 50 mM or above for MgCl2 and MgSO4. This study demonstrated that fibrochondrocyte constructs could tolerate magnesium concentrations up to 20 mM. This was an informative study as it also took into consideration the mechanical properties of the fibrochondrocytes when exposed to magnesium ions. Measuring GAG content, collagen content, and cell viability provide useful information, but the mechanical properties would also help elucidate magnesium's effectiveness as a treatment.

Dou et al. used a dynamic or temporal analysis of fluctuating amounts of magnesium to determine the effect on chondrocytes in media over time (Dou, Li, Zheng, & Ge, 2014) (Table 2). Specifically, they placed pure magnesium microspheres (99.80% wt) or MgCl2 (5, 10, 20 mM) in media with chondrocytes in 2D. In addition, they also replicated the experimental design in 3D with alginate hydrogel scaffolds. Chondrocytes were isolated from 1 year old miniature pigs and once they were placed into their respective environments they were cultured

for 1, 3, 7 days. In order to assess cytotoxicity, an MTT assay was performed along with pH measurements of the media; residual magnesium concentration in the media was also measured. GAG content and measurements of the change in Collagen types I, II, X, and Aggrecan using PCR were performed. It was found that a lower concentration of magnesium (10 mM) enhanced proliferation of chondrocytes, whereas a higher concentration (20 mM) inhibited it. GAG content was increased in the lower concentration of Mg. The authors found a discernible difference between 2D and 3D seeding with respect to GAG content; however, not much was elucidated from the effects of magnesium concentration. This study provides a reminder that results in 2D do not necessarily translate to 3D.

These three studies showed the cytotoxic range of Mg ions. 5 mM appears to be the safe end of the spectrum, whereas a concentration of 20 mM begins to have adverse effects in vitro. These findings give design criteria for future biodegradable Mg prosthetics.

The work from Pichler et al. evaluated the effects of magnesium on human growth plate chondrocytes (hGPCs) (Pichler et al., 2014) (Table 2). More specifically, they machined discs made of ZX50 (5% wt Zn, Ca, Mn, Y, balance Mg) and WZ21 (1% wt Zn, Ca, Mn, Y, balance Mg) alloy. Then, they were dissolved in media with agitation for 40 hours. Following that, the eluate from the media was applied in varying amounts (0, 0.4, 1, 2, 4, 10, 20, 40% of eluate to total volume) to cultured hGPCs from children. After this, the optimal volume percentage of eluate was determined, and used for a live cell imaging for 2 days (Cell-IQ) to see the ions' effects on the hGPCs. An MTT assay was performed to assess cell viability and metabolic activity was also measured. Finally, qRT-PCR was used to observe changes in expression for osteogenic markers and chondrogenic markers in chondrocytes. An upregulation of osteogenic markers as well as sox-9 were seen in the chondrocytes in the presence of both eluates. It was

found that ZX50 and WZ21 inhibited proliferation in hGPC. In PCR, ZX50 increased the expression of osteocalcin and sox-9 by 400 and 225% respectively in hGPCs. These results suggest that the eluates switch the chondrocytes from a proliferative to a synthesis state. It seems that there was a big gap in concentration of eluate in which magnesium had an effect. Future studies should further refine the concentration to find when the peak response occurs.

In the work by Liao et al, the authors compared their coated custom magnesium alloy to commercially available alloys and the effect of the degradation products on cartilage cells (Liao et al., 2015) (Table 2). Specifically, they investigated Mg-Nd-Zn-Zr coated with brushite (JDBM) and compared it to AZ31, WE43, pure magnesium and a Titanium alloy. Discs of the metals were cultured in media, and the extract was directly cultured with chondrocytes obtained from young rabbits for 1, 3 and 5 days. The authors measured adhesion, viability, proliferation and apoptosis of chondrocytes, as well as GAG and Col II content, mRNA expression of Col II and Aggrecan. It was found that the JDBM performed equivalent to control media without extract, while the other groups had lower responses. This study was informative in that it showed chondrocytes are very tolerant to commercially available magnesium alloys, promoting their usefulness in current and future orthopedic applications.

Similar to the osteoblasts, these studies have shown a certain range of biocompatibility amongst the magnesium alloys for chondrocytes. Also, at ranges that were not drastically different from physiological amounts, inclusion of Mg increased glycosaminoglycan production. It was also exemplified that the inclusion of magnesium could result in an upregulation of Sox-9 in chondrocytes and also collagen type X. These findings in biocompatibility and gene expression show that magnesium has promise to be incorporated in treatments to promote cartilage regeneration. There are some reservations, however, because as shown by the Pichler et al.

experiment, it would be informative to see some more studies done in 3D; the success seen in 2D may not be replicated in a 3D environment.

More mechanism studies are required to fully understand magnesium and chondrocyte differentiation. From some of the articles reviewed, it seems that magnesium can have an upregulation of chondrogenic markers such as sox 9. At the same time, the ions can also inhibit adverse mechanisms. In the study by Hu et al, magnesium supported chondrogenic differentiation through the inhibition of pro-inflammatory responses (Hu, Xu, Wang, Qin, & An, 2018). Lu et al. studied the function of transient receptor melastatin potential 7 (TRPM7) cation channel during chondrocyte differentiation. Gene expression of this channel was monitored during the study and it was found to be upregulated during proliferation, which suggests the importance of Ca and Mg ion homeostasis during chondrocyte growth. Both of these studies suggest that the importance of magnesium is bimodal: its presence promotes chondrogenic mechanisms, but it also inhibits inflammatory mechanisms.

Table 2. In vitro cytotoxicity, GAG, and gene expression results for different magnesium alloys and ions tested on chondrocyte cells.

Author	Mg Type	Preparation	Cell Line	MTT Results	GAG Results	PCR Results
Feyerabend et al.	MgSO4	Dissolved in water (ions)	Human articular chondrocytes	10 mm MgSO4 had 30% more proliferation than control (media only)	14.5 µg in 20 mM compared to 12.5 µg in control (not significant)	N/A
Hagandora et al.	MgSO4, MgCl2	Ions	Caprine costal chondrocytes	N/A	5.8 and 6.8% Collagen/DW for MgSO4 and MgCL2 respectively (20 mM)	N/A
Dou et al.	Pure (99.80 wt %), MgCl2	Pure Mg: eluate, MgCl2: ions	Porcine knee chondrocytes	MgCl2 20mM group had ~45% of cells in 2D compared to control (no Mg added)	3 µg per 2.5 µg control	230% Col X 40% Col II (Mg 500 ug/mL) 175% (5 mM MgCl2) (all compared to blank control)
Pichler et al.	WZ21 (Mn, Y), ZX50 (zinc, calcium, Mn)	Eluate	Human growth plate chondrocytes	Decrease w/ 10% eluate volume for ZX50 compared to media with no eluate	N/A	225%/160% sox9 60%/75% Col II (ZX50/WZ21 expression w/ GAPDH control)
Liao et al.	Mg (99.99%), AZ31, WE43, JDBM (Mg-Nd-Zn-Zr)	Cells culutured with disc-shaped sample	Rabbit knee chondrocytes	Coated JDBM (w/ brushite) equivalent to media control	20 µg JDBM compared to 18.5 µg of negative control (not significant)	Col II 2% and Aggrecan 25% relative to GAPDH

1.4.2 In Vivo Studies with Plates and Screws or Pins

The following studies highlight the in vivo effects, and to an extent, the degradation profile, and biocompatibility of Mg applications. These studies are important as they help establish the efficacy of placing the magnesium alloy in an active biological environment. Articles were chosen to discuss in the review if they were published within the last 10 years, and have at least 20 citations. Regions were limited to the: United States, China, and Germany. Articles not focused on in vivo magnesium were excluded. The keywords used to perform the literature search for magnesium plates were: Mg AND in vivo AND plates. Of the 13 articles that appeared in the search, 3 were relevant for this review. For review of the magnesium screws the search terms were: Mg AND in vivo AND screws. 6 of the 15 articles were chosen. Finally, to search for relevant articles on magnesium pins the following search terms were: Mg AND in vivo AND pins. 4 out of 6 articles were chosen from this search.

In the work done by Chaya et al., magnesium plates and screws were tested in a rabbit ulna fracture model (Chaya, Yoshizawa, Verdelis, Noorani, et al., 2015) (Table 3). In this study, 99.9% magnesium plates devices were used to hold the rabbit fracture in place for 4 weeks. This group was compared to devices that were made from titanium. From the micro-CT scans, new bone formation was found around the device, nearly encasing it. Histology validated this by confirming the presence of mature osteocytes and active osteoids throughout those regions – something that was not seen in the titanium device group. Histomorphologic quantification of the bone bridging at the fracture sites did not show a significant difference in new bone formation between the titanium and the magnesium groups. The authors conducted a similar experiment and published another study (Chaya, Yoshizawa, Verdelis, Myers, et al., 2015) a few months after, seeing similar results in the same model: fracture healing within 8 weeks and maturation of the bone after 16

weeks. Complete bone overgrowth was seen by the 16 week mark. The incorporation of a fracture in the animal model helped validate its future clinical application and also accentuate the usefulness of magnesium -based devices.

In the work done by Han et al., HP (High Purity, 99.99 wt%) magnesium screws were used to hold together intracondylar fractures of femurs in a rabbit model for up to 24 weeks (P. Han et al., 2015) (Table 3). These were compared to a PLLA screw group. From the micro-CT bone volume results, the magnesium screw group degraded slower from 4 to 16 weeks, but increased the degradation rate at 24 weeks. There was also a significant recovery of range of motion (ROM) at week 24 for both the HP magnesium group and the PLLA group. When compared to the PLLA group, there was significantly more bone ingrowth seen in the HP Mg screw. This was an informative study as there was an inclusion of a critical size defect which resulted in osseointegration between the interface of the implant and the bone after a 24 week time point. The release of the magnesium ions resulting from implant degradation affected osteogenic differentiation of nearby tissues and induced mature bone ingrowth inside in the HP Mg screw group.

Ezechieli et al. conducted a study to determine the effects of synovialis and synovia on the degradation of the MgYREZr (Y, Rare Earth Elements, Zr,) pins that were implanted in the intercondylar femoral notch in a rabbit model for 1, 4, and 12 weeks (Ezechieli et al., 2014) (Table 3). The magnesium alloy was compared to a control Ti6Al4V alloy. Histology was performed on the synovial fluid of the knee; qualitative scores were then given to each sample to assess the amount of inflammation in the area regarding hyperplasia of the synovial lining layer, activation of synovial stroma, and inflammatory infiltration. During the entirety of the study, both the magnesium and titanium groups showed moderate to no synovitis (scores of 0-2) of the synovial

membrane. After 1 week, 75% of the rabbits in the magnesium group exhibited synovitis, while this occurred 83% of the time in the titanium group. By four weeks, 8% of the rabbits in both groups showed moderate evidence of synovitis. By the end of the last time point, in all of the samples, there little to no synovitis found from histology.

The use of Mg in craniofacial applications and devices have not been studied in-depth. More investigation is warranted as the location is in close proximity to the brain, which makes proper selection of new biomaterials paramount. Henderson et al. implanted pure Mg and AZ31 (3% Al, 1% Zn) screws in the rabbit mandible and compared them to stainless steel screws to evaluate magnesium and its alloys as possible craniofacial fixation materials (Henderson et al., 2014) (Table 3). The time points of this study were 4, 8, and 12 weeks. Microcomputed tomography was used to quantitatively and qualitatively observe any bone remodeling and degradation of the screws. A hematoxylin and eosin stain was also performed for the 12 week samples to confirm any new bone that was seen from the microCT images. Bone degradation and remodeling was seen after 12 weeks of implantation. The pure Mg screws degraded and only had one density level, whereas the AZ31 screws had a higher-density region and a lower-density region. When comparing the remaining volume of the screws, the pure Mg had a lower total volume left when compared to the AZ31 alloy (when both lower and higher density areas are included). However, when the lower-density area is not included, then both groups have a similar remaining volume. Thus, it is hypothesized that the lower-density area is comprised of degradation products of the alloy. To this end, this data demonstrated the efficacy of using Mg-based implants for craniofacial applications.

Schaller et al. tested the in vivo degradation of Mg screws in plates in a miniature pig model (Schaller et al., 2016) (Table 3). The researchers created Mg devices that had geometries similar

to existing titanium systems used for the treatment of facial fractures. The two experimental groups used for the study were: a Magnesium Elektron WE43 (Mg, Y, Zr) implant that was not coated and one that was coated with a plasma electrolytic surface coating; both groups were compared to the control, which were titanium implants. The devices were implanted in the frontal bone (or around the forehead) in adult miniature pigs. Two time points of 12 and 24 weeks were used for endpoint evaluation of device degradation with X-rays, micro-CT, and histological analyses. From the micro-CT there was a significant difference in the volume of the screws between the control and the two experimental groups; when compared, the coated and the uncoated groups also showed differences between each other where the uncoated group showed a lower volume due to its faster rate of degradation. The area was the largest in the titanium groups whereas the lowest was seen in the uncoated magnesium group, due to most of the sample degrading. The results of this study provide important information on biodegradable metals in a non-load bearing area such as the craniofacial region.

It is important that proposed Mg devices also function in different environments such as the synovial joint. A study performed by Cheng et al. observed the healing potential of high purity (HP) magnesium screws when used to repair the anterior cruciate ligament (ACL) in rabbit knees (P. Cheng et al., 2016) (Table 3). The screws were used to fix the ACLs for time points of 3, 6, 9 and 12 weeks. In order to assess tissue regeneration in vivo, histology, a range of motion (ROM) test, a pull to failure test, and micro-CT scans were used. The ROM test showed that both the Mg group and Titanium groups were within the normal range of motion (150 – 180 degrees) by the 12^{th} week. The ultimate load of the tendon graft for the HP magnesium group showed a significantly higher ultimate load to failure after 12 weeks compared to 0 weeks following surgery (~130 N compared to ~110 N, respectively) and slightly higher, but not significantly, than the

titanium group (120 N). The rigidity of the sample still upheld even though more of it degraded. This was a novel study in that it provided a very thorough analysis encompassing a wide range of methods including a pull out test and a range of motion test.

Implantation of Mg devices inside bone marrow have also been investigated. Waizy et al. implanted MgYREZZr-alloy screws into the marrow cavity of rabbit femora. Histological assays were done 1 week, 12 weeks, and 52 weeks postoperatively (Waizy et al., 2014) (Table 3). Degradation on the threads of the screws were observed as early as 1 week. Following 12 weeks, the screw had degraded further, and bone apposition was seen to directly contact the implant. At 52 weeks the metallic portion of the implant was fully degraded in the bone marrow. It was also reported that fibrous tissue growth was apparent in some samples at 12 weeks, but only one showed slight formation of a fibrous structure at 52 weeks.

A. Bondarenko et al implanted magnesium pins into the tibial medullae of New Zealand rabbits (n = 46) in order to observe peri-implant osteogenesis (Bondarenko et al., 2014) (Table 3). Three different alloys were observed for this study: MgCa0.8 (0.8 wt% Ca), LAE442 (4 wt% Li, 4 wt% Al, 2 wt% rare earth composition metal), LANd442 (4 wt% Li, 4 wt% Al, 2 wt% Nd) and ZEK100 (1 wt% Zn, <1 wt% Zr, < 1 wt% rare earth elements). The pins were allowed to degrade in the implantation site for 3 and 6 months. From the results, Titanium proved to have the highest initial osteopontin (OPN) expression and overall bone reaction scores. Both MgCa and LANd exemplified a statistically significant increase in osteocalcin and bone regeneration (bone reaction scores), respectively, over time from 3 months to 6 months. Besides the control, the LAE alloy had the highest 3 month osteocalcin score, but saw significant decreases in all 3 parameters at 6 months. It is hypothesized that the combination of aluminum (could have a possible toxic effect on osteoblasts) and low-toxicity rare earth metals could have played a role in this observation.

This study was novel in that the authors considered statistical correlation with bone formation and osteocalcin or osteopontin expression. They also identified the discrepancy of their results between each group could be attributed to different degradation mechanics and time – MgCa0.8 and LANd degraded the fastest and demonstrated increased osteocalcin expression whereas LAE had decreased osteocalcin expression most likely due to the decreased degradation.

Evaluation of the degradation of Mg devices in an environment with direct contact to muscle would also assist in providing design considerations for future orthopedic devices. Erdmann et al., compared MgCa0.8 screws to surgical steel (S316L) screws in vivo; both bone formation and soft tissue biocompatibility were assessed (Erdmann et al., 2010) (Table 3). Screws of both types were implanted in rabbit tibia underneath the cranial tibial muscle. Postoperative follow ups were 2, 4, 6 and 8 weeks. In as early as 2 weeks, fibrous tissue formed between the muscle and the implant site in both the Ti and Mg groups. Tissue cavities, which were assumed to be by-products of hydrogen accumulation from the degrading material, were seen only in the Mg screw group; however, this did not seem to adversely affect the host. The inflammatory response of the hosts implanted with Mg were reportedly higher than the Ti group, but neither exceeded a moderate level, making the use of MgCa 0.8 in soft tissue applications feasible.

A possible concern for using Mg devices in vivo is the possibility of gas bubble formation from degradation. Li et al. tested the cytotoxicity and degradation characteristics of a binary alloy, Mg-1Ca (1% wt Ca) (Z. Li, Gu, Lou, & Zheng, 2008) (Table 3). Pins made of the alloy were also placed in the femoral shaft of male New Zealand white rabbits (n = 18). For comparison, pins made of titanium were placed in the cortical bone of the femur. The 3 month time point of the Mg-1Ca pin group showed new bone formation around the implant; this was not seen in the control commercially pure Titanium pin group. Correspondingly, there was a large decrease of weight of

the Mg alloy pins. After 1 month, the average pin weight was 0.11 g, 0.09 g by 2 months, and by the 3 months, the pins had an average weight of 0.03g. This experiment provides more information on Mg-Ca alloys along with the study performed by A. Bondarenko et al (Bondarenko et al., 2014). This, in particular, is an interesting composition as calcium is mineralizing agent; however, the range for how much Ca is put into the alloy is limited as with increasing Ca, there is increasing brittleness of the alloy. There could also be a small concern with gas formation from magnesium degradation at the alloy composition, as there was some seen after implantation, but this disappeared after 2 and 3 months.

One study not only tested the cytotoxicity of a new metal alloy, but also directly compared different degradation profiles and responses when Mg is implanted in different tissues. Reifenrath et al. studied the corrosion of a Mg-La-Nd-Zr (magnesium, lanthanum, neodymium, zirconium) magnesium alloy in vitro and in vivo (Reifenrath, Marten, Angrisani, Eifler, & Weizbauer, 2015) (Table 3). For the in vivo studies, the alloy was extruded into cylindrical pins with a 1.5 mm diameter and 7 mm length. The pins were then implanted in 3 different ways inside the female Lewis rat: subcutaneously, intramuscular, and intramedullary (n = 6 for each method). The intramedullary pins' corrosion rate (0.63 ± 0.08 mm/year) far exceeded that of the subcutaneous and intramuscular pins (0.06 ± 0.04 and 0.02 ± 0.07 mm/year, respectively) when calculated by weight loss. When treated with acid to get rid of the corrosion products on the samples, the calculated weight loss values were 0.28± 0.05, 0.28 ± 0.06, and 1.12 ± 0.15 mm/year for the subcutaneous, intramuscular and intramedullary pins, respectively. The cell culture results showed no significant difference in cell metabolic activity, nor cell proliferation in any of the extract dilutions when compared to the negative control; there were only significant differences when compared to the cytotoxic, positive control. All values for metabolic activity and cell proliferation

were higher than 70%, which is the accepted threshold for cytotoxicity. The undiluted extract resulted in 95.3% metabolic activity and 88.6% of relative proliferation. This paper was informative as it did compare the in vivo degradation of the magnesium alloy in multiple in vivo environments. The authors stated that they did not expect the intramedullary space to induce the fastest degradation, but when compared to Chaya et al. 2015, in which the portions of the screw that were inserted in the intramedullary space corroded faster than those on the surface of the bone, these results coincide. This demonstrates the effect of the different environments on corrosion rate and how consideration for materials in different areas are necessary.

1.4.2.1 Discussion

The aforementioned studies show promise for magnesium-based implants to be used in future orthopedic or maxillofacial procedures. All of the alloys showed no signs of cytotoxicity. One foreseeable drawback of using magnesium implants would be their tendency to cause gas accumulation near the site due to the degradation reaction; however, in the studies done by Chaya et al. and Li et al. the gas formation did not adversely affect the implant site. Additionally, Li et al. confirmed that the hydrogen gas was self-absorbed by 2 months. Other studies have extensively tested the cytotoxicity of alloys of the metal and have not seen any adverse effects.

The studies conducted in vivo are very broad in terms of application and types of alloys used, but determining the benefits of each type of Mg alloy would via a meta-analysis would be informative to those trying to incorporate Mg into devices for different applications. For example, strontium has been studied as a possible Mg alloy (X. N. Gu, Xie, X.H., Li, N., Zheng, Y.F., Qin, L., July 2012; J. Han, Wan, P., Sun, Y., Liu, Z., Fan, X., Tan, L., Yang, K., March 2016; Tarafder, December 2013). The inclusion of it has shown to increase the compressive strength of the alloy, as well as improve biocompatibility and bone formation in vivo (Y. Li, Wen, C.,

Mushahary, D., Sravanthi, R., Harishankar, N., Pande, G., Hodgson, P., 2012). It has even been proposed that it enhances osteogenic activity more than pure Mg when implanted (Tie et al., 2016). Zinc is another commonly used metal in Mg alloys where studies have observed slower degradation rates and promising bone responses (D. Chen et al., 2011; S. Chen et al., 2012; Hofstetter et al., 2015; Huan, Leeflang, Zhou, Fratila-Apachitei, & Duszczyk, 2010; Sun et al., 2013; H. Wang et al., 2011; Xia, May 2012; S. Zhang, Zhang, X., Zhao, C., Li, J., Song, Y., Xie, C., Tao, H., Zhang, Y., He, Y., Jiang, Y., Bian, Y., 2010). Regarding the cell response when Mg devices are implanted, there were two different layers of tissue observed near a Mg-Zn-Mn implanted in rat femurs which contained numerous fibroblasts (E. Zhang, Xu, L., Yu, G., Pan, F., Yang, K., September 2009). This could be a response indicative of a critical sized bone defect rather than an osteogenic effect. As seen in some of the aforementioned studies, Mg alloys containing calcium are also viable as their incorporation increases the strength (Wu et al., 2008) as well as their observed ability to enhance osteoblast adhesion (Yang, 2012; Zeng, April 2012).

Although it was not covered in depth in this manuscript, Mg has been tested in polymers, blends, and coatings in vivo. There have also been a few studies that have investigated hybrid materials of polymers and Mg in devices to induce osteochondral regeneration. A type I collagen scaffold combined with magnesium-doped hydroxyapatite crystals in another layer was tested in the nude mice model and found osteogenic differentiation and deposition of ECM following 8 weeks (Sartori et al., 2017). Wollastonite and macroporous fibrin biphasic scaffolds also saw regeneration of cartilage and the subchondral bone in vivo (Shen, June 2018). PLGA combined with Mg hydroxide was another considered material to regenerate cartilage in an osteochondral defect. Following 4 and 8 weeks implantation, there was increased COL2 expression within the defect in the PLGA and MH group compared to PLGA-only (Park et al., 2018). Because the

mechanism for the release of Mg may be different in these types of constructs, another review of these materials could be warranted.

The largest benefit seen is the cellular effects of magnesium. Osteogenic activity has been observed in multiple studies with Mg-based implants with the upregulation of OC, Runx2, OPN, and Col1a1. The metal's chondrogenic effect can also lend itself to osteochondral applications with its ability to upregulate cartilage matrix synthesis. When loaded onto TiO_2 films and placed in the tibia of rabbits for 3 weeks, there was a noticeable increase in the osteogenic markers OC, RUNX-2 and IGF-1 from the specimens (Galli, 2014). Mg ion presence has also been observed to upregulate collagen type I and OPN expression (M. Q. Cheng et al., 2016). Mechanisms of how Mg affects osteoclast activity was observed when compressed, pure $Mg(OH)_2$ was implanted into a rabbit femur (Janning et al., 2010). At 4 weeks the osteoclast surface was significantly reduced, whereas an increase in the osteoid surface was observed. This finding could suggest that not only is osseointegration promoted, but bone resorption could also be mitigated.

Table 3. Summary of magensium plates and screws, and pin in vivo studies.

Author	Mg Type	Animal	Location of Implant	Time Points	Observations
Chaya et al	99.9% Mg Plate and Screws	Rabbit	Ulna	4 weeks	Bone formation on top of ulna.
(P. Han et al., 2015)	99.99% Mg Screws	Rabbit	Femur condyle	4-24 weeks	Osseointegration was seen around the screws.
Ezechieli et al	MgYREZr (Y, Zr, Rare Earth Elements) Pin	Rabbit	Femur Condyle	1, 4, 12 weeks	Less cases of inflammation compared to Titanium group.
Henderson et al	99.9% Mg, AZ31 (Al, Zn)	Rabbit	Mandible	4, 8, 12 weeks	Bone remodeling seen after 12 weeks.
Schaller et al	Mg Elektron WE43 (Y,Zr) Screws	Pig	Frontal bone (forehead)	12, 24 weeks	Uncoated alloy degraded faster.
Cheng et al	99.99% Mg Screw	Rabbit	ACL	3, 6, 9, 12 weeks	Mg implant stronger in pullout test
Waizy et al	MgYREZr (Y, Zr, Rare Earth Elements) Screw	Rabbit	Tibia	1, 12, 52 weeks	Bone apposition at 12 weeks.
(Bondarenko et al., 2014)	MgCa0.8 (0.8% Ca) Pin	Rabbit	Tibia	3, 6 months	Increase in osteocalcin expression
Erdmann et al	MgCa0.8 (0.8% Ca) Screw	Rabbit	Tibia	2, 4, 6, 8 weeks	Inflammation and fibrous tissue formation
Li et al	Mg-Ca (1% Ca) Pin	Rabbit	Femur	1, 2, 3 months	Bone formation following 3 months.

1.4.3 Conclusion

From the aforementioned literature, there are promising results in terms of magnesium biocompatibility. The studies have shown, for both of the cell types, there is a range in which they are cytocompatible with Mg in the environment. Studies could have included a Mg ion release measurement; some experiments only gave a quantitative amount of magnesium in the media by using an eluate dilution. This is important as it was shown that magnesium does have benefits for osteoblasts and chondrocytes as there was an upregulation of both osteogenic and chondrogenic markers in vitro; however, it was also shown that high concentrations of Mg ions proved to be deleterious to the cells in which there were observed decreases in function and proliferation. It is paramount that this range is more established for the different alloys of magnesium as the release profile and in vivo behavior may be different for each one.

Many of the assays performed were cytotoxicity and proliferation tests. Although this is important to know, it does not seem widely reported on what osteogenic and chondrogenic markers magnesium has an effect on for both osteoblasts and chondrocytes. More quantitative information on these markers from q-PCR with different alloys would be more informative. The fact that it has deleterious effects when beyond a physiological composition may make these associated endeavors more difficult, but from this research, there is further evidence that magnesium can have beneficial effects on bone and cartilage. Also, from observing the in vivo studies, all of the alloys tested did not exemplify cytotoxicity in any of the implanted regions. This shows that the implants are degrading slow enough to not reach a concentration that would otherwise reach cytotoxic levels.

2.0 Viscoelastic Compressive Properties of the Different Regions in the TMJ Disc and Mandibular Condylar Cartilage

2.1 Introduction

The temporomandibular joint (TMJ) is a bilateral synovial joint that is imperative for execution of daily activities such as eating and speaking. Injury or deteriorating function of the tissues of the TMJ may lead to more downstream problems and affect quality of life. Temporomandibular joint disorders (TMD) include: locked jaw, headaches, and downstream joint degeneration. There are approximately 10 million Americans affected by TMD. If left untreated and undiagnosed, further degeneration will occur, this resulting in irreversible damage and possibly the need for TMJ total joint prosthetics. As of now, there are currently no regenerative treatments for TMD that are commercially available. In order to create an optimal tissue regeneration alternative for this complex joint, knowledge of the mechanical properties of the articulating tissues are required.

The TMJ has two types of articulating fibrocartilage: the TMJ disc and the mandibular condylar cartilage (MCC). Currently, there is a gap in knowledge in how the mechanical properties of the MCC and TMJ disc compare to one another in terms of viscoelastic properties. Past studies have evaluated the viscoelastic properties of the porcine disc and MCC under compression, but with different loading methods and models for characterization. For example, Lamela et al. performed a compressive test for the disc in a dynamic loading, and different fits were used (Lamela, Fernandez, Ramos, Fernandez-Canteli, & Tanaka, 2013; Lamela, Prado, Fernandez, Fernandez-Canteli, & Tanaka, 2011). Commisso et al. measured compressive properties, with

quasi-static loading, of the TMJ disc and described the stress-strain behavior by the quasi-linear viscoelastic model (Commisso, Calvo-Gallego, Mayo, Tanaka, & Martinez-Reina, 2016). Allen et al. performed unconfined compression on porcine TMJ discs at fast strain rates and fitted the data with a Kelvin model (Allen & Athanasiou, 2006). Singh et al. also performed regional stress relaxation tests in unconfined compression on the MCC using the Kelvin model (Singh & Detamore, 2009). These models do not reliably capture the stress-strain behavior of a ramp stress and relaxation test of the disc and MCC at strain rates of around 4.5%/min, and do not provide fit constants/parameters with physical meaning.

Biphasic models do provide a good model for the stress-strain behavior of TMJ articulating tissues at slow strain rates, with constants/parameters that have physical meaning. Mow et al. first developed the biphasic theory to model stress relaxation behavior in articular cartilage (Mow, Kuei, Lai, & Armstrong, 1980). Kim et al. then characterized the regional mechanical properties of the articular cartilage of the fossa and the superior surface of porcine TMJ discs, by indenting with creep, and then using linear biphasic isotropic theory (Kim, Wong, Helfrick, Thomas, & Athanasiou, 2003). A transversely isotropic biphasic model was used previously by us to fit the compressive behavior of goat discs and MCC due to the tissues having a transverse collagen fiber alignment, with 10% strain increments at 9%/min strain rate (C. K. Hagandora, Chase, T. W., Almarza, A. J., 2011). The current study proposes to use the same transverse isotropic biphasic theory to model the stress-relaxation behavior of the disc and the MCC in pig, but at a lower strain rate of 4.5%. In addition, the parameters resulting from the model will be compared regionally, and between structures to elucidate differences within the TMJ disc and the MCC while understanding their functions. Moreover, this study will determine if the transverse isotropic

biphasic theory provides a robust equation for viscoelastic biomechanical data of the soft tissues of the porcine TMJ.

2.2 Methods

2.2.1 Sample Preparation

Porcine heads were acquired from the local abattoir at slaughter age (6 – 9 months). The right TMJs were then extracted from 6 pigs. The matching disc and condyle were used for mechanical testing. 4mm biopsy punches were taken from 5 regions of the disc and MCC: anterior, posterior, central, medial, and lateral. The acquired punches were then embedded in OCT and frozen sectioned to an appropriate testing thickness. The average thickness of the tested disc and cartilage samples were 1.66 ± 0.32 mm and 1.61 ± 0.32mm, respectively. The average samples diameter for the disc and cartilage were 3.73 ± 0.21 mm and 3.68 ± 0.23 mm respectively.

2.2.2 Unconfined Compression

Unconfined compression with stress relaxation was performed on all tissue samples. Test samples were first loaded with a 0.02 N preload, followed by submerging them into a PBS bath at 37 °C. The buoyancy of the water was taken into account once the sample was submerged. A 10 cycle preconditioning procedure to 10% strain at 4.5% strain/minute was performed prior to testing. Finally, a stress relaxation test to 10% sample strain was performed at a rate of 4.5%

strain/minute and then allowed to relax for 30 minutes. Preliminary test showed that the biphasic model did not fit well when a strain rate of 9%/min was used, as done in our previous goat study (C. K. Hagandora, Chase, & Almarza, 2011), on the disc when compared to the MCC. As such, we decided to use have the speed, 4.5%/min, and the model seemed to fit well for both tissues.

2.2.3 Curve Fitting

The peak force and stress were determined at 10% strain, and stress was calculated as the force (N) divided by the cross-sectional area. In order to calculate the stiffness and the tangent modulus, the last 10% linear portion of the curve was determined and the slope was calculated for that region, for the load-elongation and stress-strain curves respectively. The transversely isotropic biphasic theory equations used to compute the viscoelastic coefficient were used from the aforementioned study (C. K. Hagandora, Chase, T. W., Almarza, A. J., 2011). The coefficients that were analyzed were: elastic modulus in the transverse plane (E_1), elastic modulus in the axial plane (E_3), Poisson's ratio in the transverse plane (ν_{21}), the Poisson's ratio in the axial plane (ν_{31}), and the permeability coefficient in the transverse plane (k). Initial guesses for the coefficients were made in order to fit the equation and the error measured from the initial was determined by the least squares method. Since the nature of the equation will allow for multiple answers, bounds for the viscoelastic parameters dictate the final outputs. 81 different combinations of initial values were used to perform the fit, utilizing 3 guesses for each parameter. The three initial guesses for each parameter ranged in equal increments from 0.1 to 0.5 for ν_{21} and ν_{31}, 0.1 MPa to 10 MPa for E_1, and 1×10^{-14} m^4/N▪s to 7×10^{-14} m^4/N▪s for k. The final parameters that were reported were the resulting average of all solutions with an error less than 1.5 times the minimum error found for

the 81 combinations of initial guesses, that also complied with defined thermodynamic restrictions (Lempriere, 1968).

2.2.4 Statistical Analysis

For statistics, MiniTab was used to perform a two way ANOVA in order to see if the individual animal and the region where the sample was taken had an effect on each of the calculated variables. A Tukey's post-hoc test detected individual differences ($p<0.05$) between each of the regions performed. No significant differences were found amongst animals, thus only regional differences are reported.

2.3 Results

2.3.1 TMJ Disc

Peak force that the disc experienced under compression was the highest in the posterior band (0.26 ± 0.10 N, Figure 1), which was significantly higher ($p<0.05$) than the lateral and central areas. The stiffness (average value and standard deviation for all regions, Figure 2) and percent relaxation (average value and standard deviation for all regions, Figure 3) of the disc showed no significant difference between the regions. The max stress (average value and standard deviation, Figure 4) and the tangent modulus (average value and standard deviation, Figure 5) of the disc were the highest in the posterior region and significantly higher ($p < 0.05$) than the anterior, medial

and lateral areas. The transverse Young's modulus (E_1) (279.97 ± 112.7 kPa, Figure 6) and the out-of-plane Young's modulus (E_3) (39.27 ± 13.80 kPa, Figure 7) were found to be the highest in the posterior region of the disc and significantly higher compared to each of the other 4 regions ($p < 0.05$). Both the Poisson's ratio ν_{21} (average value and standard deviation for all regions, Figure 8) and ν_{31} (average value and standard deviation for all regions, Figure 9) had no difference between the 5 regions. The posterior region of the TMJ disc had the lowest calculated permeability (k) ($1.11*10^{-14} \pm 0.57*10^{-14}$ $m^4/N\cdot s$), Figure 10) when compared to the lateral and anterior bands.

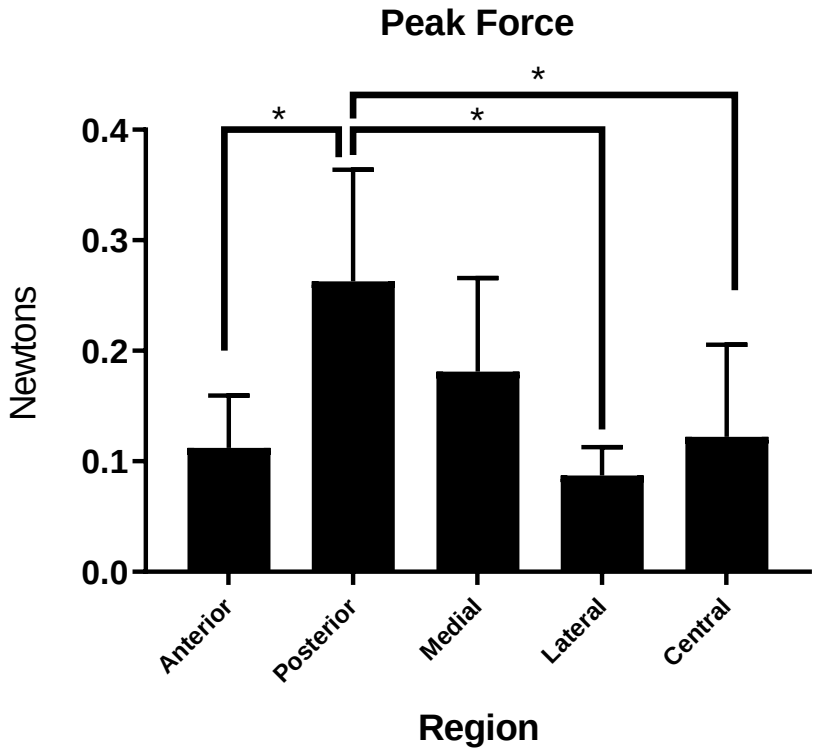

Figure 1. Bar graph of the peak force for for the temporomandibular joint disc. Asteriks represents the post-hoc Tukey's test having $p < 0.05$.

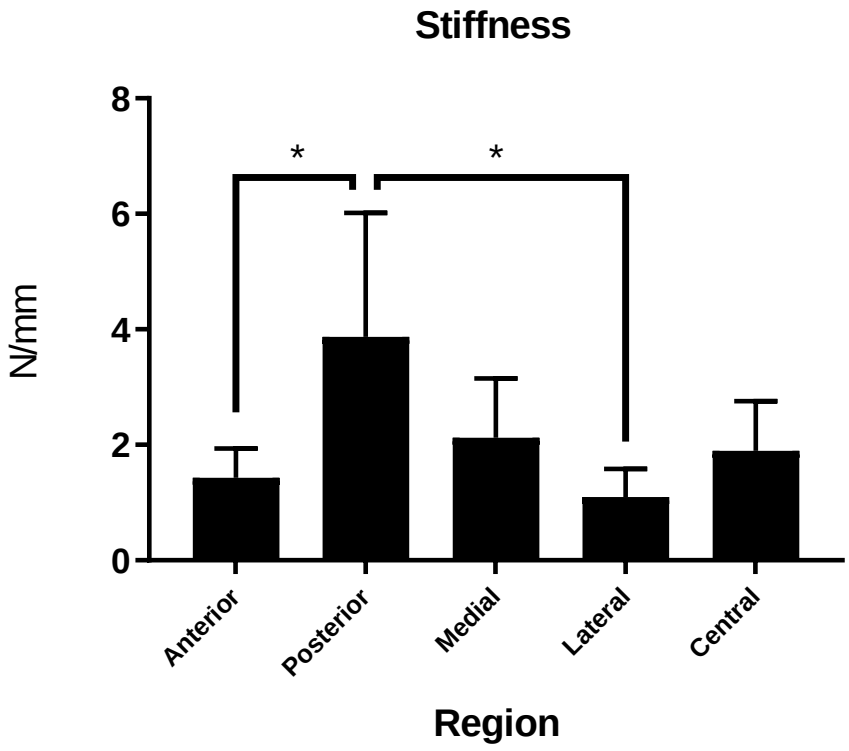

Figure 2. Bar graph of the stiffness (N/mm) for the five different regions of the temporomandibular joint disc. Asteriks represents the post-hoc Tukey's test having $p < 0.05$.

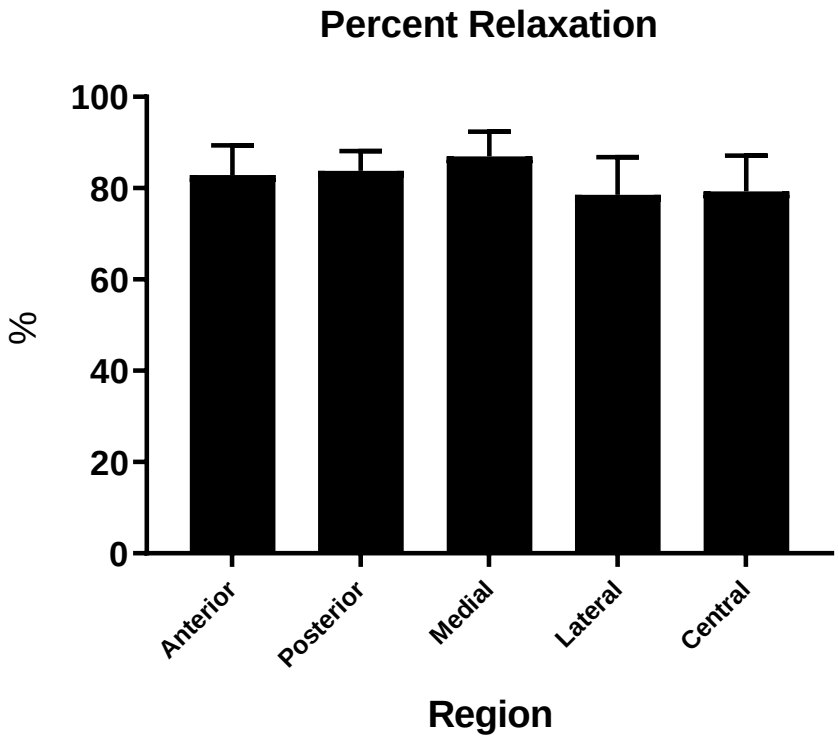

Figure 3. Bar graph of the percent relaxation for the five different regions of the temporomandibular joint disc.

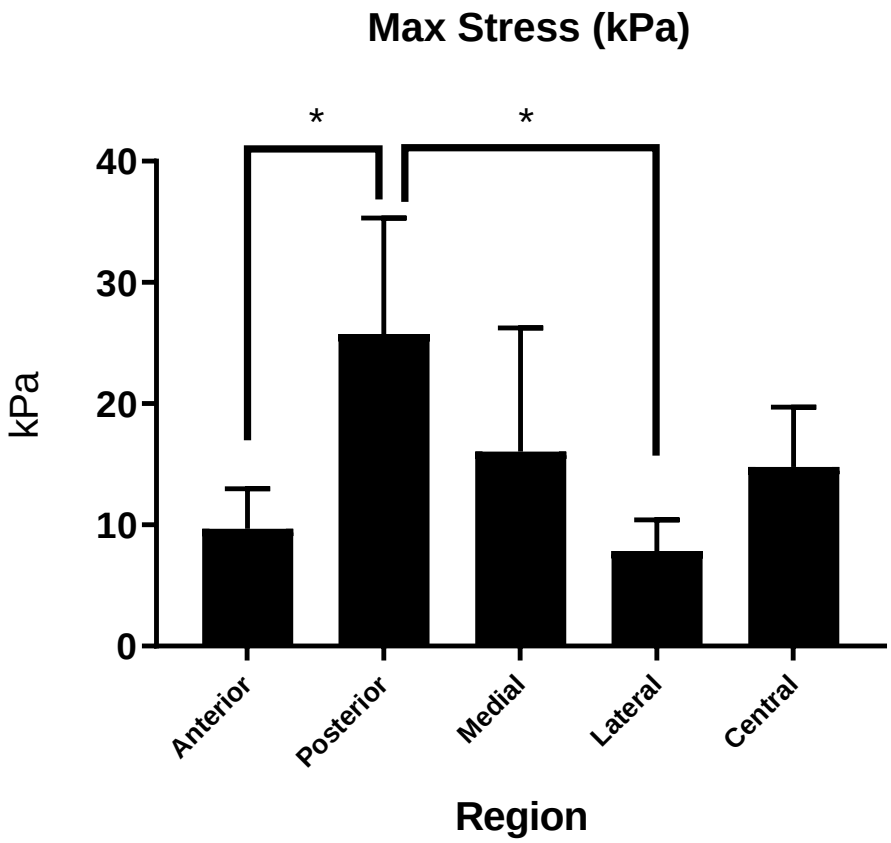

Figure 4. Bar graph of the max stress (kPa) of the five regions of the temporomandibular joint disc. Asteriks represents the post-hoc Tukey's test having $p < 0.05$.

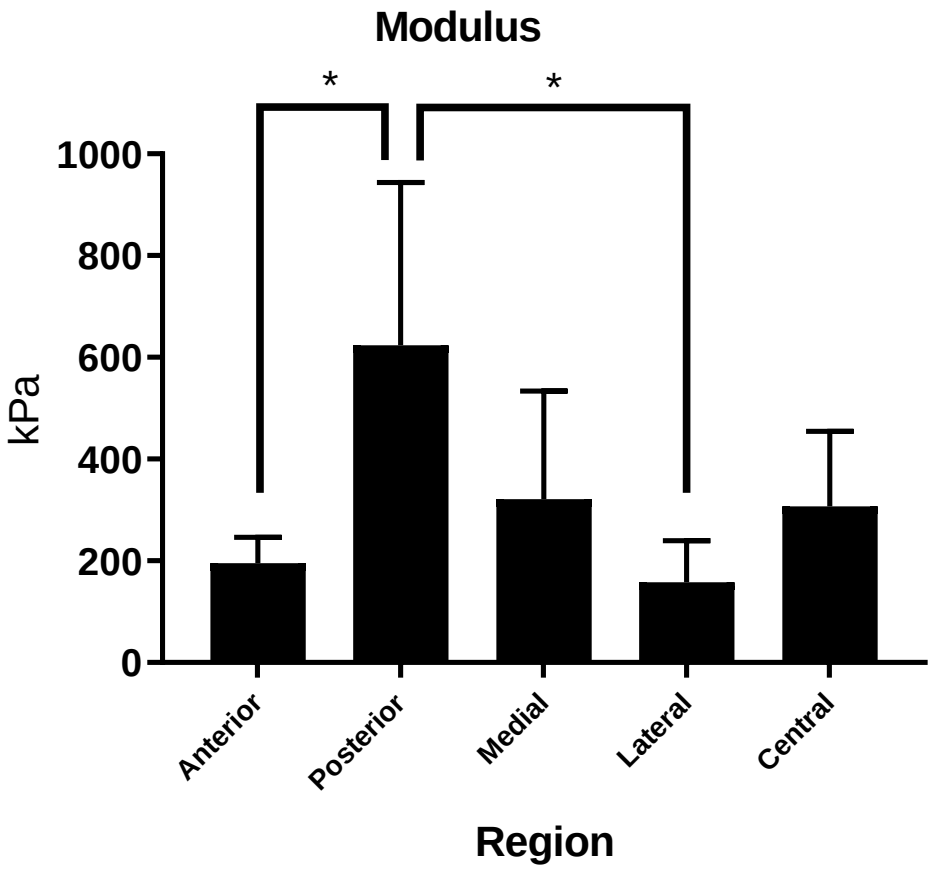

Figure 5. Bar graph of the modulus for the five different regions of the temporomandibular joint disc. Asteriks represents the post-hoc Tukey's test having a significance of $p < 0.05$.

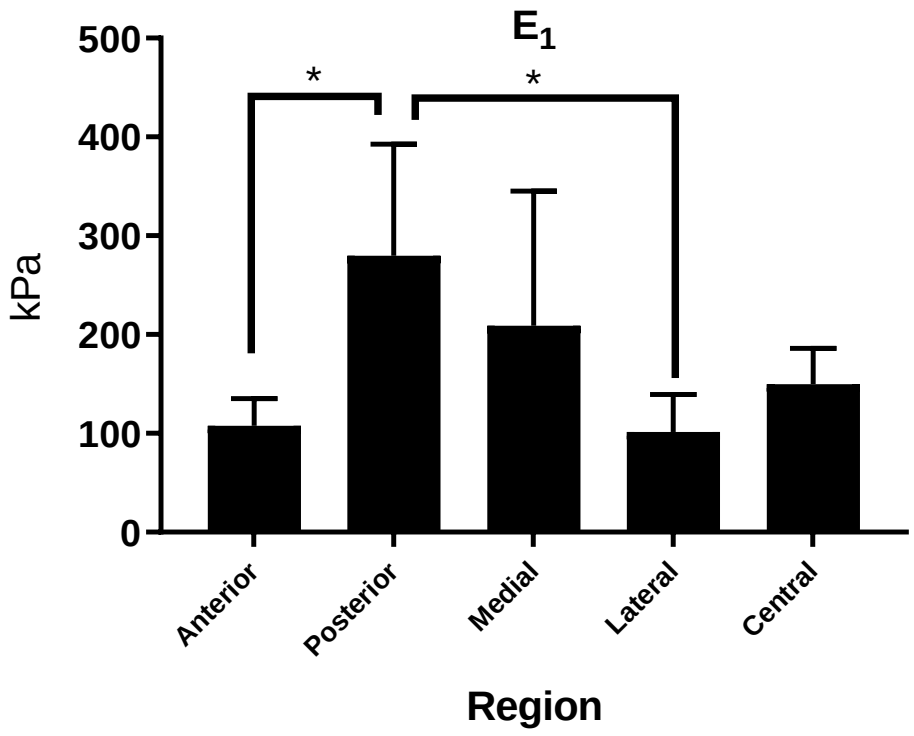

Figure 6. Bar graph of the Young's, in-plane modulus for the five different regions of the temporomandibular joint disc. Asteriks represents the post-hoc Tukey's test having a significance of $p < 0.05$.

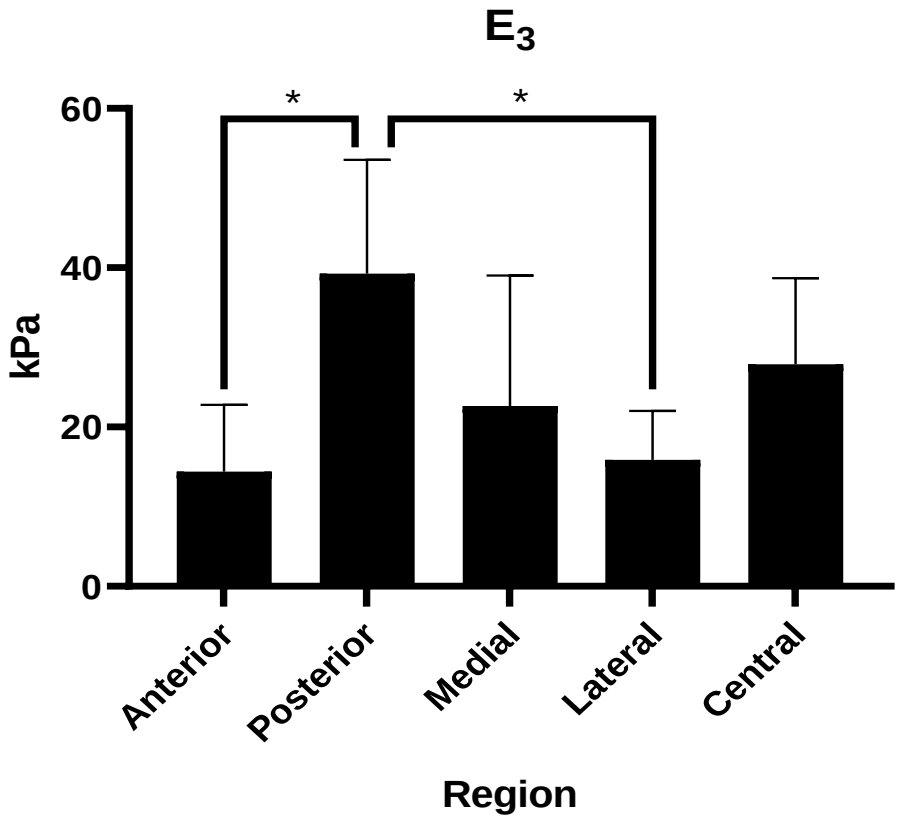

Figure 7. Bar graph of the Young's, out-of-plane modulus for the five different regions of the temporomandibular joint disc. Asteriks represents the post-hoc Tukey's test having a significance of $p < 0.05$.

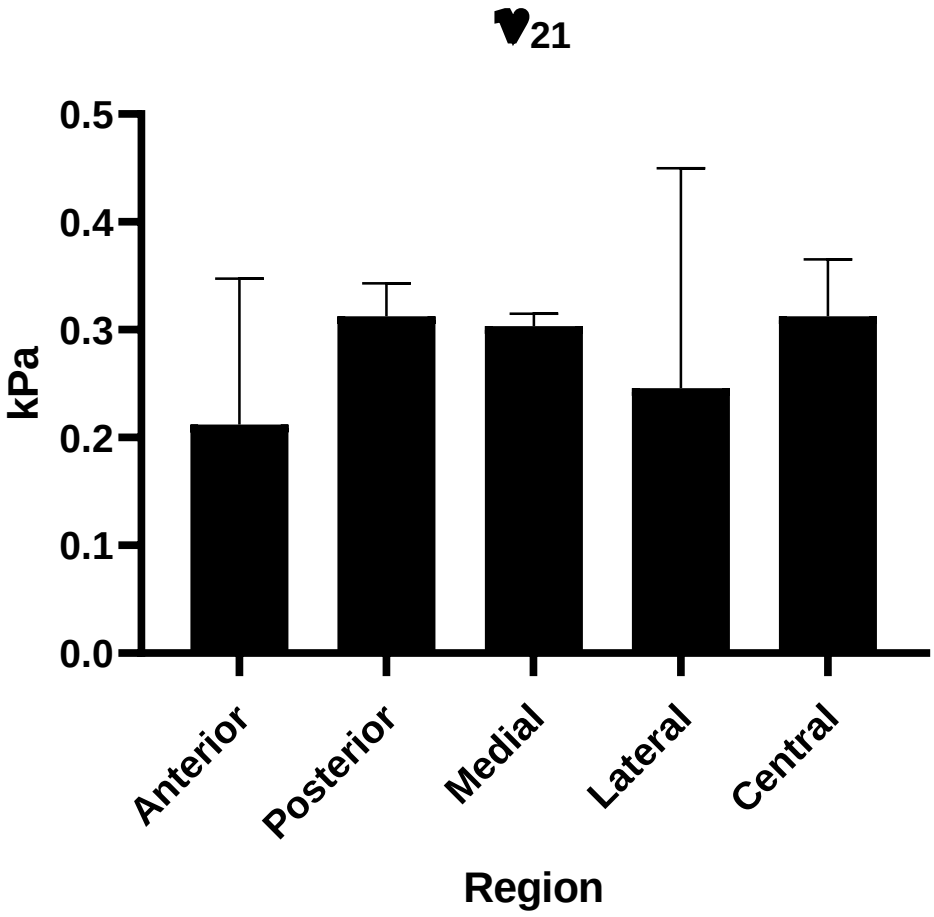

Figure 8. Bar graph of the Poisson's ratio of the in-plane modulus for the five different regions of the temporomandibular joint disc.

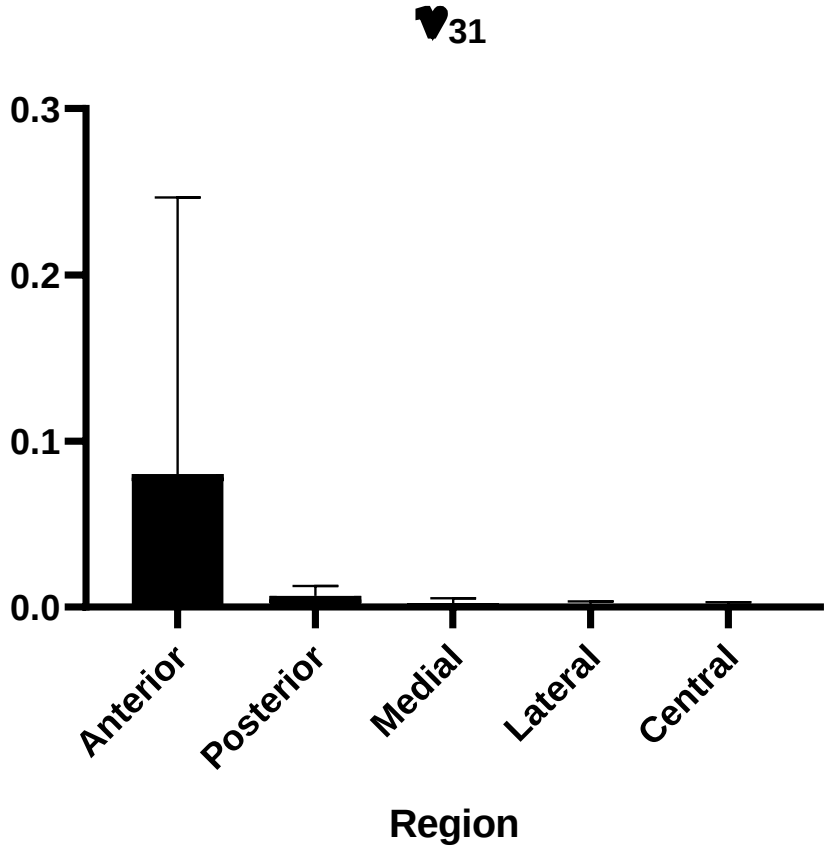

Figure 9. Bar graph of the Poisson's ratio of the out-of-plane modulus for the five different regions of the temporomandibular joint disc.

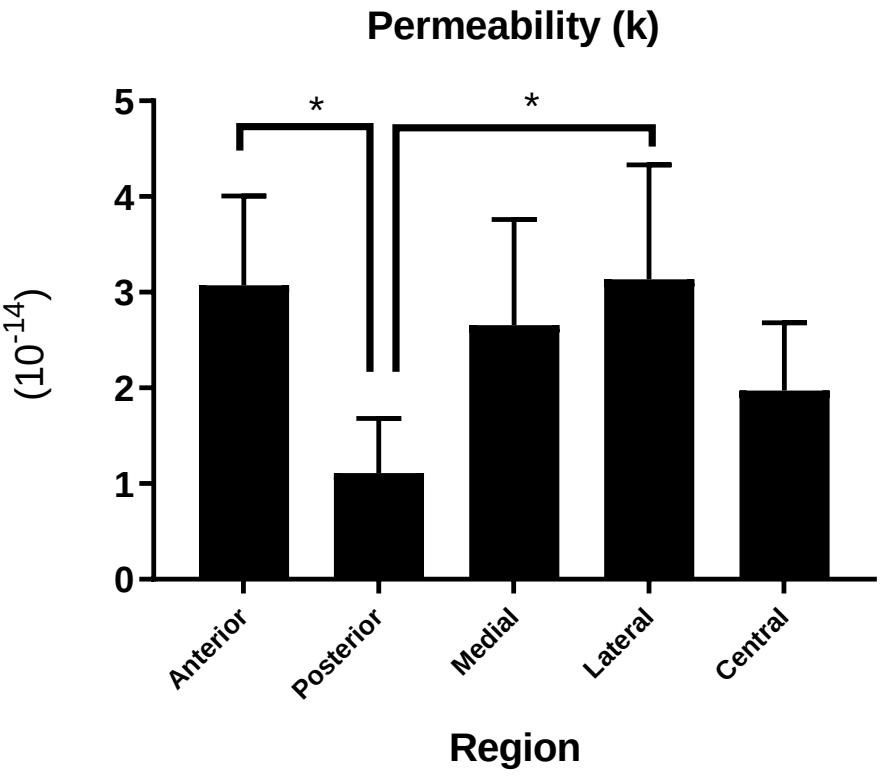

Figure 10. Bar graph of the permeability (10^{-14} m^4/(Ns)) for the five different regions of the temporomandibular joint disc. Asteriks represents the post-hoc Tukey's test having a significance of $p < 0.05$.

2.3.2 Mandibular Condylar Cartilage

The peak force (average value and standard deviation for all regions, Figure 11) and the stiffness (average value and standard deviation for all regions, Figure 12) of the cartilage was not significantly different in the 5 regions. In addition, there was no difference in the percent relaxation (average value and standard deviation for all regions, Figure 13) or the peak stress (average value and standard deviation for all regions, Figure 14) between each region. The tangent modulus also showed no differences between the regions (average value and standard deviation for all regions, Figure 15). The results of the transverse Young's modulus, E_1 (304.5±108.7 kPa, Figure 16) showed the lateral region of the cartilage was significantly higher than the posterior region). The out-of-plane Young's modulus, E_3, was not found to be significantly different throughout regions (average value and standard deviation for all regions, Figure 17). Both the in-plane Poisson's ratio ν_{21} (average value and standard deviation for all regions, Figure 18) and the transverse ratio ν_{31} (average value and standard deviation for all regions, Figure 19) showed no differences between the different areas of the cartilage either. The posterior region of the cartilage seemed to have highest permeability (average value and standard deviation), but was not statistically different from the other regions (Figure 20).

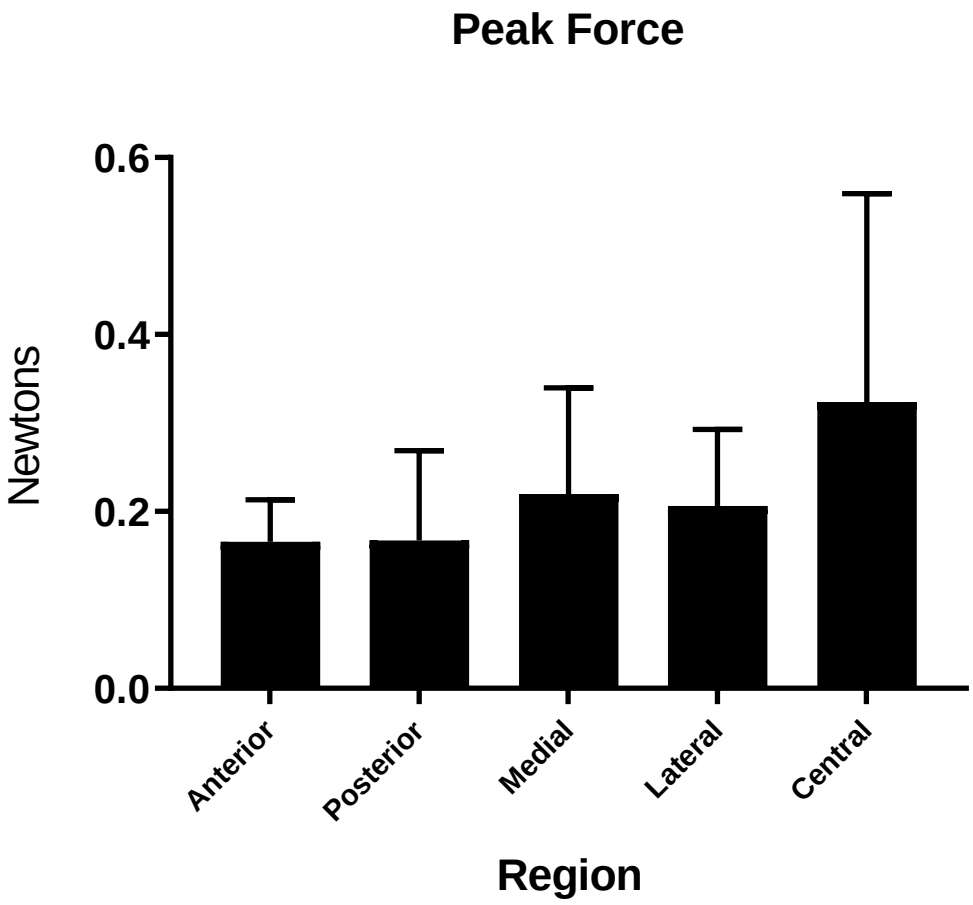

Figure 11. Bar graph of the peak force for the mandibular condylar cartilage.

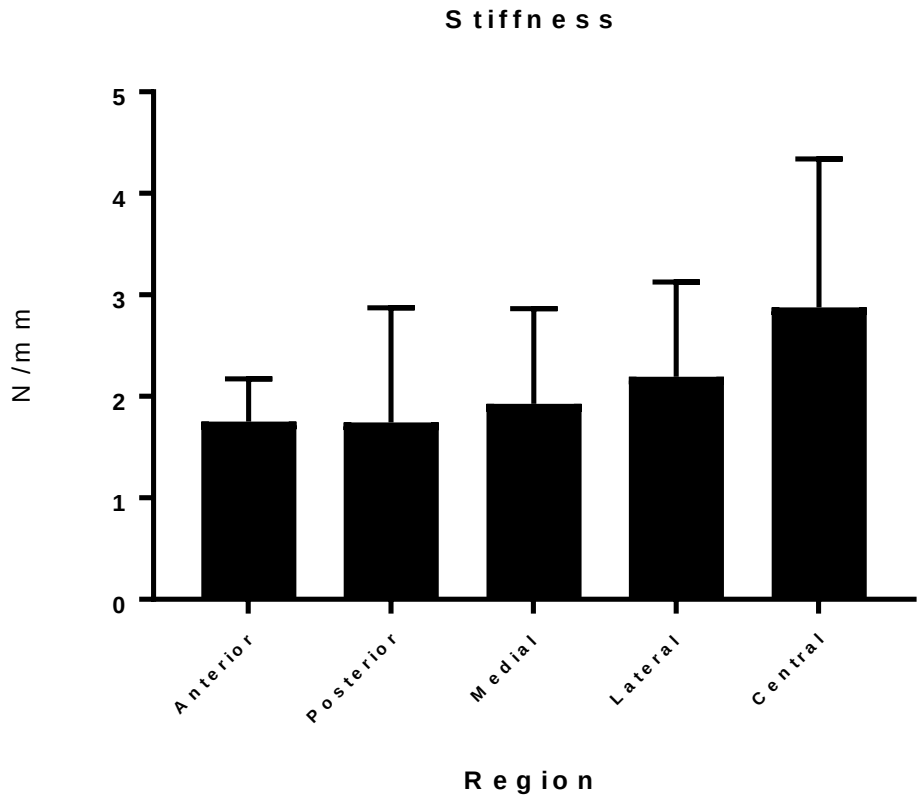

Figure 12. Bar graph of the stiffness (N/mm) for the five different regions of the mandibular condylar cartilage.

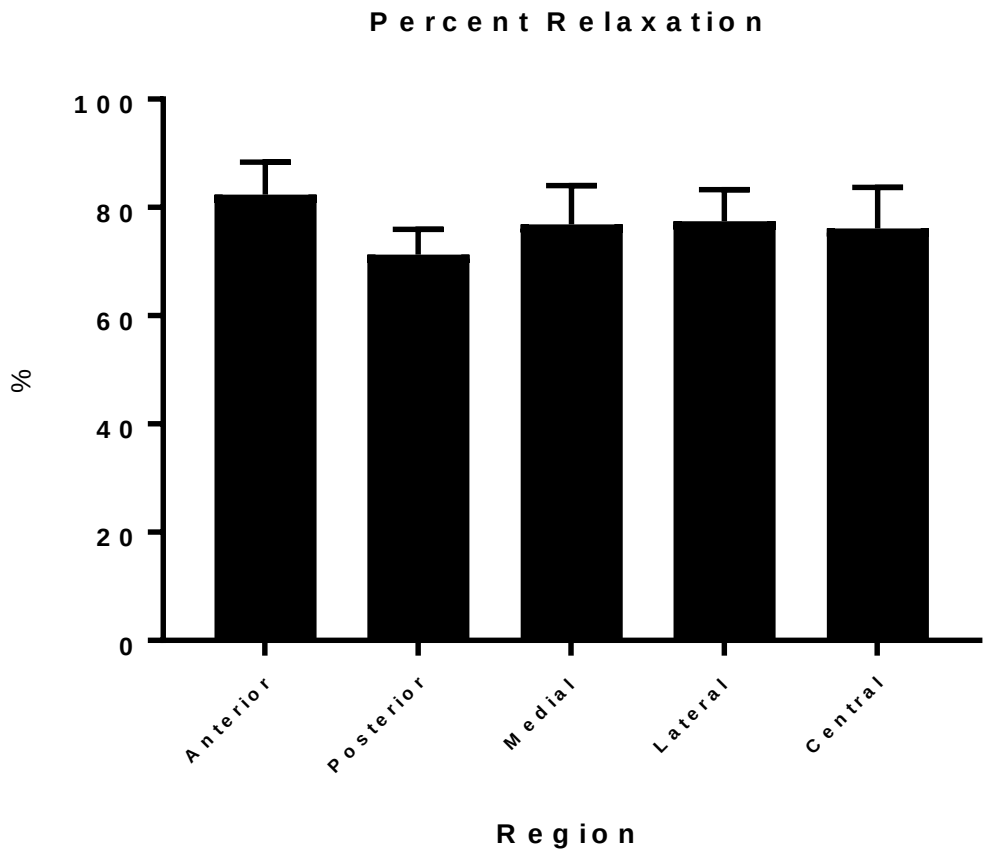

Figure 13. Bar graph of the percent relaxation for the five different regions of the mandibular condylar cartilage.

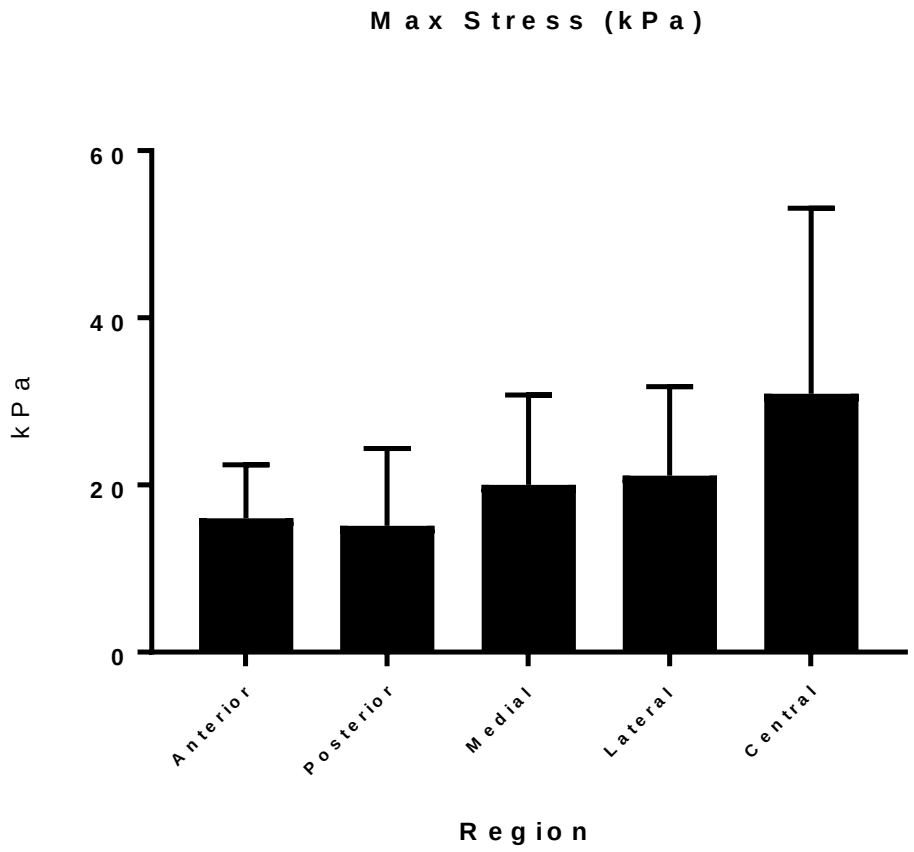

Figure 14. Bar graph of the max stress (kPa) of the five regions of the mandibular condylar cartilage.

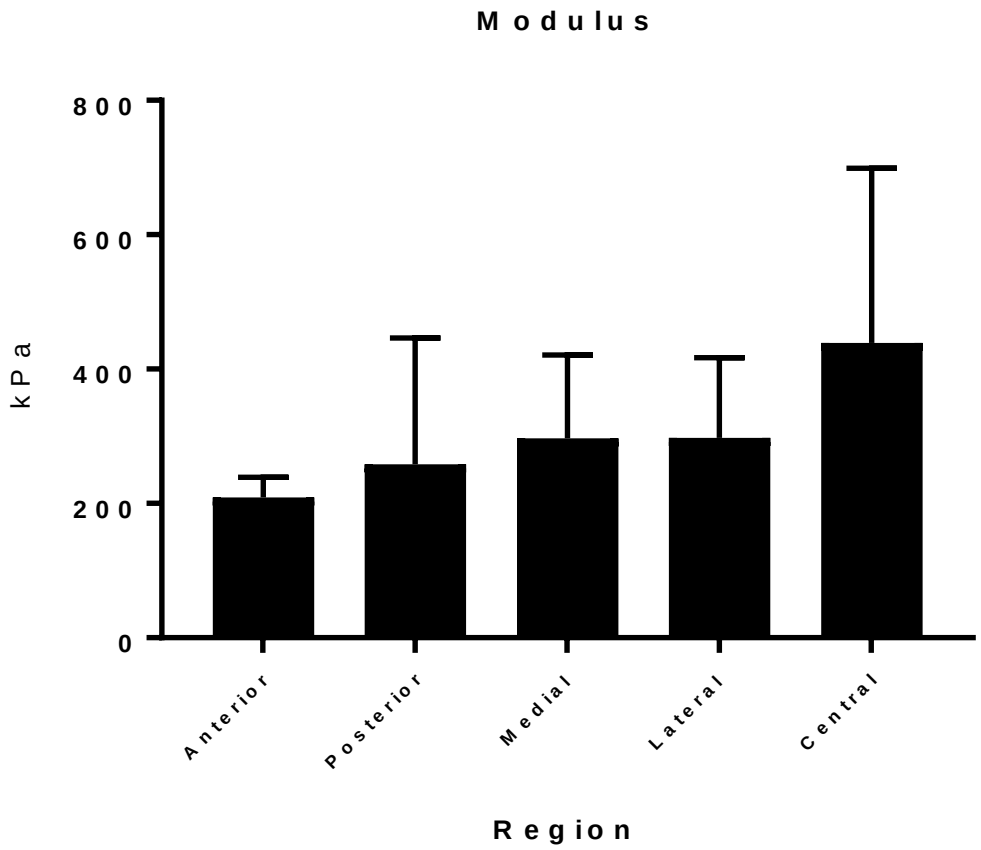

Figure 15. Bar graph of the modulus for the five different regions of the mandibular condylar cartilage.

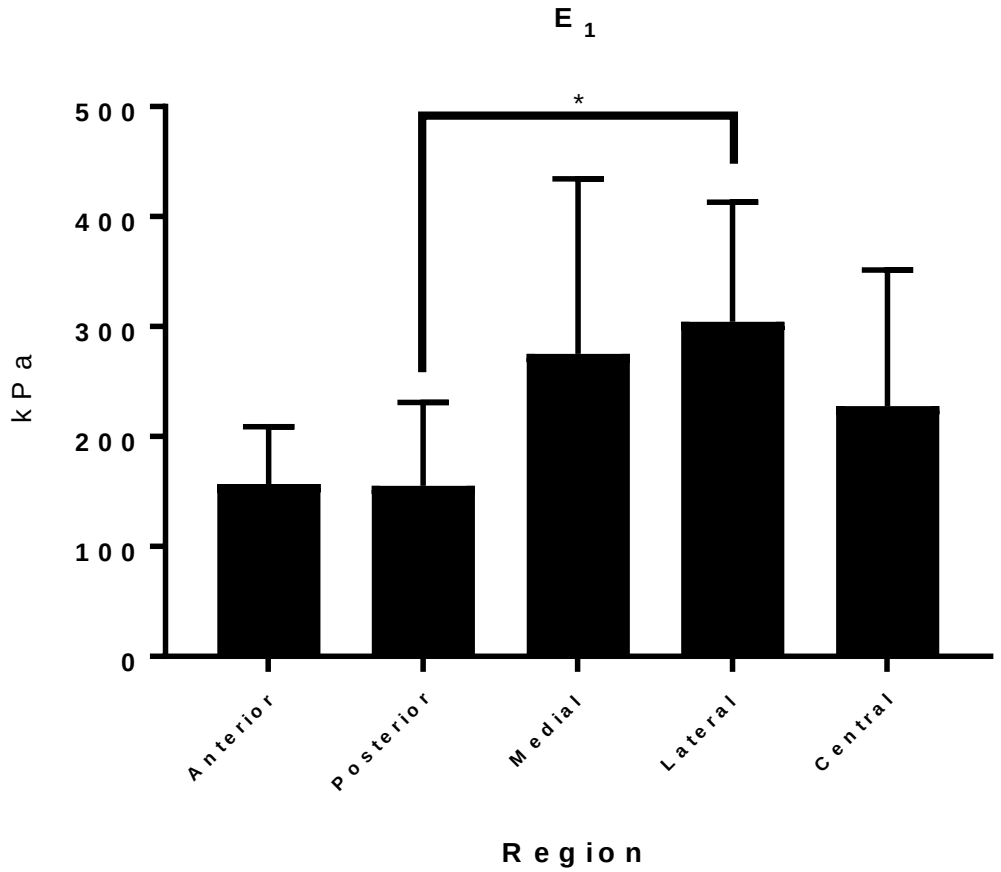

Figure 16. Bar graph of the Young's, in-plane modulus for the five different regions of the mandibular condylar cartilage.

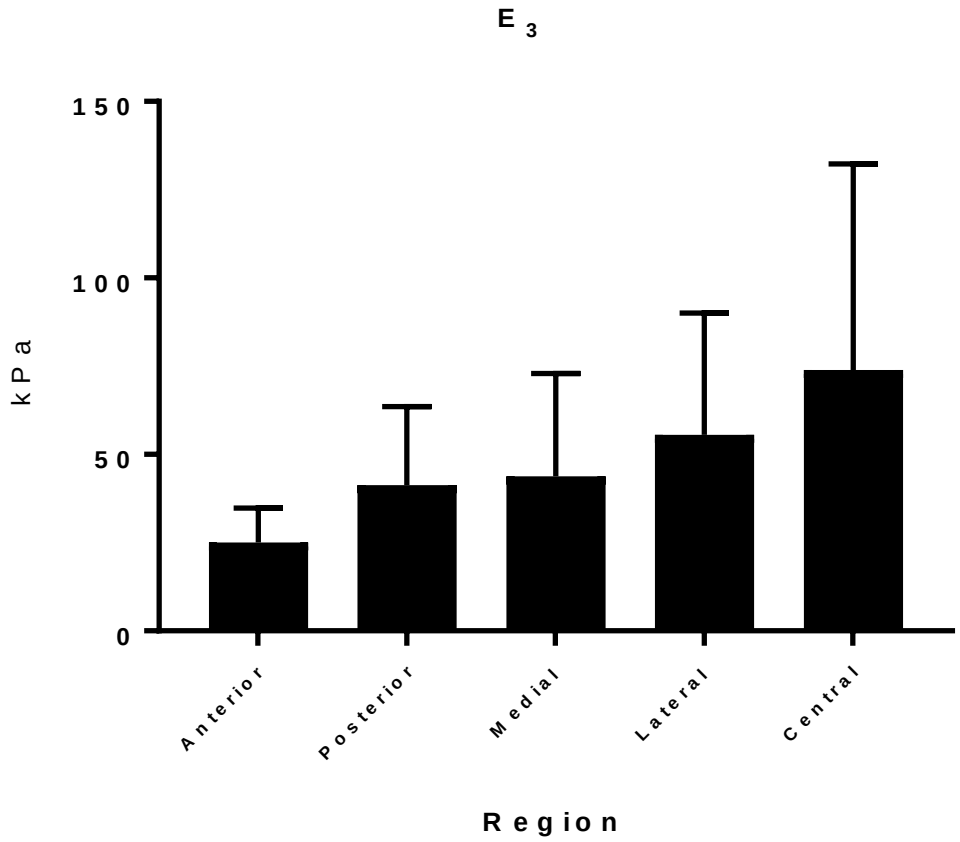

Figure 17. Bar graph of the Young's, out-of-plane modulus for the five different regions of the temporomandibular joint disc.

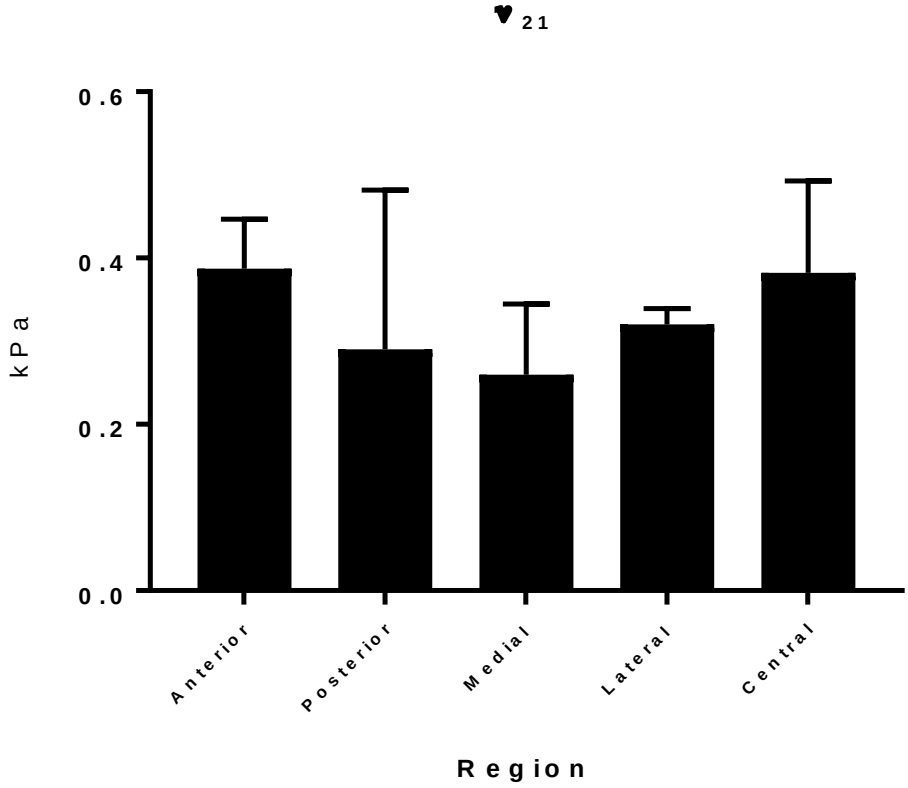

Figure 18. Bar graph of the in-plane Poisson's ratio of the different regions of the mandibular condylar cartilage.

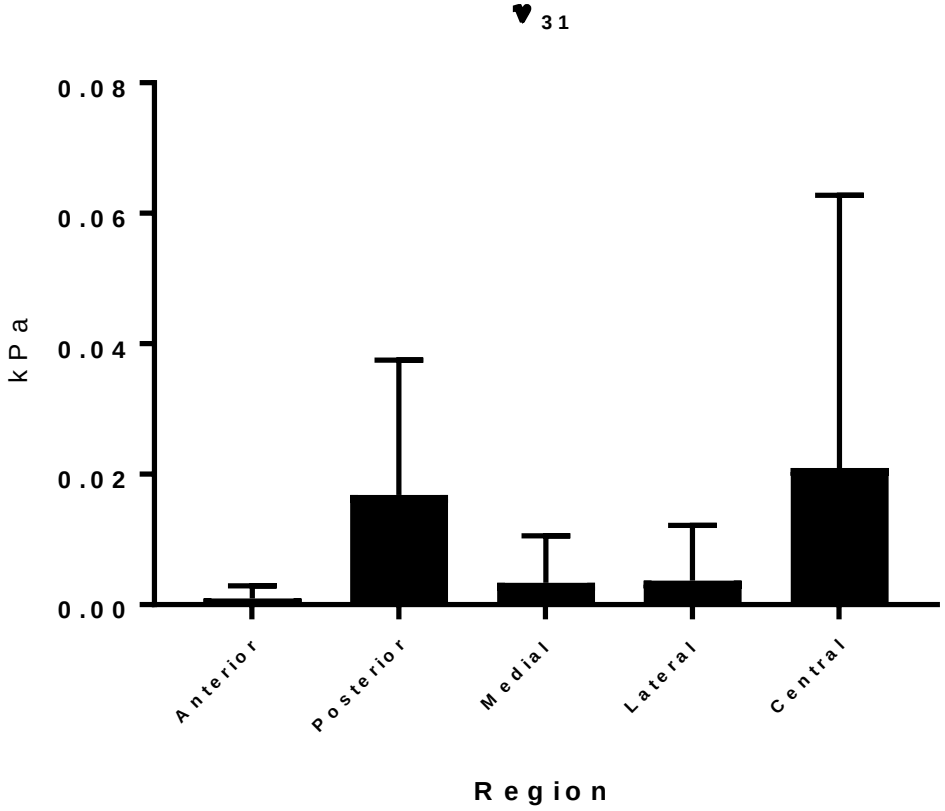

Figure 19. Bar graph of the in-plane Poisson's ratio of the different regions of the mandibular condylar cartilage.

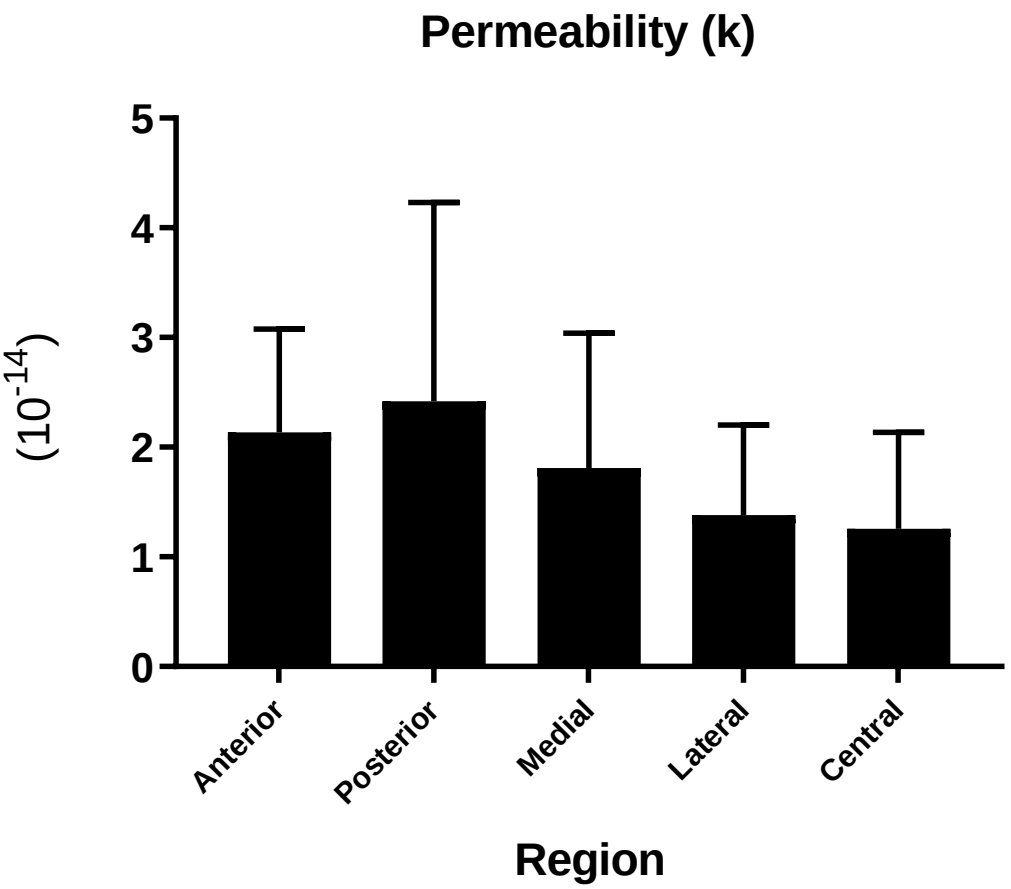

Figure 20. Bar graph of the permeability (10^{-14} m^4/(Ns)) for the five different regions of the temporomandibular joint disc.

Table 4. Percent relaxation of the temporomandibular joint disc for the five different regions. The numbers represent the average plus/minus the standard deviation.

Region	Relaxation (%)
Anterior	82.85±6.56
Posterior	83.79±4.31
Medial	86.95±5.41
Lateral	78.56±8.26
Central	79.31±7.78

Table 5. Percent relaxation of the mandibular condylar cartilage for the five different regions. The numbers represent the average ± standard deviation.

Region	Relaxation (%)
Anterior	82.39±5.97
Posterior	71.33±4.63
Medial	76.88±7.15
Lateral	77.46±5.84
Central	76.15±3.49

Table 6. Table of the peak force for the temporomandibular joint disc for for the five different regions. The right column represents the average ± standard deviation.

Region	Peak Force (N)
Anterior	0.11±0.05
Posterior	0.26±0.10
Medial	0.18±0.08
Lateral	0.09±0.03
Central	0.12±0.08

Table 7. Table of the peak force for the temporomandibular joint disc for for the five different regions. The right column represents the average ± standard deviation.

Region	Peak Force (N)
Anterior	0.17±0.05
Posterior	0.17±0.10
Medial	0.22±0.12
Lateral	0.21±0.09
Central	0.32±0.21

2.4 Discussion

The results from this study showed that the stress-strain behavior for an unconfined compression test under stress-relaxation was similar between the disc and the MCC in the pig for both magnitude of values and overall behavior. In terms of the fit, the biphasic model was able to fit the data for the disc (Figure 21) and the MCC (Figure 22), yet there were notable differences in how well the model fit between two tissues. Because of the ultrastructure of the extracellular matrix (collagen fibers) of the disc, the tissue was able to relax faster than the MCC. The faster drop in the stress-strain curve resulted in a slightly higher calculated error from the curve-fitting. It was also apparent that peak stress for both tissue types contributed to the behavior of the model as a higher stress still creates a larger absolute difference from peak to relaxation stress. This confirms our observations that the model begins to fail to describe the stress-strain behavior when there is a steeper decline in stress at the initial portion of relaxation. Again, these findings are mainly applicable to slow strain rates, which minimize the viscoelastic contribution of the fluid phase, and maximize the elastic contribution of the solid phase.

The pig model was chosen due to its similarities in its anatomical shape of the TMJ to humans (Almarza et al., 2018; Almarza, Hagandora, & Henderson, 2011). As such, there has been extensive testing of the mechanical properties of the porcine TMJ disc and MCC . When compared to other porcine TMJ disc compression studies, the study by Allen et. al (4), is close in terms of unconfined compression stress-relaxation tests. Allen et al. used the Kelvin model to characterize the compression results of the porcine TMJ disc (4), and it fit fairly well. The researchers found that the posterior region was stiffer than the central, lateral, and medial regions of the disc, which is similar to the results of the current study. The main difference between the two studies is that this current study was performed at 4.5% strain/min, and Allen et al. was performed at a very high

loading rate of 50% strain/second. Although this strain rate might be closer to physiological, it is very fast and pushes the accuracy of the loading system. This compounding error makes it difficult to replicate results. Furthermore, the kelvin fit does not provide constants with physical meaning, and as such, other fits might be desired.

When compared to other porcine MCC compression studies, our results compare well to Singh et al., where a regional analysis of the compressive properties was performed (Singh & Detamore, 2009). The tangent modulus was determined with a slower rate at 2 mm/ min and the stress relaxation test was performed at a strain rate of 0.5 mm/min in order to determine an elastic modulus. The authors also experienced a difficulty fitting the Kelvin model to the entire stress-strain curve due to the fast relaxation time seen at the beginning of the test. As a result, the curve was separated into two portions: one for the initial relaxation of the curve prior to 5 minutes and another post-5 minutes for fitting purposes. In the discussion, the authors mentioned that more sophisticated constitutive models could provide other relevant information about the mechanical properties of the cartilage.

The fit of parameters of the linear transverse isotropic biphasic theory of the TMJ disc revealed that the posterior region is much stiffer than the lateral region. We can assume that the differences seen are due to the types of stresses and functions those regions serve for the disc. The posterior band is the thickest band attached to the TMJ disc; the function of the posterior band is to move the disc back in place during jaw movement. We can contrast this to the lateral side of the disc which is only attached to the mandibular condyle and is not required to move – it is hypothesized the posterior region of the disc must be reasonably more mechanically robust than the lateral side. This could also have contributed to the findings seen in the estimation of the mechanical properties: the posterior region had a lower permeability value compared to the other

regions. A lower permeability of the tissue could indicate that the tissue is less porous and there is higher concentration of collagen fibers.

The current study aimed to improve upon this by employing a model that fit the entire curve. There was still some difficulty with fitting the curve to the initial portion of the test, as seen by the fit near the peak of the curve for both the disc (Figure 21) and the MCC (Figure 22), but the offset was reasonable enough to warrant using the transverse isotropic biphasic fit. In the future, a model that is also strain dependent in combination with biphasic, could also be used to be fit to compression data. Nevertheless, this work reveals that the transverse isotropic model does show robustness in calculating viscoelastic parameters of soft tissues that experience relaxation such as the mandibular condylar cartilage as well as the TMJ disc. The parameters calculated from the model help us characterize the TMJ disc even further. In the future, the relationships between composition, ultrastructure/alignment/density, and mechanical properties need to be fully elucidated in order for regenerative therapies to be successful.

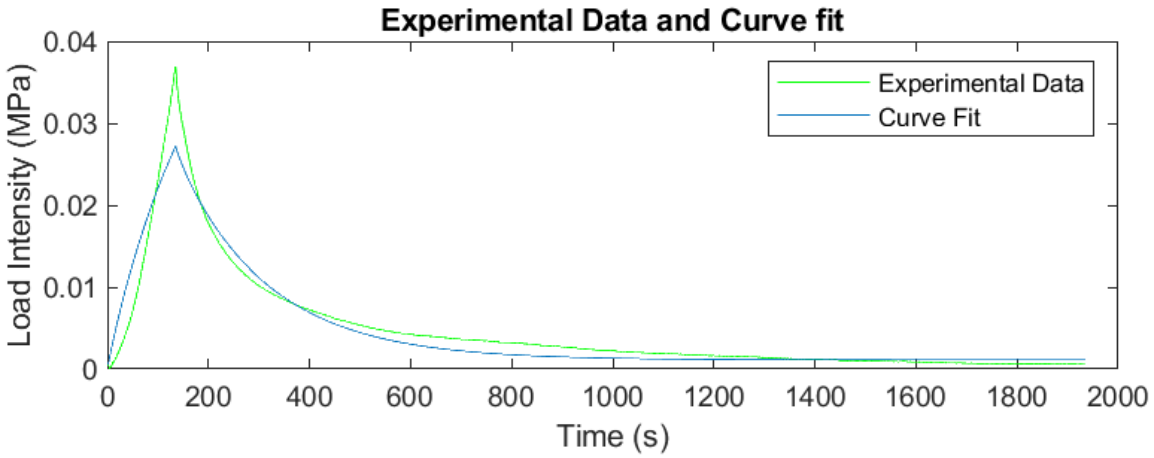

Figure 21. Representative graph of the experimental data plot (green) versus the estimated curve fit calculated by MATLAB for the temporomandibular joint disc.

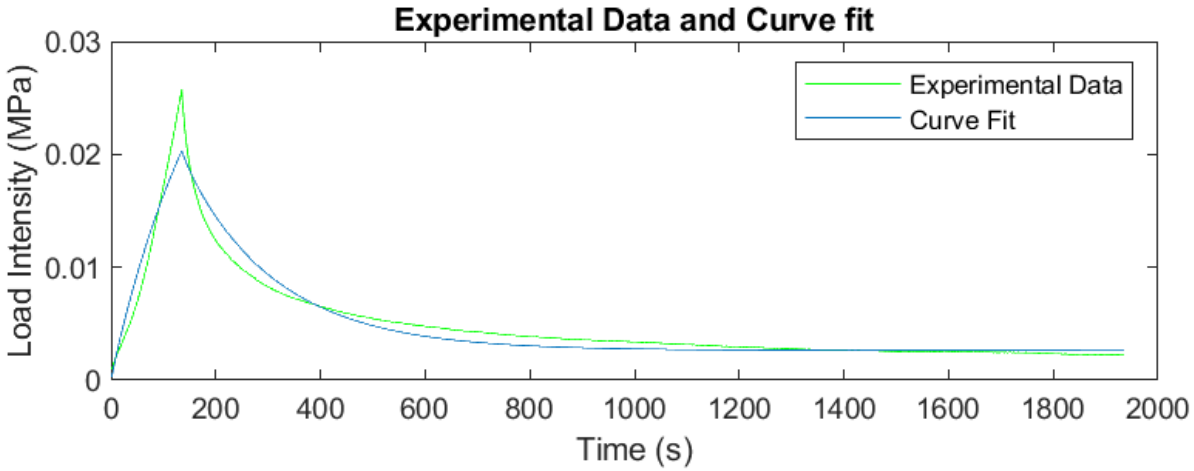

Figure 22. Representative graph of the experimental data plot (green) versus the estimated curve fit calculated by MATLAB for the mandibular condylar cartilage.

3.0 Regenerative Potential of Various Soft Biomaterials: An In Vivo Pilot Study

The second aim was to assess various soft biomaterials in vivo. The purpose of this pilot study was to establish a new animal and injury model for the MCC and to determine the feasibility of using soft biomaterial scaffolds for regeneration of the fibrocartilage and subchondral bone of the TMJ. To do this, scaffold sponges using the previously mentioned biomaterials were produced and inserted into osteochondral defects of the mandibular condyle in skeletally mature goats. The caprine model was chosen due to the accessibility of the TMJ as opposed to the commonly used porcine model (Almarza et al., 2011). Scaffolds and condyles were then evaluated following 12 weeks of healing.

3.1 Materials and Methods

3.1.1 Biomaterial Preparation

Skeletally mature (4-6 years old) female Spanish Boer goats were used for the surgeries. These goats were purchased from K Bar Livestock (Sabinal, TX). The Institutional Animal Care and Use Committee at the University of Pittsburgh approved all the animal procedures, which were performed in accordance with the National Institutes of Health guidelines for the use of laboratory animals.

Six goats were used in our study to evaluate 4 different experimental groups: 1) an empty control, 2) PGS with Mg ions, 3) gelatin with Mg ions, and 4) gelatin with both Mg ions and

trimagnesium phosphate (TMP) powder. Mg salts were added to all the polymer groups, and was also delivered as a powder in the TMP group. The purpose of this was to have both a quick delivery of Mg via salts, and then a slower method of delivery via trimagnesium phosphate, as the latter requires enzymatic processes to dissolve. Bilateral surgeries were performed on each goat, thus the total number of goat condyles analyzed was n=12. With 4 groups and 12 condyles, each group had a sample size of n=3. The same group was never performed on both condyles of the same animal.

The PGS scaffolds were prepared as previously described (Gao, Ensley, Nerem, & Wang, 2007). The PGS was made into a sponge using porogen leaching of 75-150 μm. The PGS with this pore size has shown to facilitate fibroblast diffusion and attachment [9]. PGS scaffolds were autoclaved and then soaked in 70%, 50%, 25% ethanol and PBS prior to implantation. Gelatin methacrylate scaffolds were made in house with a 10% methacrylated gelatin solution in PBS. The solution was then photo polymerized into a hydrogel (the photoinitiator was lithium phenyl-2,4,6-trimethylbenzoylphosphinate (LAP)), lyophilized and then put into an oven to baked at 100 °C overnight to form sponges. The gelatin scaffolds were manufactured with a sterile process; the hydrogel precursor was sterile filtered and the scaffolds were baked. For the fourth group, TMP was added to the gelatin hydrogel precursor at 10mM before the slow freezing. Prior to implantation, all scaffolds sponges were soaked in a saturated (20% w/v) concentration magnesium sulfate solution.

3.1.2 Surgical Procedures

Surgeries were performed by first making an incision near the temporal lobe of the goat. Following the incision, the lateral pterygoid muscle along with others were separated to access the

TMJ space. Once inside the joint space, 1 mm drill bit was used to create a trough-like defect on the superior surface of the mandibular condyle, moving in the mediolateral direction beginning at the center of the condyle. This was performed while a spatula was situated between the drill and the TMJ disc to preserve the structural integrity of the rest of the joint. The drill was then inserted roughly 2-3 mm below the superior surface of the mandibular condyle and allowed to enter the condyle to a depth of no more than 10 mm. Upon reaching this depth, the drill was then moved upward to remove the fibrocartilage layer superior to the subchondral bone. After making the osteochondral defect, blood in the surrounding areas were allowed to clot before the scaffold was inserted, then the underlying muscles tissue was sutured, then the skin was sutured to completely close the incision. All animals were then immediately returned to a normal diet.

3.1.3 Histology

Mandibular condyles were retrieved after 12 weeks of healing and fixed in 10% formalin overnight. Condyles from similarly aged female goats were obtained from K Bar Livestock to use as a native control. Paraffin sectioning was performed by Alizée Pathology (MA) as well as hematoxylin and eosin staining. Safranin-O for glysosaminoglycan (GAG) detection and Masson's Trichrome staining for collagen were performed in-house. The collagen II immunostaining, to visualize the cartilage layer, was performed at the Research Histology Services of the Starzl Institute at the University of Pittsburgh using anti-human collagen type II produced in mouse (MP Biomedicals, Cat#: 008631711). Briefly, samples were first incubated overnight in a NA3PO4 buffer of pH 6 in an oven at 56 °C, blocked with Avidin, Biotin, and serum, incubated with 1:1000 diluted Coll II overnight at 4 °C, with the secondary antibody biotinylated anti mouse

(MP Biomedicals, Cat#: 08631711), and with ABC reagent (kit). Then AEC chromogen was applied, with counterstaining using aqueous hematoxylin and Scott's Tap Water.

3.2 Results

The native condyle from two Spanish Boer goats, in hematoxylin and eosin images, exemplify the discrete layers of the mandibular condylar cartilage (Figure 23a,d). The safranin-O images showed glycosaminoglycan presence in the same zone as the hypertrophic cells for the same condyle (Figure 23b,e). In the Masson's trichrome stain, there was a clear collagen layer beneath the fibrous layer of the native condyles (Figure 23c,f).

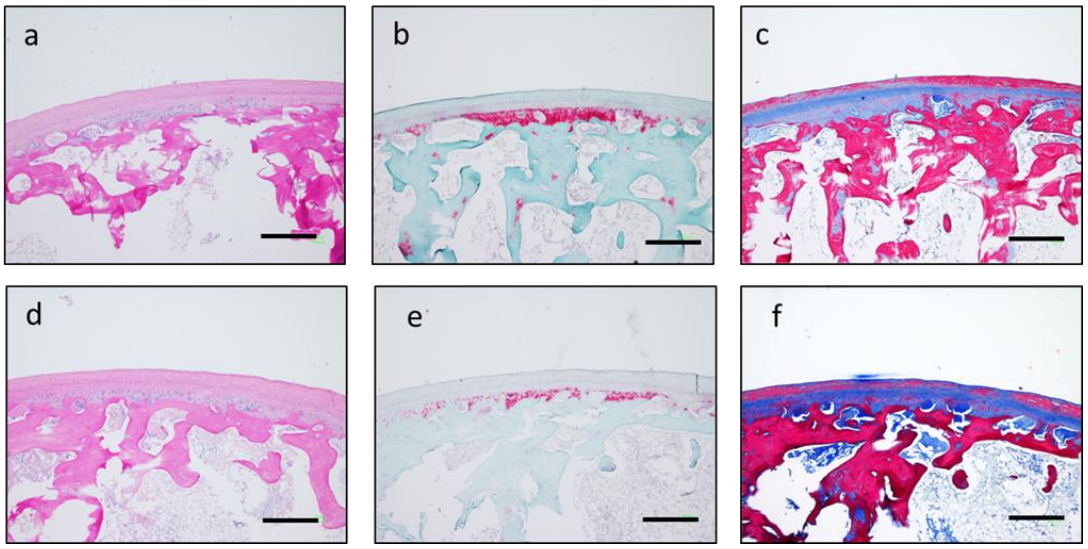

Figure 23. H&E (a,d) , safranin-O (b,e) , and Masson's trichrome (c,f) stain for the native condylar cartilage of 2 goats.

The empty control on the first goat showed no signs of cell infiltration and only fibrous tissue surrounding the edges of the defect (Figure 24a). The safranin-O image supported that the tissue was fibrous since there was no staining for GAG (Figure 24b). The faint blue in the Masson's trichrome of the empty control condyle also suggested fibrous tissue growth over the defect (Figure 24c). On the second goat, there also appears to be fibrous tissue in-growth with bone remodeling in the fibrous scar (Figure 24d,e,f). The third goat did not seem to have a full defect, and resembled the native condyle with a small tear in the condylar cartilage and a small hole in the subchondral bone (Figure 24g, 2h, 2i).

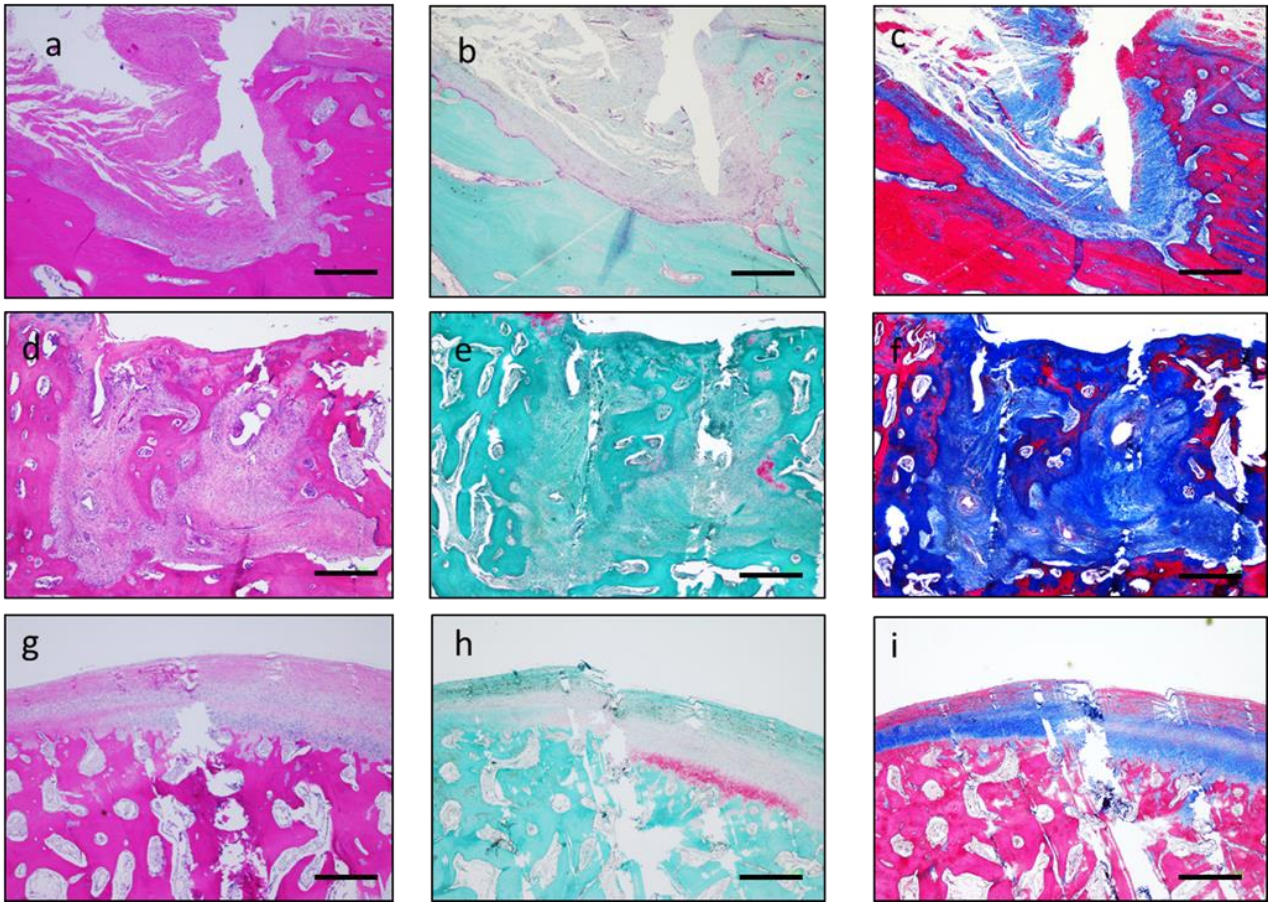

Figure 24. H&E (a,dg,g), safranin-O (b,e,h), and Masson's trichrome (c,f,i) of the empty control group (osteochondral defect, but not biomterials inserted, n=3).

The PGS group showed cellular infiltration within the osteochondral defect (Figure 25a) in the first goat. The safranin-O stain of the PGS-implanted scaffolds (Figure 25b) show robust GAG presence at the site of the surgery. From the Masson's trichrome, there was collagen formation inside the defect (Figure 25c). In the second goat, the created defect was apparent, but the regeneration of the cartilage layer did not seem as robust (Figure 25d) as the first goat due to the majority of the tissue being fibrous. Along the edges of the defect in the second goat, there were was a very small amount of GAG, but still seems to be mostly fibrous tissue (Figure 25e); collagen was still seen in the defect (Figure 25f). The third goat of the group had histological artifacts, but half of the defect is still visible with minor cell presence (Figure 25g). There was no GAG (Figure 3h), but there was a noticeable amount of collagen in the regenerated area (Figure 25i).

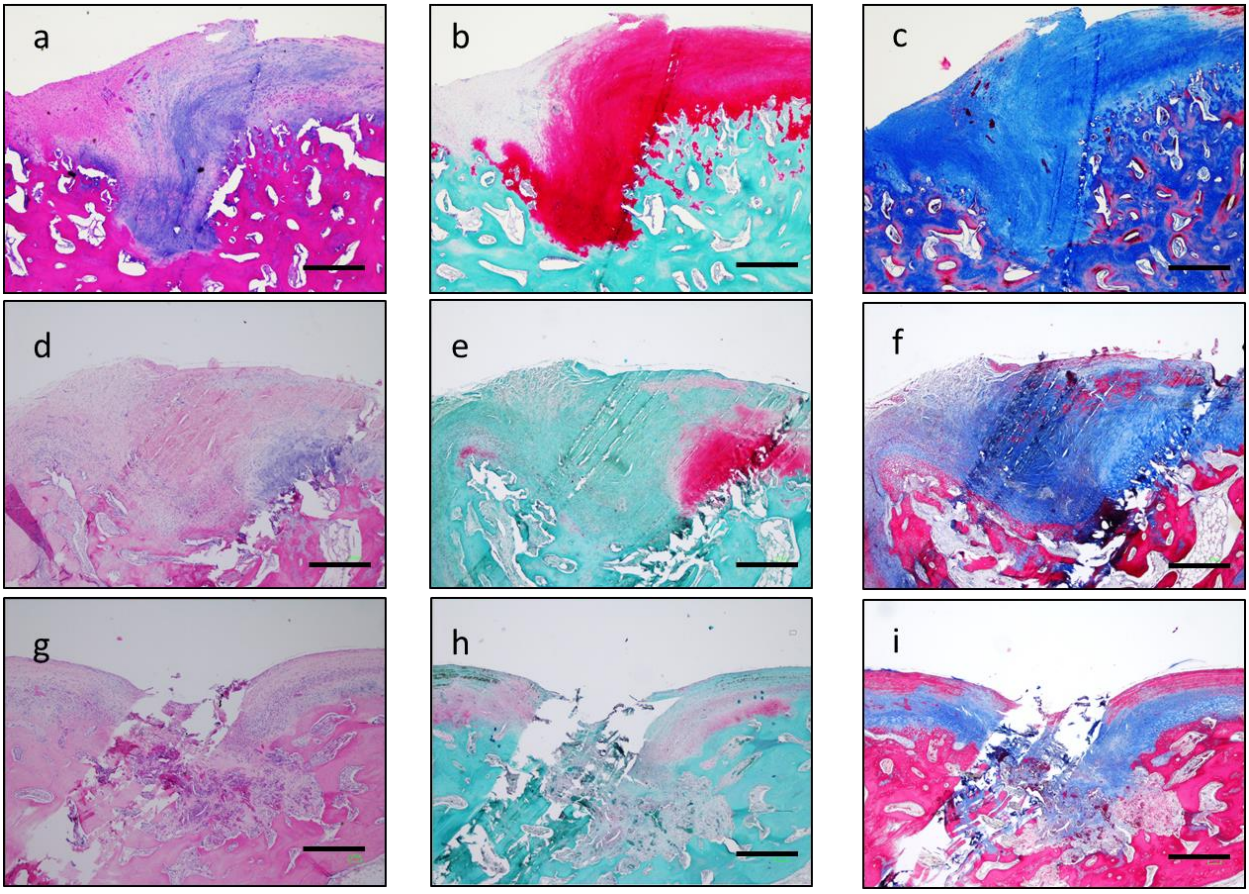

Figure 25. H&E (a, d, g), safranin-O (b,e,h), and Masson's trichrome of ostechondral defects filled with a gelatin sponge scaffold (n=3).

The gelatin group also showed cellular infiltration in the first goat (Figure 26a), along with some portions of non-degraded scaffold. In addition, right above the cell layer of the regenerated tissues there appeared to be a fibrous layer – similar to that found in the native mandibular condylar cartilage. The same was observed for the safranin-O stain; fibrous tissue on the surface of the condyle with a GAG layer underneath it (Figure 26b). The trichrome stain showed collagen as expected (Figure 4c). The second condyle had no in-growth of fibrous tissue (Figure 26d,e,f).. The third goat of the group had histological artifacts, but the drilled bone was still apparent in the sections as there was a small collection of cells in the right portion of the defect (Figure 26g). GAG was seen in the same portion of the defect where the cells were (Figure 26h). Judging from the trichrome stain, there was a mixture of fibrous tissue and collagen in the regenerated area (Figure 26i).

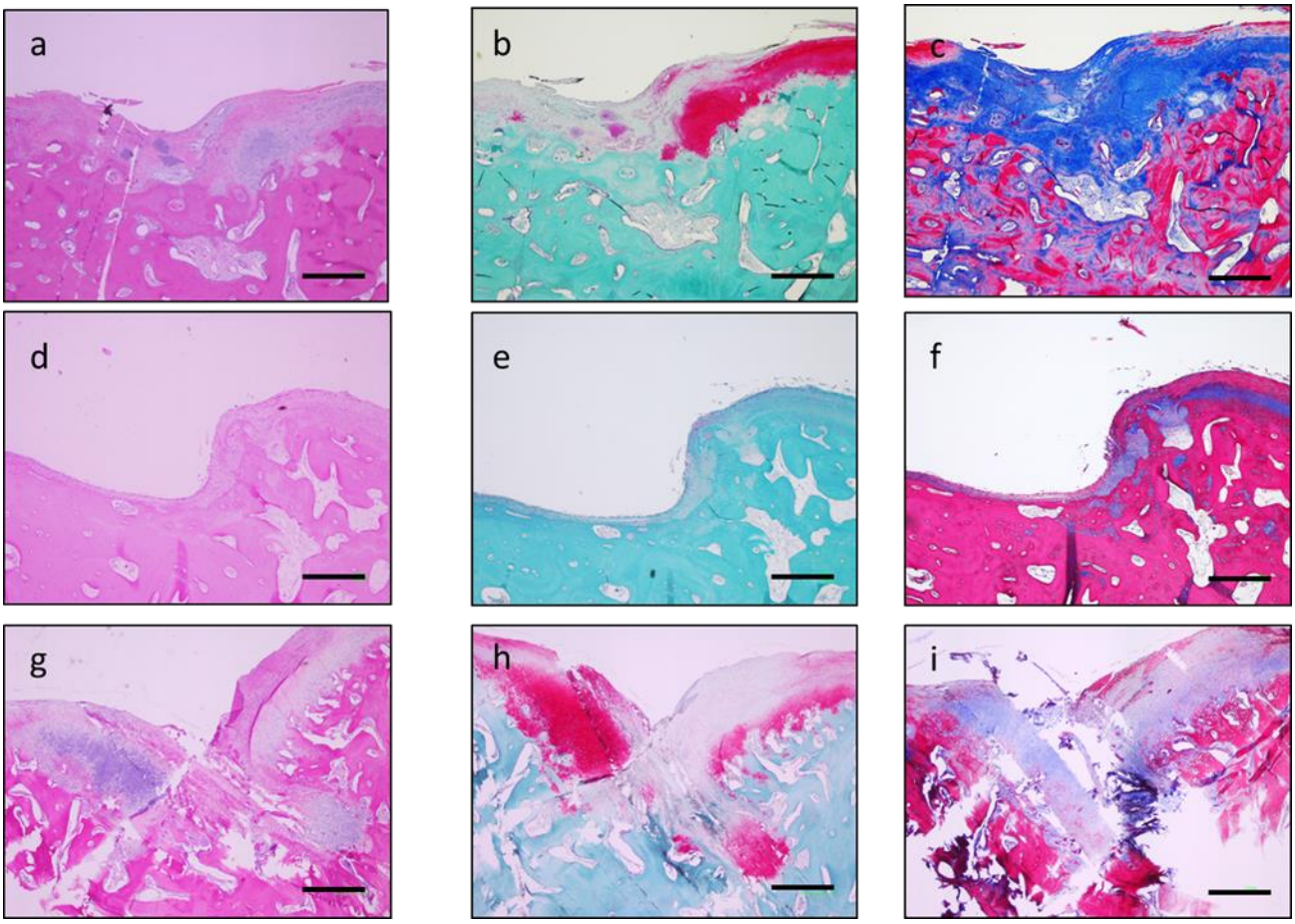

Figure 26. H&E (a, d, g), safranin-O (b,e,h), and Masson's trichrome of ostechondral defects filled with a gelatin sponge scaffold (n=3).

The gelatin and TMP constructs did not completely degrade by the end of 12 weeks (Figure 27a); however, between the pores of the non-degraded scaffold, there appears to be formation of neotissue as evidenced by the cells in each pore. The safranin-O (Figure 27b) and Masson's trichrome (Figure c) stains revealed mostly fibrous tissue between the pores of the scaffold. The second condyle of the group only had fibrous tissue growth in the defect (Figure 27d, e, f). The condyle of the third goat was lost during histological processing.

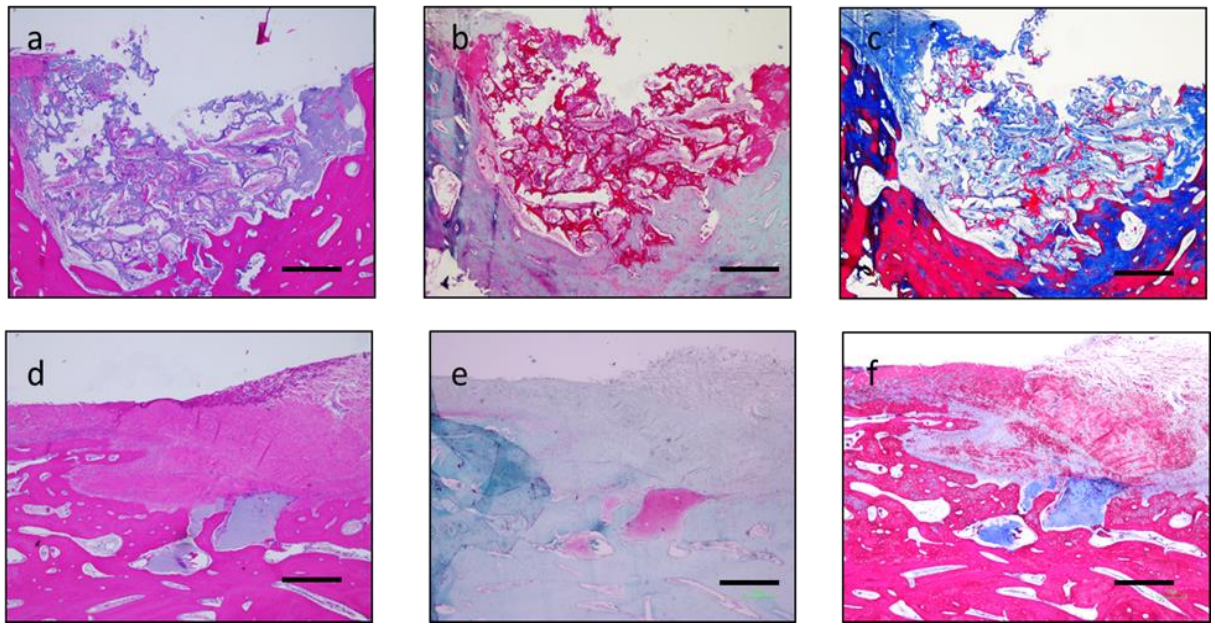

Figure 27. H&E (a, d), safranin-O (b, e), and Masson's trichrome of the gelatin sponge scaffold with trimagnesium phosphate.

Immunohistochemistry staining for collagen II was only performed on two condyles: the PGS only group, and the gelatin scaffold only group (Figure 28a, b, respectively). The immunostain demonstrated collagen II growth within the defect of the PGS only group (Figure 28a). This was also seen in the gelatin scaffold group, although to a lesser extent.

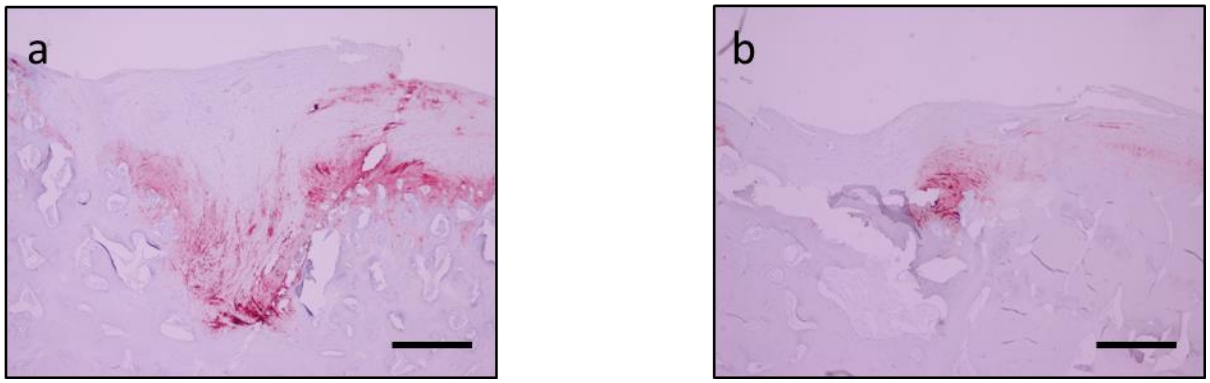

Figure 28. Collagen II immunostain of the PGS group (a, first sample) and the gelatin sponge group (b, first sample). The red signifies presence of collagen II and the background of the sample is light blue.

3.3 Discussion

In the past, the adult porcine model has been commented as the gold standard model for TMJ anatomy (Almarza et al., 2011). We believe that our goat model offers a key benefit. The anatomy of the farm pig proves to be a hindrance when it comes to executing repeatable procedures in the joint space. The zygomatic arch of the porcine model impedes access to the TMJ, while the arch is minimal in the goat. For this experiment, not only was it easy to insert the drill into our surgical area, but there was plenty of space between the glenoid fossa and the superior surface of the mandibular condyle. Thus, we believe that this work starts a paradigm shift in the ideal TMJ surgical model.

Our findings from the PGS group demonstrate the viability of the material as a means of cartilage regeneration in condylar defects. A large amount of cellular infiltration was observed with the presence of cartilage with GAG and collagen in the same area. An immunostain for collagen II confirmed the type of collagen that regenerated in the osteochondral defect (Figure 6a). In the future, a collagen X stain should be performed to determine if there are hypertrophic chondrocytes in the region. Similar outcomes were observed with the gelatin scaffold group, as there were both GAG and collagen II within the defect (Figure 6b). Although this group did not see the same degree of cellular infiltration as the PGS group, it was interesting that one defect regenerated the fibrous layer that was seen on top of the cellular layer – something that is characteristic of the native TMJ mandibular condyle.

For future iterations of this study, magnesium metal (as opposed to ions) could be incorporated into these scaffolds to provide a better healing template for bone. As the results showed, there was insufficient evidence of bone regeneration from these biomaterials alone. The lack of subchondral bone regeneration could be due to the disparity of the mechanical properties

of both the scaffold and the bone at the interface. A limitation of the current study is that all polymer scaffold sponges were soaked in magnesium, and there was not a comparison to a pure scaffold control. In addition, we do not know if the scaffolds remained inside the defect throughout the duration of the healing period.

The healing responses observed with the gelatin-TMP scaffolds was much different than just gelatin. From the condyles in this particular group, all of them showed a non-degraded scaffold still lodged in the defect and little GAG formation. An observation was made that the TMP group scaffolds were considerably stiffer than the gelatin-only scaffolds. In one condyle, the scaffold was stiff enough to prevent proper section of it; hence, there only being two available condyles of the TMP group for histology. A more ideal method of incorporating the magnesium would be to deliver them via microparticles as ions – this would decrease the stiffness of the scaffold while also providing a more controlled delivery.

The lack of time points for temporal analysis is another future consideration for this experiment. For the pilot study we had only chosen one time point due to limited resources as well as choosing a time point well within the range for complete degradation for gelatin and PGS. Shorter time points could give more insight on when the earliest formation of collagen II or GAG occurs within the defect. This would be something worthwhile to pursue especially for Mg-based scaffolds as we have found that the one containing trimagnesium phosphate would more than likely require more than 12 weeks to degrade fully. Another limitation of the study is the variance seen in the size and shape of the injury (Figure 2). Future studies will endeavor to create a more standard defect.

The need for a biodegradable polymer for TMJ regeneration is paramount. Total joint devices device come with the risk of revision surgery. An intervention that does not require

secondary surgeries would be the most ideal treatment. From the histology results of this pilot study, the use of soft polymers such as gelatin and poly (glycerol sebacate) show promise as biomaterials for cartilage and fibrocartilage regeneration in the TMJ.

4.0 Controlled Stem Cell Differentiation and Primary Cell Behavior in Gelatin-Based Hydrogels: An In Vitro Study

The third aim of the thesis follows through with the findings of the *in vivo* results, and utilizes gelatin biomaterials because of their versatility. With gelatin, these subsequent studies aim to build around a promising hydrogel, and modify its composition to fit the specific regenerative needs of the mandibular condylar cartilage.

Hydrogels are a well-studied material due to their physical ability to mimic the matrix composition of cartilage. In addition, they have the benefit of being able to carry cells and drugs, and deliver growth factors. These favorable characteristics have elicited novel studies to develop these hydrogels for various applications. The consideration to switch from a gelatin sponge to a hydrogel was based on the degradation and the cellular attachment seen in previous *in vivo* studies for similar efforts with this material (Conrad et al., 2018; Nichol et al., 2010). The growth plate and the MCC are similar because the population of cells differs from the proximal to the distal ends of the tissue.

Regeneration of either cartilage, growth plate or MCC, requires modification of the gelatin hydrotel in order to prevent for chondrocyte hypertrophy and stem cell dedifferentiation, which is a challenge in itself during soft tissue regeneration. Chondrocytes to have the ability to produce glycosaminoglycans and collagen II inside gelatin scaffolds (Chin, Gao, Wang, Taboas, & Almarza, 2018); however, if not properly controlled in *in vitro* conditions, chondrocytes may undergo hypertrophy, which enlarges the cell and induces apoptosis (Cheung et al., 2003).

The first part of this study investigates stem cell behavior when seeded in a gelatin and gelatin-composite hydrogel scaffold. An *in vitro* study first analyzes the differentiation potential

of the two different gelatin hydrogels by exposing the cell-laden scaffolds to either chondrogenic media or osteogenic media. Next, the second part of the aim shifts to understanding possible long term effects of cells once they have differentiated. In order to do this terminally differentiated primary cells (osteoblasts, costal chondrocytes, and mandibular condylar chondrocytes), were isolated from goat mandibles acquired by the local abattoir in order to understand primary cell behavior within these hydrogels. Cells were then seeded in the same manner as the first part of the aim. Biochemistry, biomechanical, and histological assays were done on scaffolds cultured between 0 to 4 weeks.

4.1 Stem Cells and Gelatin Based Scaffolds

4.1.1 Introduction

The mandibular condylar cartilage is a unique cartilage in the body with its various layers that make up the entire fibrocartilage. The cell population from the cartilage varies from the superior portion of the condylar cartilage, to the layer just before the subchondral bone.

With gelatin showing the ability to foster both fibrous and cartilage growth from the previous aim, we have looked towards using similar materials used to regenerate soft tissues in discrete layers by controlling the local spatial distribution of stem cell differentiation. Specifically, we will explore the addition of Poly (ethylene glycol) (PEG) and Heparin to the gelatin polymer. PEG is a biomaterial that has been used as scaffolds to host cell attachment and regeneration in addition to gelatin. Heparin is a biomaterial with a highly negative charge associated with it structure, which allows for growth factors to have a better affinity of binding to it than other

materials. With this characteristic, it is possible to improve the delivery of growth factors for the purpose of enhancing tissue regeneration.

4.1.2 Materials and Methods

4.1.2.1 Cell Isolation

Goat BMSCs were isolated from bone marrow aspirates taken from the iliac crests of 3-month-old female goats. A 16G bone marrow biopsy needle attached to a 10mL syringe was loaded with alpha MEM containing 180U/mL heparin. Following the manufacturer's protocol, erythrocytes were removed via Ficoll-paque PLUS. The extracted cells were plated and the tissue culture adherent cells were taken as BMSCs.

4.1.2.2 Hydrogel Material Modification

PEG (molecular weight: ~4000), type B gelatin taken from bovine skin (molecular weight: ~45000), dichloromethane, triethlyamine, diethyl ether, molecular sieves (4Å) , methacrylic anhydride, and dialysis tubing were obtained from Sigma-Aldrich. Heparin sodium salt (molecular weight: 15000) and other chemicals used for material synthesis were from Thermo Fisdher Scientific (Hampton, NH).

PEG was modified the same way as previously done by Lin-Gibson et al. (79). The unmodified PEG was briefly dissolved in dichloromethane and reacted with methacrylic anhydride and trimethylamine in the presence of freshly activated molecular sieves (4Å). The mixture was left to react for 4 days at room temperature in the dark. The modified PEG (PEGDA) was then

allowed to precipitate in diethyl ether, followed by dialysis against distilled water for 48 hours. The material was the removed, frozen, and lyophilized.

Gelatin was modified using the same method as in Nichol et al. (6) and Schuurman et al. (80). The unmodified gelatin was dissolved in phosphate-buffered saline (PBs) and reacted with methacrylic anhydride at 50 °C for 1 hour. The newly modified gelatin (GEL-MA) was then neutralized to pH 7.4 and dialyzed against PBS for 48 hours. The dialyzed material was removed, frozen, and lyolphilized.

Heparin was modified using the same method as Benoit et al (81). The unmodified heparin was dissolved in distilled water and reacted with methacrylic anhydride at pH 8.5. Following the initial reaction, the mixture was allowed to react for 12 hours at 4 °C. Once the mixture was removed, the pH was increased back to 8.4 due to the prolonged reaction and temperature causing a decrease in the pH. Modified heparin (heparin methacrylate) was precipitated in ethanol and dialyzed against distilled water for 48 hours, and lyophilized.

For all materials, 1H NMR was used to verify the methacrylation (Bruker Avance III 300MHz). Lithium phenyl-2,4,6-trimethylbenzoyl phosphinate (LAP) was synthesized as in Majima et al. (82) and was used as a cross liking agent that reacts to ultraviolet (UV) light.

4.1.2.3 Hydrogel Preparation

Two different hydrogels were used in the *in vitro* experiment: a composite hydrogel with a volume ratio of 3:4:3 of PEG, gelatin, and heparin, respectively (PGH hydrogel) and a pure gelatin hydrogel. The materials were hydrolyzed at 10% w/v in PBS. Trypsinized BMSCs were seeded into the PGH mixture at a density of 30 million cells/ mL of scaffold. In order to cross-link the hydrogel, 2 μL of lithium phenyl-2,4,6-trimethylbenzoyl phosphinate (LAP) was added per 100 μL of hydrolyzed mixture of the precursor. The scaffolds were then pipetted into a large

rectangular silicone mold, and exposed to 2.5 J/cm^2/mm UV-A light (365 nm) for about 3 minutes. Cylindrical hydrogel scaffolds were cut using 4mm biopsy punches.

4.1.2.4 Scaffold Culture

Hydrogel scaffolds were culture in osteogenic or chondrogenic media. Osteogenic media used for cell culture contained: alpha MEM, 10% fetal bovine serum, 10 nM dexamethasone, 50 μM ascorbic acid, and 10 mM β glycerol phosphate (Fisher SKU 50020). Chondrogenic media was made using Dulbecco's modified eagle's medium 5% Insulin Transferrin Selenium (ITS), 5% non-essential amino acids, 100 nM dexamethasone, 100 μM ascorbic acid, 40 μg/mL L-proline, and 10 ng/mL TGF-β3. This made for a total of 4 different experimental groups that were observed: 1) BMSCs seeded in gelatin, cultured in chondrogenic media (n=3), 2) BMSCs seeded in gelatin, cultured in osteogenic media (n=3), 3) BMSCs seeded in PGH, cultured in chondrogenic media (n=3), and 4) BMSCs seeded in PGH, cultured in osteogenic media (n=3). Hydrogel scaffolds were cultured in 6 well plates for 4 weeks, and replenished with media (3 mL) every other day.

4.1.2.5 Histology

Following 4 weeks, the hydrogel scaffolds were immediately removed from culture and fixed in 10% formalin. Sucrose water was then used to remove water from the sample overnight. Hydrogels were immersed in 40% OCT overnight prior to submerging them in OCT, and freezing them with liquid nitrogen for frozen sectioning. The resulting slides underwent hematoxylin & eosin, safranin-O, Von Kossa stains.

4.1.3 Results

From culture of BMSCs *in vitro*, chondrogenesis was seen in both the PGH and the GEL scaffolds (Figure 26, A and B). With the safranin-O stain, there was stronger staining for GAG in the pericellular region and overall for the gelatin scaffolds cultured in chondrogenic media. There was no evidence of GAG staining for scaffolds cultured in osteogenic media (Figure 26, C and D). Signs of osteogenesis with von kossa were seen for gelatin scaffolds in osteogenic media (Figure 27, D); however, there was no mineralization seen for the PGH scaffolds in osteogenic media (Figure 27, C). No mineralization was observed in either hydrogels cultured in chondrogenic medium (Figure 29, A, and B).

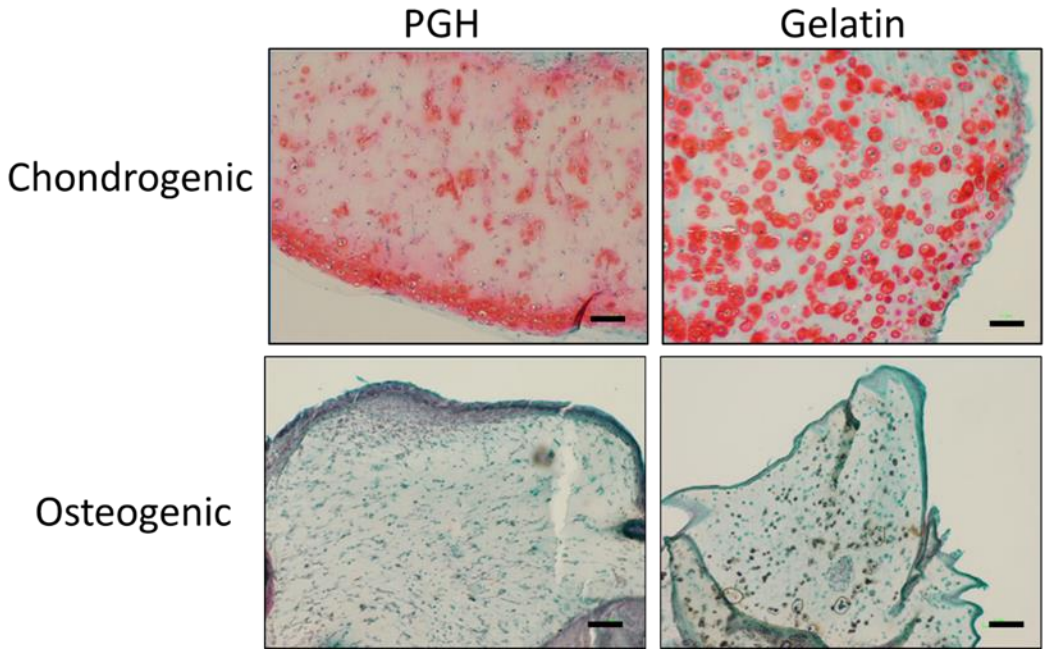

Figure 29. Safranin-O stain of the four different hydrogel groups seeded with BMSCs: A) PGH in chondrogenic media, B) GEL in chondrogenic media, C) PGH in osteogenic media, and D) GEL in osteogenic media.

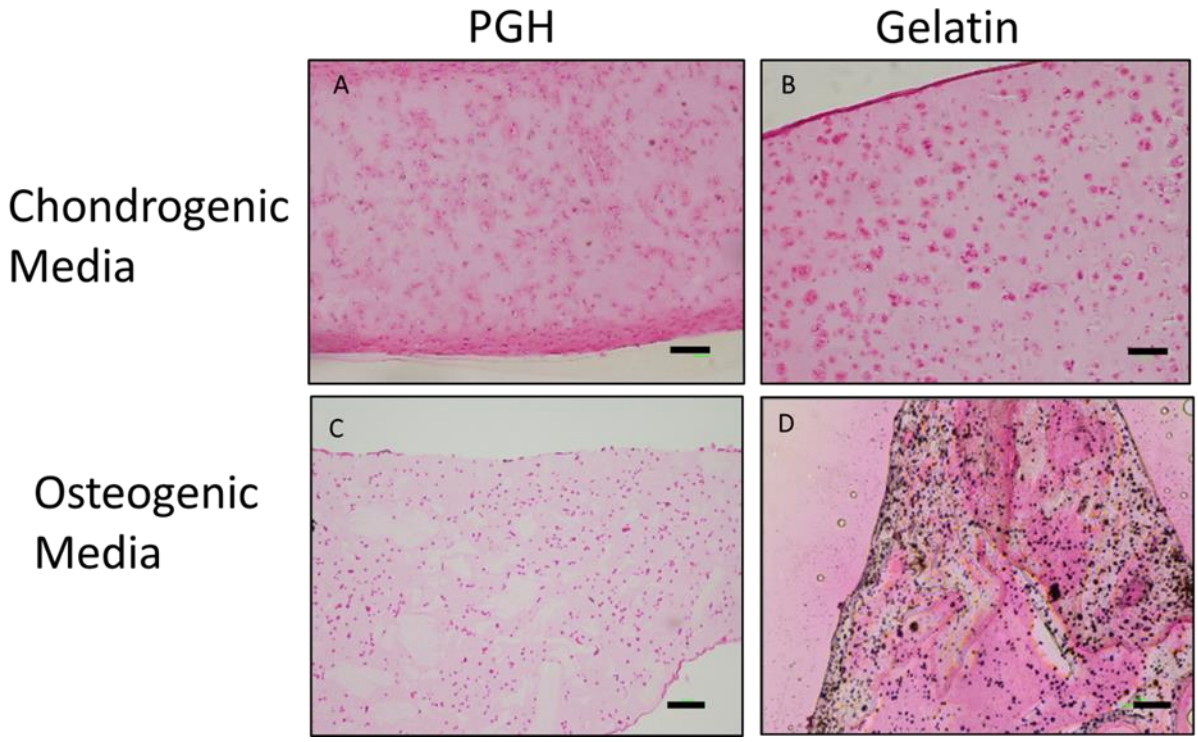

Figure 30. Van Kossa stain of the four different hydrogel groups seeded with BMSCs: A) PGH in chondrogenic media, B) GEL in chondrogenic media, C) PGH in osteogenic media, and D) GEL in osteogenic media.

4.1.4 Discussion

From these findings PGH combination hydrogels show their efficacy as a biomaterial that can induce material-controlled differentiation of stem cells. Indeed, the PGH hydrogel prevented mineralization of BMSCs, which was the main goal of this new hydrogel. One caveat is that the level of cartilage differentiation did not seem to be as robust as the pure gelatin hydrogel. It would be interesting to observe the phenotype of the MSCs in the long term. With the anti-hypetrophic effects of the PGH, it would be beneficial to see the time dependence of how long the material can keep the cells at a pre-hypertrophic state while taking into consideration for how long it will take for the material to fully degrade.

4.2 Primary Cells and Gelatin Based Scaffolds

4.2.1 Introduction

The results from the first part of the aim gave an understanding of how BMSCs could be pushed towards different cell lineages based on the material they were seeded in. In this case, it would be ideal to create a therapy in which an autologous cell source, such as bone marrow stem cells, could be implanted into the degenerated or damaged area create different layers of regenerated tissue through material-controlled stem cell differentiation. Nevertheless, it is imperative to also understand the impact of these biomaterials on primary cells. Primary cells could migrate and populate these scaffolds as well, and BMSCs after differentiation become

primary cells. This part of the aim focuses on the material effects on primary cells when seeded inside of the hydrogel.

4.2.2 Methods

4.2.2.1 Material Preparation

The same protocol for biomaterial preparation in the first half of this aim was used for this portion of the study.

4.2.2.2 Cell Isolation

Goat heads were acquired from a local abattoir; all animals were slaughtered less than 24 hours before cell isolation. Mandibular condyles with the temporomandibular joint disc attached were extracted from the head using sterile tools. The condyles were then moved to a sterile hood to scrape off the mandibular condylar cartilage from the surface of the condyle using a sterile scalpel. Retrieved cartilage was put into high glucose DMEM supplemented with mg/mL collagenase (Catalog #11965092). Cells were incubated for 3 days at 37 °C, trypsinized, and frozen at 2 million cells/ 1mL of freezing media.

Osteoblasts were isolated after cartilage removal. First, a syringe filled with sterile PBS was used to flush out the trabecular bone of the mandibular condyle. The bone was minced using a sterile pin and ligature cutter. Retrieved bone was immersed into a petri dish with alpha MEM GLUTAMAX supplemented with 2 mg/mL collagenase. After 7 days of culture, the migrated and attached osteoblasts were trypsinized and frozen at 2 million cells/ 1 mL of freezing media.

Costal chondrocytes from the goat were isolated from the ribs of young (<1 year) female goats obtained from the local abattoir within 4 hours of slaughter. Obtained fibrocartilage from the ribs were minced and digested in 2 mg/mL type II collagenase (Thermo Fisher catalog # 17101015) overnight in an incubator at 37 °C and 5% CO_2 with mechanical agitation on an orbital shaker. The isolated fibrochondrocytes were then passaged three times in Dulbecco's modified Eagle medium (DMEM)/ high glucose, 10% fetal bovine serum, 1% non-essential amino acids, and 1% penicillin-streptomycin.

4.2.2.3 Cell Culture and Scaffold Preparation

All primary cells were passaged until P3 and frozen prior to seeding. Hydrogel scaffolds were manufactured in the same manner as part A of this aim. Osteoblasts (OB) were seeded in gelatin and PGH hydrogels and cultured in osteogenic media (described in part A) for 0-4 weeks. Both costal chondrocytes (CC) and mandibular condylar chondrocytes (MCC) were seeded into PGH hydrogels and gelatin hydrogels, which were cultured in chondrogenic media (described in part A) for 0-4 weeks. This resulted in 6 experimental groups: 1) osteoblasts seeded in gelatin, 2) osteoblasts seeded in PGH, 3) costal chondrocytes seeded in gelatin, 4) costal chondrocytes seeded in PGH, 5) mandibular condylar cartilage cells seeded in gelatin, and 6) mandibular condylar cartilage cells seeded in PGH. The cell seeding densities for all 3 groups were 30 million cells/ mL of scaffold. Scaffolds were placed in a 12 well plate with 2.5 mL media in each well. Plates were left on a mechanical rocker in the incubator, and 3 mL of media was changed every other day.

4.2.2.4 Histology

For each group, n = 3 scaffolds were prepared the same way as the first half of this aim. Two time points were observed: 2 weeks and 4 weeks of culture. The frozen sections were stained for hematoxylin & eosin, safranin-O, Von Kossa, and alizarin red.

4.2.2.5 Biochemistry

Samples for each group (n = 3 for week 0 and n = 6 for week 4) were used for biochemistry assays. The samples were first digested in 0.1M Papain at 65 °C overnight. Following digestion, the hydrogels were then mechanically agitated to break up the scaffolds. Samples were then stored at -20 °C prior to the biochemical assays. DNA quantification was done using a picogreen assay (Molecular Probes, Inc.). The total amount of glycosaminoglycans (GAG) was measured using a 1,9-dimethylmethlyene blue colorimetric assay where chondroitin-4-sulfate was the standard. In order to compare the difference in GAG for each time point, the DNA content for the scaffolds were used to normalize this amount.

4.2.2.6 Unconfined Compression

Samples (n = 6 for 24 hours and 4) were immediately removed from culture and stored at 4 °C in 24 well plates filled with PBS. For scaffolds taken at 24 hours, the scaffolds were allowed to swell in PBS overnight prior to testing. The diameter of the constructs were measured using calipers; thickness was measured using a micrometer. An MTS Insight 1 kN testing apparatus with a 10 N load cell was used to perform unconfined compression of the hydrogels.

Samples were placed in a cylindrical water bath that is 10 cm in height and 6.5 cm in diameter. Once loaded, a preload of 0.005 N was applied to the hydrogels and the height was recorded. The water bath was then filled with 0.1 M PBS and the samples were subjected to 10 cycles of preconditioning at 9% strain/mm to 10% strain. After preconditioning, the samples had 10% strain applied to them at a rate of 9% strain/mm, and were allowed to relax for 30 minutes.

The compression data was then processed in MATLAB in a similar manner as in Specific Aim 1. Once the loading and viscoelastic parameters were estimated, a one-way ANOVA with a post-hoc Tukey's comparison was done to detect differences between the 6 groups.

4.2.3 Results

4.2.3.1 Histology

After 4 weeks of culture the Von Kossa stain was positive for mineralization throughout the gelatin hydrogel (Figure 31). When the osteoblasts were seeded in PGH, there was no mineralization seen after 4 weeks of culture from the Von Kossa stain (Figure 32).

Gelatin hydrogels with costal chondrocytes did show GAG deposition from the safranin-O stain at 4 weeks. Specifically, there was a positive stain for GAG around the periphery of the cells and throughout the construct (Figure 33). Cell morphology showed the chondrocytes beginning to demonstrate hypertrophy. In the PGH group, at 4 weeks, the GAG appeared to localize around the edges of the scaffold and the cells were only beginning to form lacunae (Figure 34).

For the mandibular condylar chondrocytes seeded in gelatin, after 4 weeks of culture, the amount of GAG appeared to increase (Figure 35). Similar to the costal chondrocytes, the cells

appeared to undergo hypertrophy at 4 weeks. GAG deposition appeared to stay towards the middle of the scaffolds, whereas fibrous tissue was present on surface of the scaffold. When cultured in the PGH material, the mandibular condyle fibrochondrocytes appeared to take on a fibrous phenotype from its morphology and lack of GAG from the safranin O stain at 4 weeks (Figure 36).

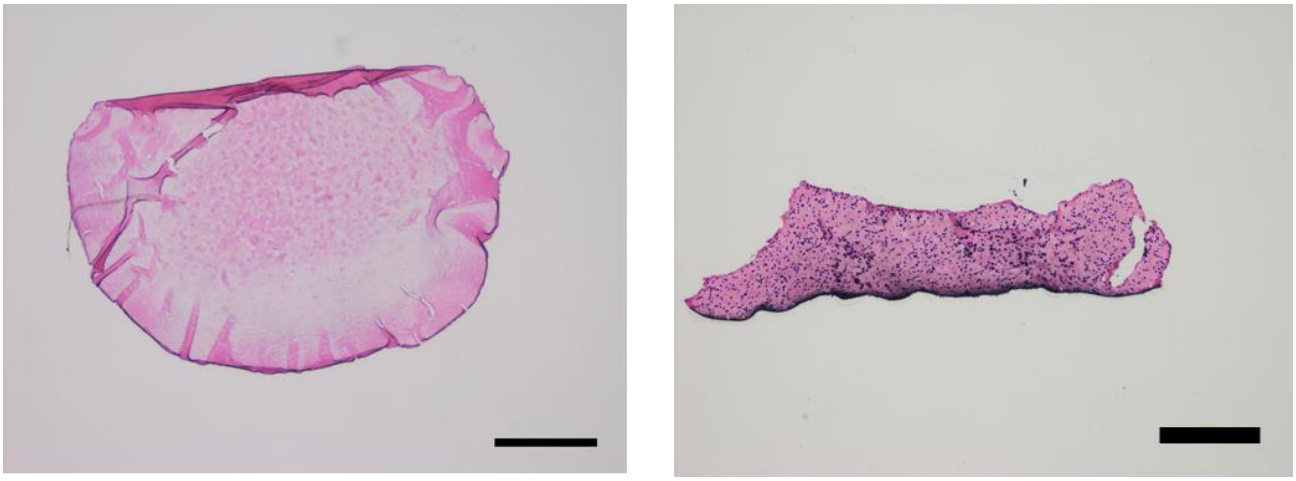

Figure 31. H&E stain for gelatin hydrogels seeded with osteoblasts at 4 weeks (left) and a Von Kossa stain of a gelatin hydrogel seeded with osteoblasts (different replicate) at 4 weeks (right). For the Von Kossa stain, pink is the background stain and black signifies calcium ions bound to phosphates. Scale bar = 500 µm.

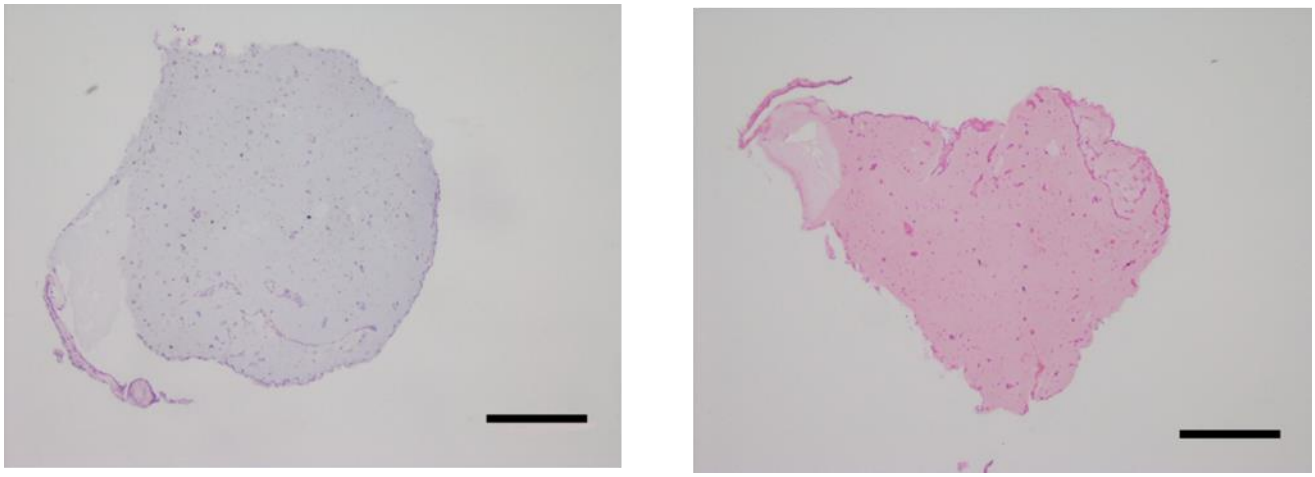

Figure 32. Hematoxylin & eosin (left) and a Von Kossa stains (right) of osteoblasts seeded into PGH hydrogel scaffolds after 4 weeks of culture. Scale bar = 500 µm.

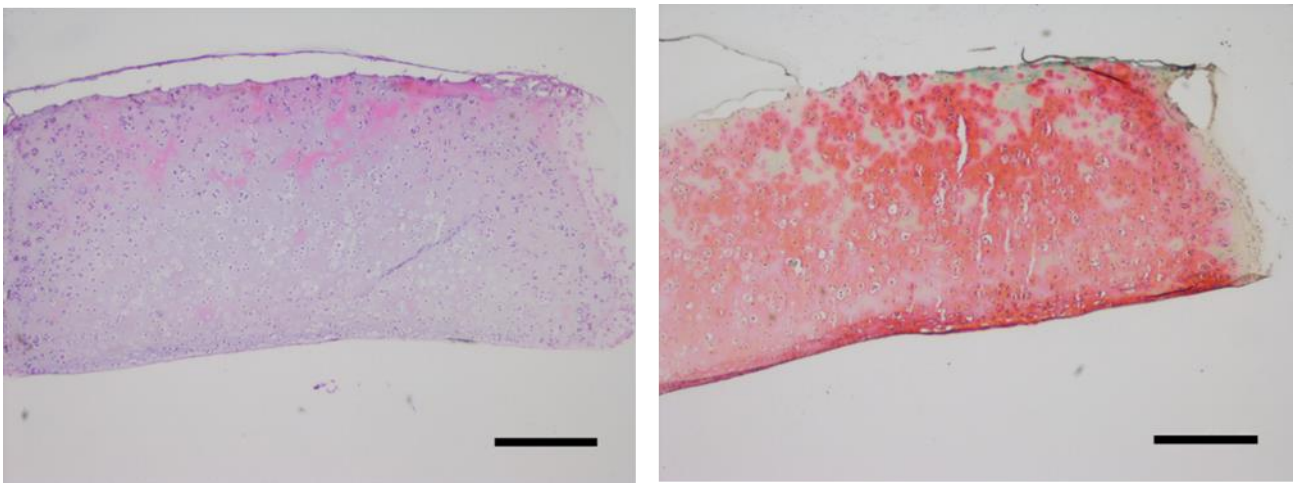

Figure 33. Hematoxylin & eosin (left) and safranin-o (right) stain of costal chondrocytes seeded into gelatin hydrogels after 4 weeks of culture. Scale bar = 500 µm.

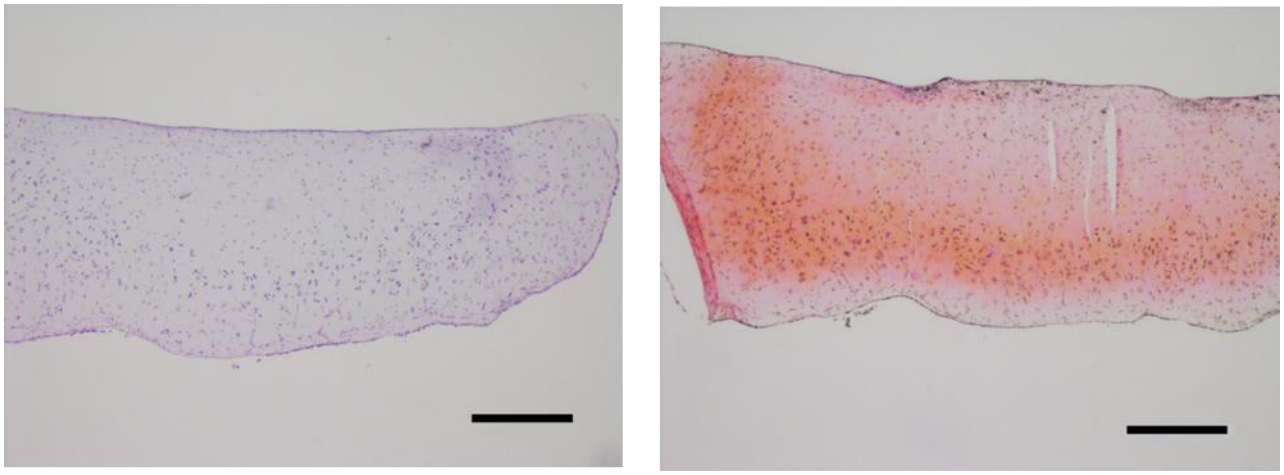

Figure 34. Hematoxylin & eosin (left) and safranin-o (right) stain of costal chondrocytes seeded into PGH hydrogels after 4 weeks of culture. Scale bar = 500 µm.

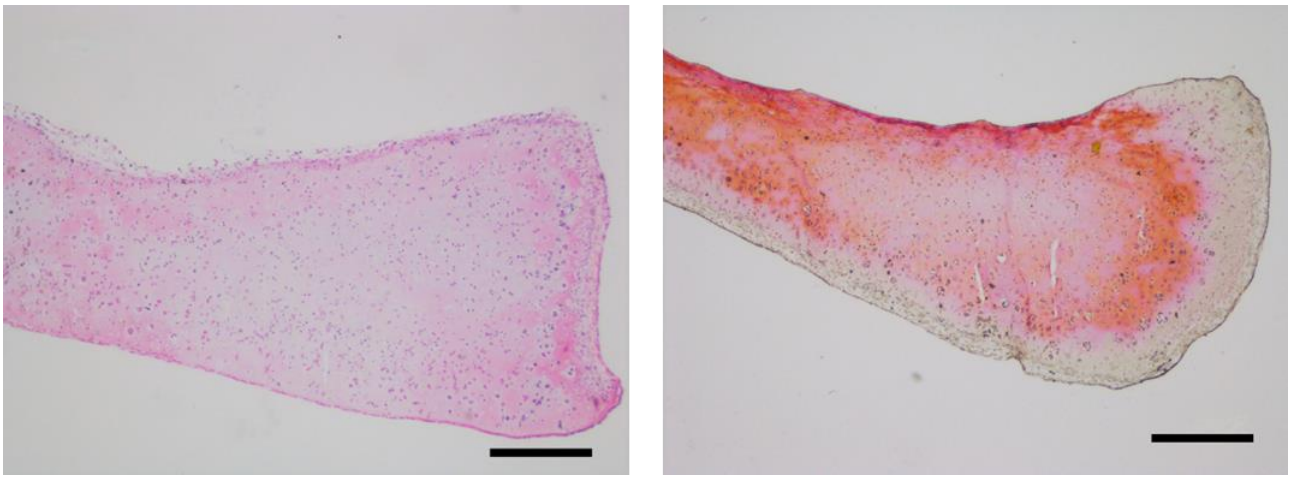

Figure 35. Hematoxylin & eosin (left) and safranin-o (right) stain of mandibular condyle chondrocytes seeded into GEL hydrogels after 4 weeks of culture. Scale bar = 500 µm.

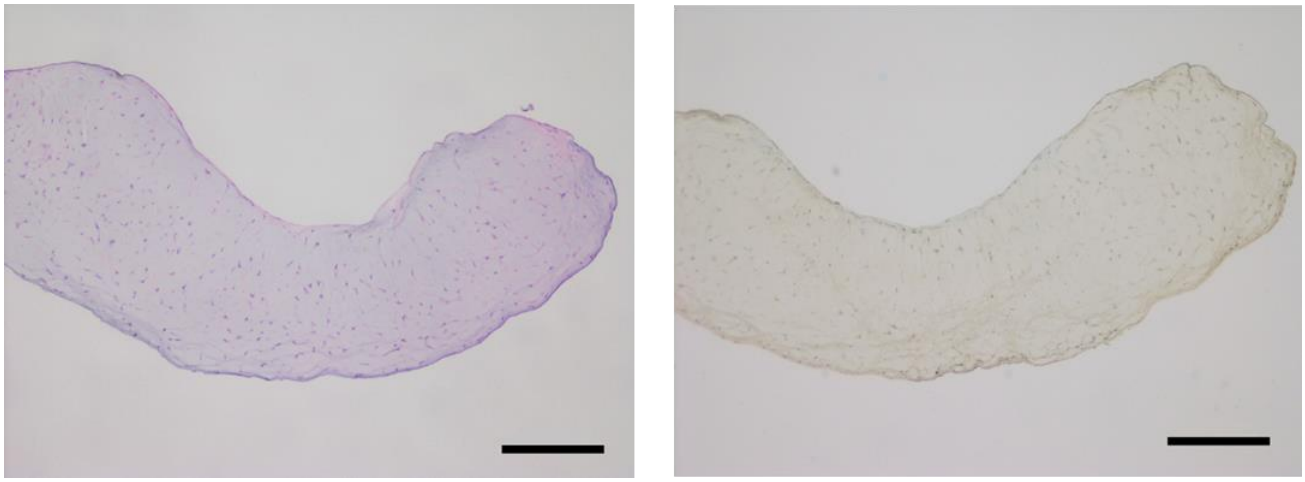

Figure 36. Hematoxylin & eosin (left) and safranin-o (right) stain of mandibular condyle chondrocytes seeded into PGH hydrogels after 4 weeks of culture. Scale bar = 500 µm.

4.2.3.2 Biochemical Assay

The scaffolds after 0 and 4 weeks of culture underwent a picogreen assay to quantify the DNA content of each structure. Figure 37 shows the comparison of the DNA content between these two time points for the 6 different experimental groups. An ANOVA revealed that material and the types of cells made a significant difference ($p < 0.05$) where. A post-hoc analysis showed that there was a significant difference ($p < 0.05$) in DNA content between weeks 0 and 4 in all of the groups except for the MCC PGH group. The GEL groups overall had more proliferation, and the scaffolds with costal chondrocytes also resulted in a higher proliferation when conducting a post hoc test to determine specific differences in cell population and gel material (both $p < 0.05$).

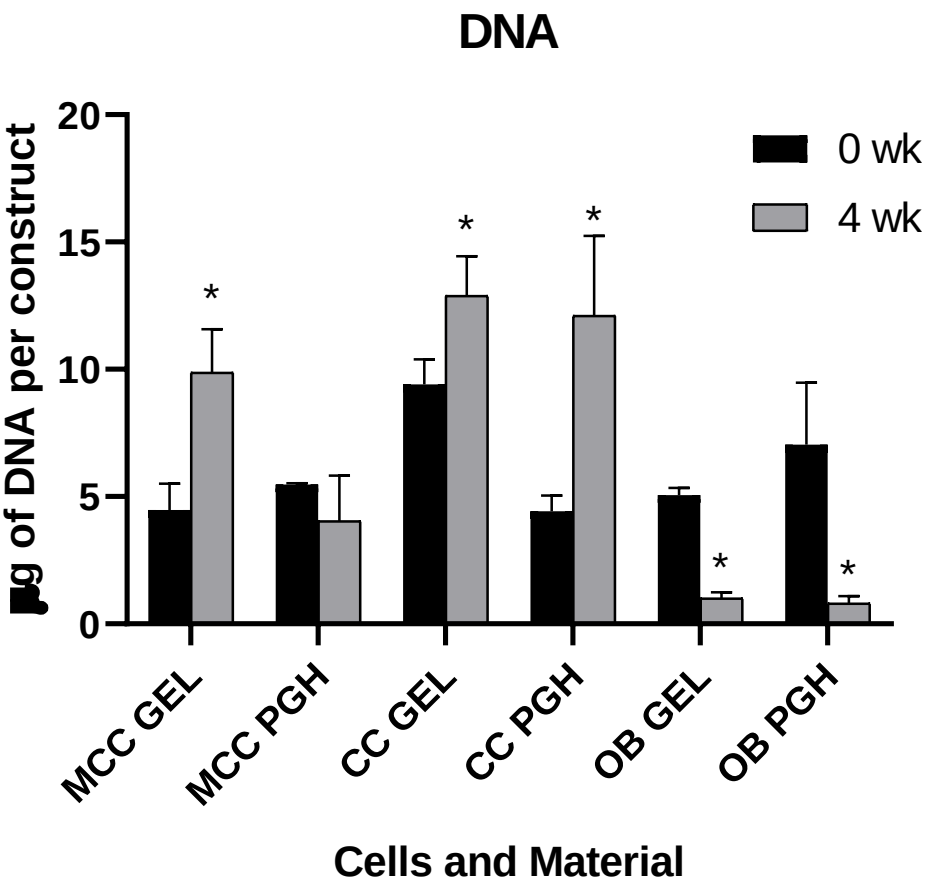

Figure 37. DNA quantification (µg) of the experimental groups at both 0 and 4 weeks (n = 6 for each time point). Black bars represent the DNA content (µg) after 0 weeks, and the gray bars represent the DNA content after 4 weeks. A * represents a significant difference ($p < 0.05$) between 0 and 4 weeks within the group.

Figure 38 represents the GAG quantity for the scaffolds at both time points. The costal chondrocyte group, when seeded in PGH and GEL, had the highest overall GAG production after 4 weeks when compared to the MCCs and both were significantly higher than the rest of the groups from a posthoc Tukey's comparison ($p < 0.05$). With that said, there were no statistical differences were observed between the GEL and PGH hydrogels when seeded with costal chondrocyte. There were initial amounts of GAG in the PGH scaffolds due to heparin (a disaccharide) being a

component of the hydrogel. There was lack of GAG presence in the PGH scaffold seeded with MCC cells due to their phenotype becoming fibrous and degradation of the heparin in the hydrogel.

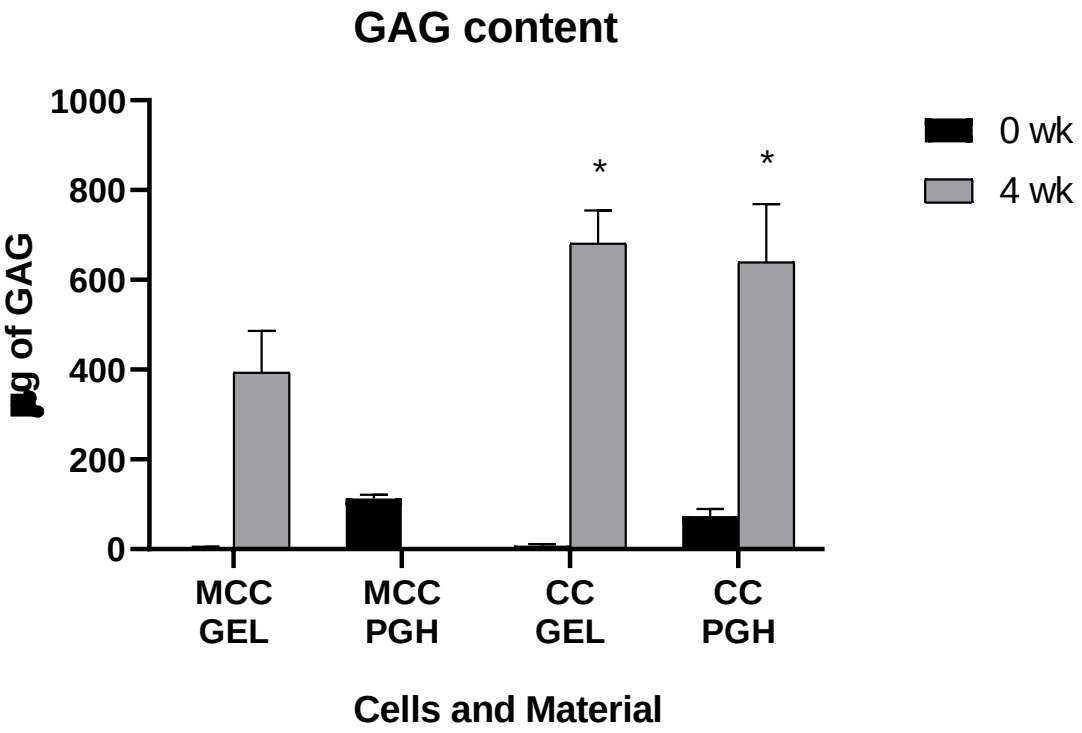

Figure 38. GAG quantification (µg) of the hydrogel scaffolds at 0 and 4 weeks (n = 6 for each time point). Black bars represent the DNA content (µg) after 0 weeks, and the gray bars represent the DNA content after 4 weeks. A * represents a significant difference to all other groups besides the groups with an *.

After determining both the overall amount of DNA and GAG (both in μg), the GAG to DNA ratio was calculated (Figure 39). There was a significant effect of the cells seeded ($p < 0.05$) and the material of the scaffold ($p < 0.05$). A post hoc analysis confirmed that scaffolds seeded with costal chondrocytes were significantly higher than the other groups. The ratio for the CC cells were higher than the MCC cells seeded in the GEL hydrogel ($p < 0.05$). In the PGH hydrogel, the MCC group did not have a detectable amount of GAG by the 4 week time point.

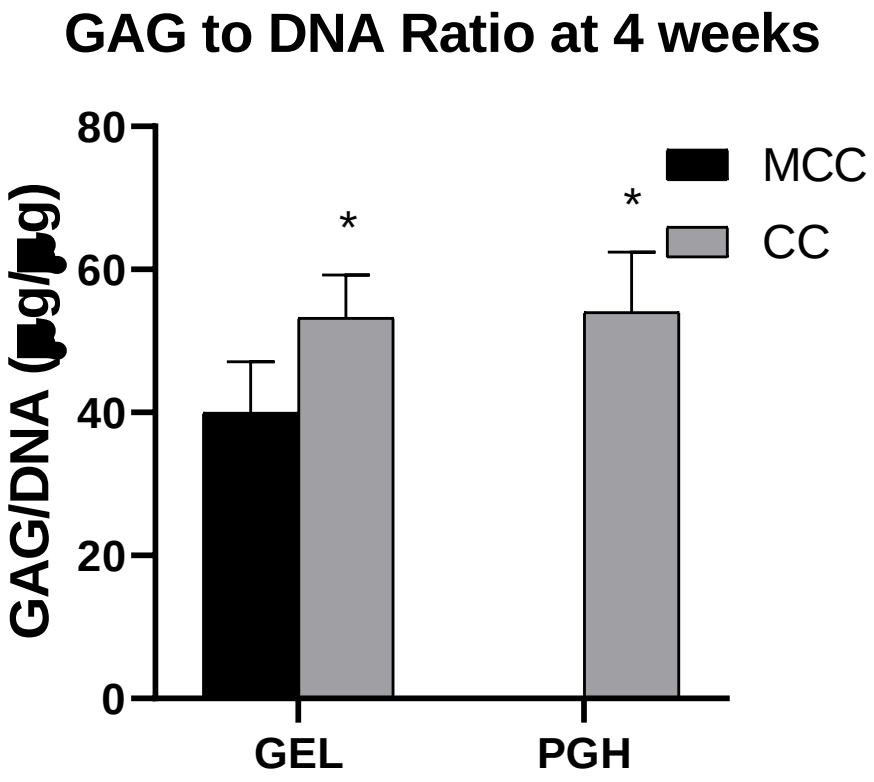

Figure 39. GAG to DNA ratio analysis for chondrocytes (mandibular condylar cartilage and costal chondral) seeded in both PGH and GEL materials (n = 6). A * represents a significant difference to all other groups besides the groups with an *.

4.2.3.3 Biomechanics

The results of the peak stress of the stress relaxation tests showed that the CC cells in GEL had the highest peak stress from a post hoc analysis ($p < 0.05$) (Figure 40). In addition, the material ($p < 0.05$) and cell type ($p < 0.05$) had an effect on the peak stress. The modulus for the experimental groups is shown in Figure 41. The same trend was seen, in both materials, with the costal chondrocytes being the highest ($p < 0.05$), and the osteoblasts having the lowest value ($p < 0.05$). Percent relaxation of the scaffolds seemed to also be determined by the cell type as scaffolds seeded with MCC cells had the highest relaxation ($p < 0.05$), and the scaffolds with osteoblasts had the lowest ($p < 0.05$) (Figure 42).

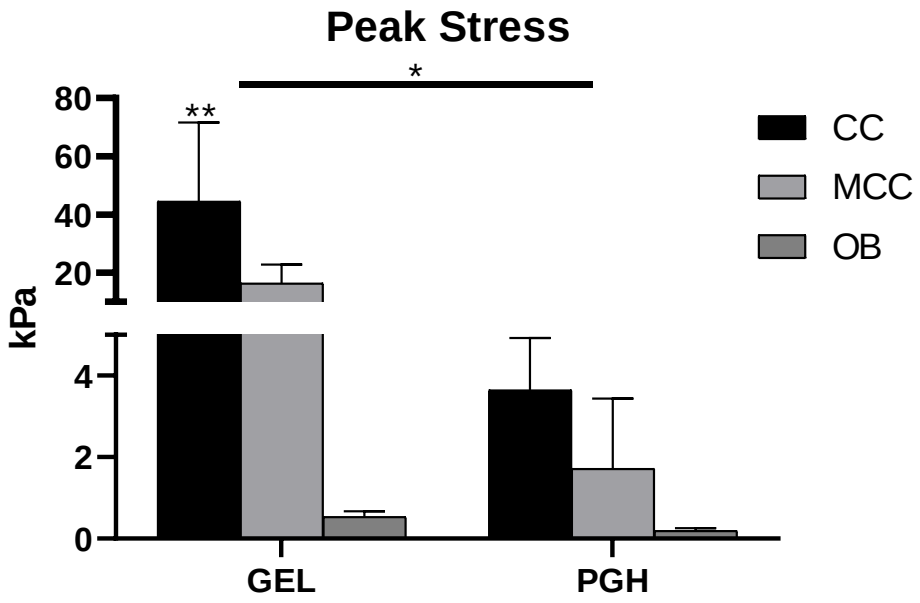

Figure 40. Peak stress of the different hydrogel groups at 4 weeks. The bars represent standard deviation. * indicates a significant difference ($p < 0.05$) between the two materials, GEL and PGH. ** represents a significant difference to all other

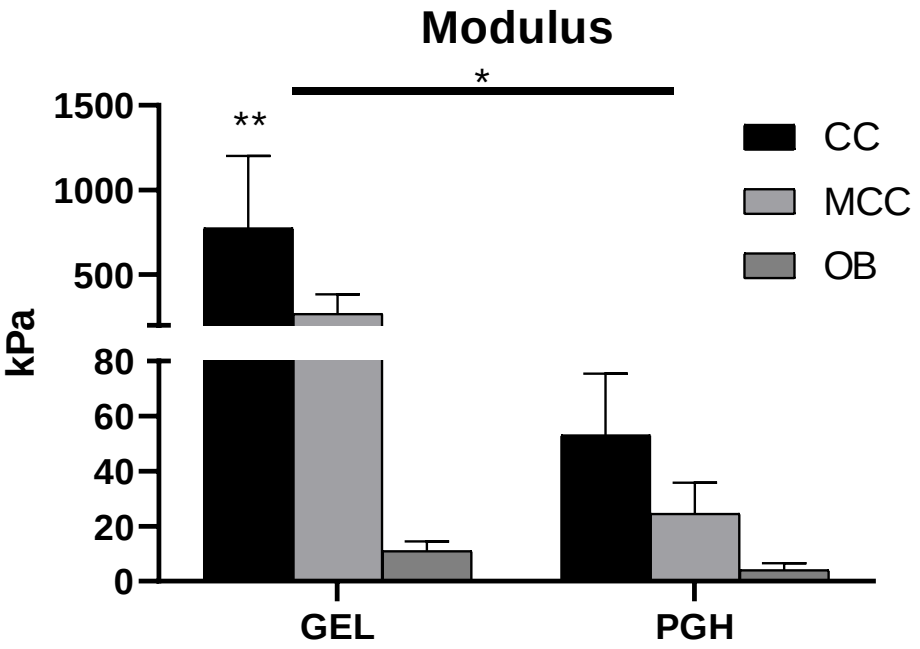

Figure 41. Modulus of the different hydrogel groups at 4 weeks. The bars represent standard deviation. * indicates a significant difference ($p < 0.05$) between the two materials, GEL and PGH. ** represents a significant difference to all other groups ($p < 0.05$).

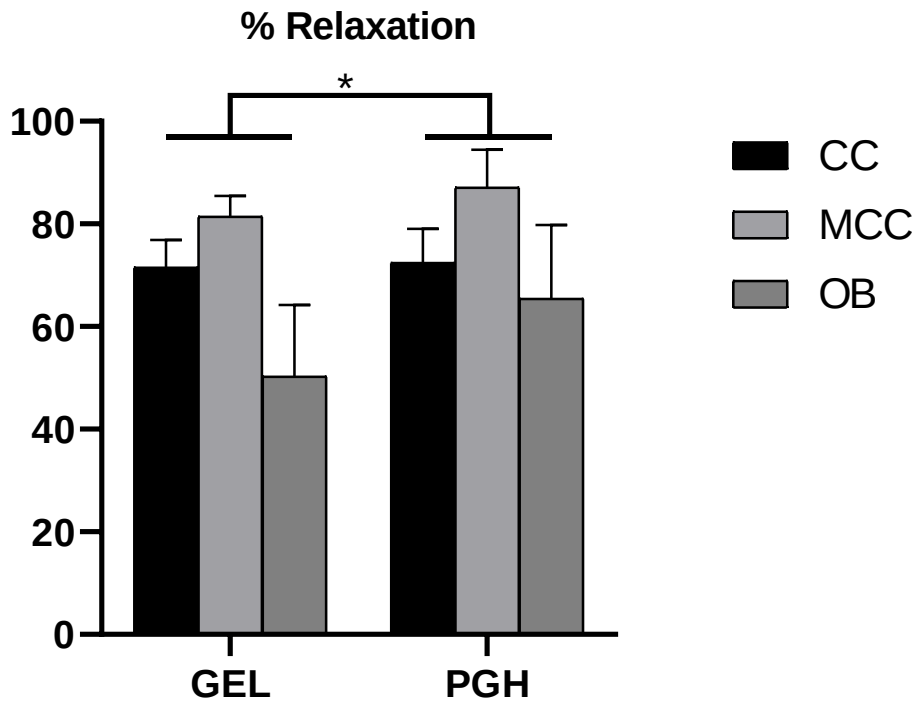

Figure 42. Percent relaxation of the hydrogel groups at 4 weeks. Bars on the graph represent standard deviation. * indicates a significant difference between both materials ($p < 0.05$).

As for the estimated viscoelastic parameters, the in-plane Young's modulus (E_1) was highest in the group where costal chondrocytes seeded in gelatin scaffolds; it was significantly greater than all other groups except for MCC GEL ($p < 0.05$) (Figure 43). The Young's out-of-plane modulus (E_3) was also the highest in the CC GEL group, where it was significantly greater than the rest ($p < 0.05$) (Figure 44). The in-plane Poisson's ratio (ν_{21}) was the highest in hydrogels seeded with mandibular condylar cartilage cells as it significantly higher than all other groups except the CC GEL and MCC PGH groups ($p < 0.05$) (Figure 45). The out-of-plane Poisson's ratio (ν_{31}) was the highest in the CC PGH group ($p < 0.05$) (Figure 46). PGH hydrogels seeded with osteoblasts were estimated to have the highest permeability (k) compared to the other groups ($p < 0.05$) (Figure 47).

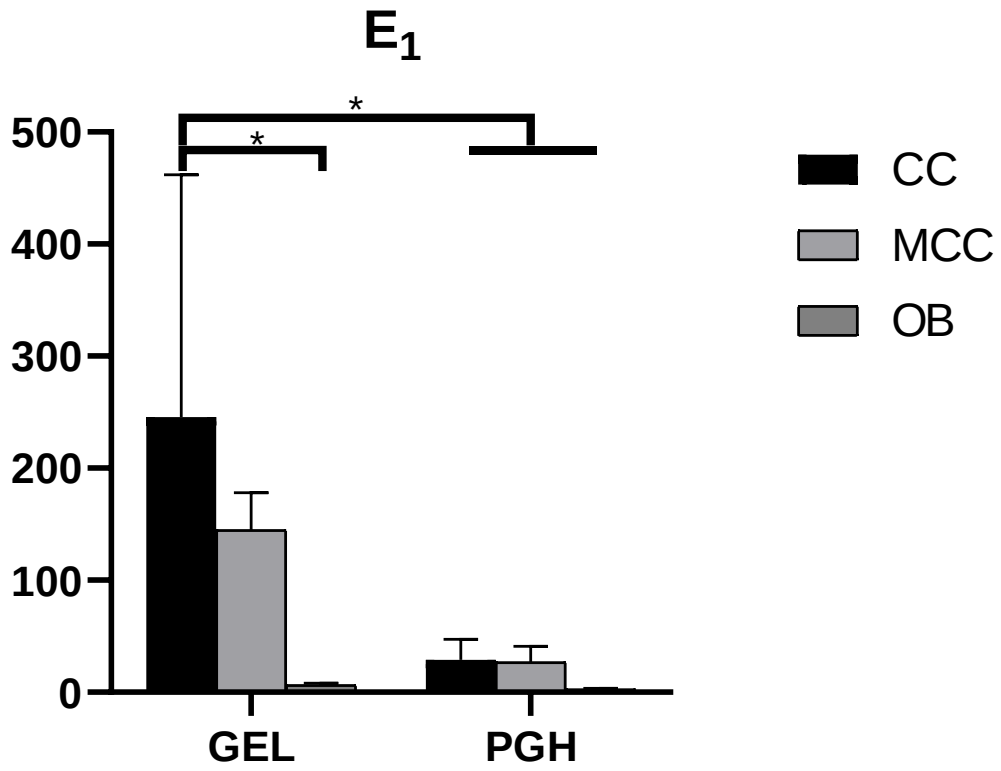

Figure 43. Young's in-plane modulus of the different hydrogel groups at 4 weeks. * indicates a significant difference ($p < 0.05$).

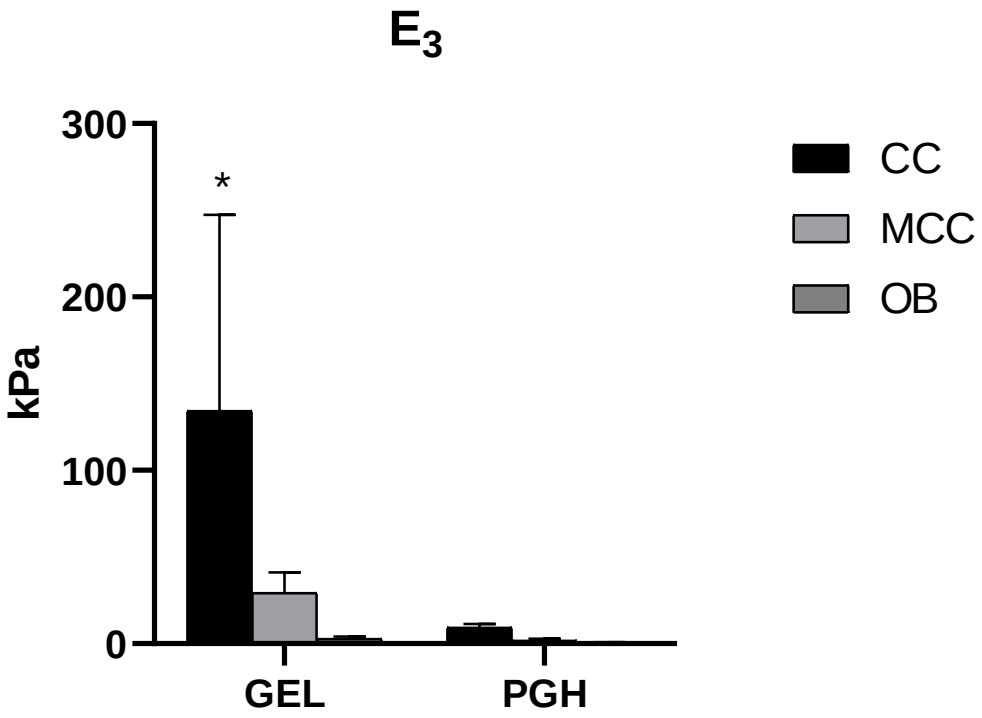

Figure 44. Young's out-of-plane modulus for the different hydrogel groups at 4 weeks. Bars represent standard deviation. * indicates a significant difference ($p < 0.05$) from all other groups.

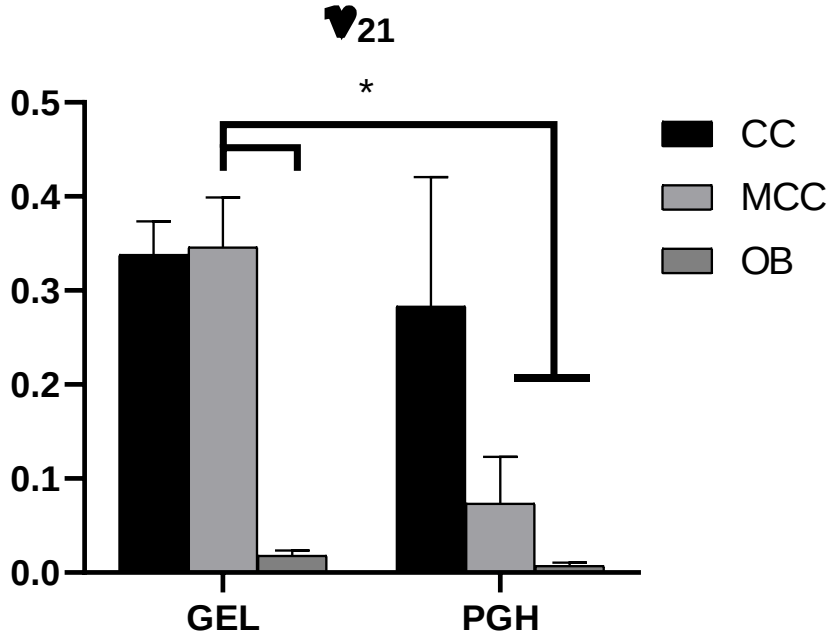

Figure 45. In-plane Poisson's ratio of the different hydrogel groups at 4 weeks. Bars represent standard deviation. * indicates a significant difference ($p < 0.05$).

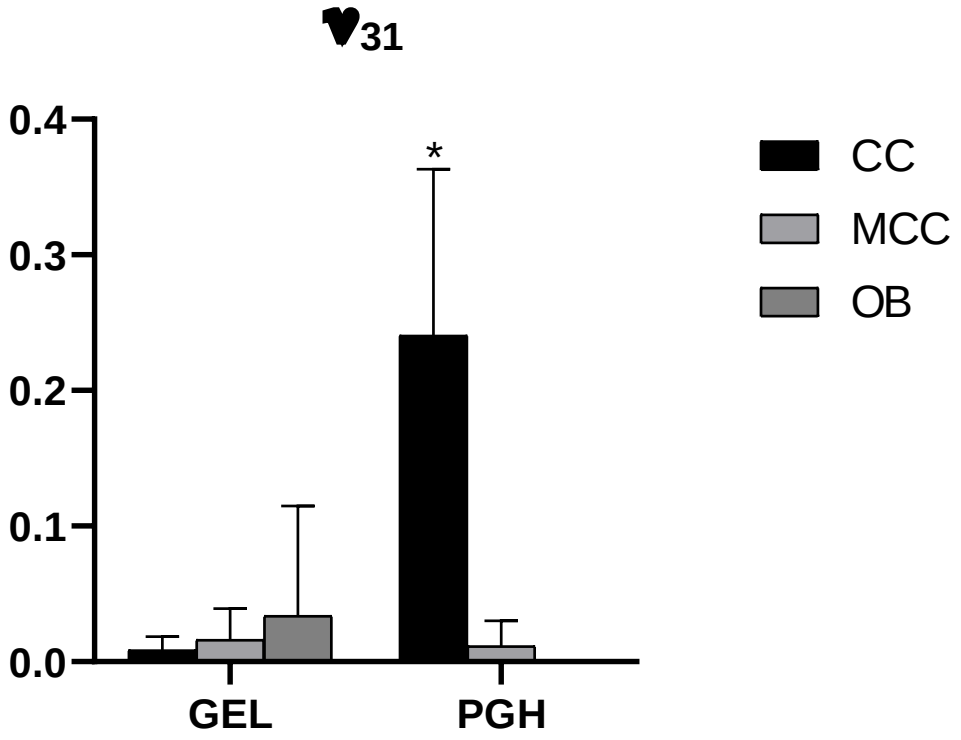

Figure 46. Out-of-plane Poisson's ratio of the different hydrogel groups at 4 weeks. Bars represent standard deviation. * indicates a significant difference from all other groups ($p < 0.05$).

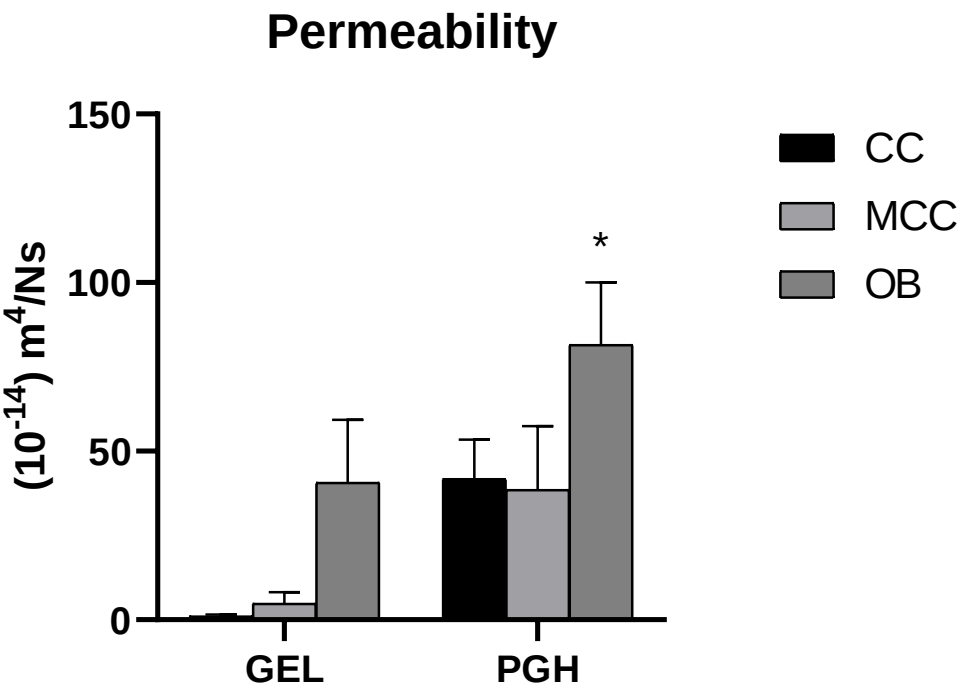

Figure 47. Permeability of the different hydrogel groups at 4 weeks. Bars represent standard deviation. * indicates a significant difference from all other groups ($p < 0.05$).

4.2.4 Discussion

The results from this part of the specific aim supports what was concluded in the part A, but also begins to elucidate what would occur if the native cells of the mandibular condyle were to be seeded into the proposed biomaterials. As with any other tissue engineering alternative, the importance of recapitulating the native cells must be taken into account, especially for a moving joint such as the temporomandibular joint.

Histology supported the theme of PGH inhibiting mineralization, as seen in part A of this aim. In addition, osteoblasts continued to demonstrate the deposition of minerals after 4 weeks inside gelatin hydrogels. This gives reason to believe an *in vivo* therapy for the bone of the

condyle, could use gelatin hydrogels along with other growth factors to induce osteogenesis, such as BMP-2, which has shown positive results when used in rabbit femoral ankles (Zhao et al., 2016).

In terms of cartilage regeneration, gelatin scaffolds seemed to have promoted cartilage regeneration to a greater degree than the PGH scaffolds when considering the GAG formation. The only caveat, however, is the incidence of chondrocytes hypertrophy and hyperplasia that was observed. Certain cartilage layers have different densities of cells, uncontrolled growth would warrant concern as an excess of cells would alter the homeostasis of the regenerated area, but also change the mechanical properties. In addition, hypertrophy could also be studied for a longer period based on these results; however, no mineralization of the chondrocytes occurred after 4 weeks from this study. Likewise, the mechanical properties of MCC cells in gelatin hydrogels were comparative to that of the mandibular condylar cartilage. The peak stress of the majority of the native porcine MCC of specific aim 1 and that of the MCC GEL group were both around 20 kPa. The moduli between the two were also similar, both measuring close to 250 kPa.

By comparison, the PGH hydrogels had lower compressive properties, regardless of the cells that were seeded inside of them. The benefit of this hydrogel composite, however, is the observed control of cell phenotype that was seen in this experiment. As opposed to the gelatin groups, the costal chondrocytes seeded in PGH did not appear to swell. A longer time point would be required to determine if the cells would undergo a similar change to those in gelatin, as there was cell hyperplasia in the CC PGH scaffold group according to DNA quantification. Likewise, there was no significant difference in the GAG to DNA ratio for CC or MCC cells in GEL or PGH scaffolds. However, the lack of GAG production from MCC cells in PGH could potentially limit the types of cells seeded in inside the material for cartilage regeneration, or utilize the material for fibrous tissue formation.

5.0 Discussion – Conclusions

The dissertation has focused on both the compressive properties of the mandibular condylar cartilage, as well as investigating analogues that could be used to regenerate as part of a proposed therapy. First, an understanding of how the disc and mandibular cartilage behave under compression was obtained with the transversely isotropic biphasic theory. Next, PGS and gelatin sponge scaffolds were tested *in vivo* to assess their ability to regenerate the cartilage and bone of the mandibular condyle. Finally, *in vitro* studies of gelatin-based hydrogels and their ability to support BMSC and primary cell osteogenesis and chondrogenesis were studied.

The compressive properties of the different regions of the temporomandibular joint and the MCC were evaluated in Chapter 2 of this thesis. Regional differences were found in the temporomandibular joint, but not in the MCC in terms of the peak stress and modulus. These measured properties were also in range of past studies of these tissues. However, with the transversely isotropic biphasic theory and a stress relaxation test, the viscoelastic parameters were also estimated. The calculation of these values revealed the disc also has differences in viscoelastic properties for each region, including the Young's modulus in different directions, Poisson's ratio, and permeability. To this end, the combination of these parameters helps explain the role of the TMJ disc. The decreased permeability and mechanical properties of the posterior region of the disc coincides with the anatomy of it, where this region is attached to retrodiscal tissue. With the rotation, and translation of the mandibular condyle during daily activities, the disc moves in and out of the pocket of the glenoid fossa. The retrodiscal tissue is responsible for retraction of the disc back into its socket when closing the jaw. Although not significantly different, the max stress and modulus of the central region of the MCC were the highest. There was also a significant

difference between the lateral and posterior region for the in-plane Young's modulus. The other compressive properties of the different regions were not found to be significantly different, but gives a baseline for the measurements for comparisons for future studies of the viscoelastic properties of the MCC. Compressive parameters such as the modulus and peak stress of tissue engineering constructs are often reported, but the need for an understanding of viscoelastic parameters and mechanical differences in these regions gives rise to considerations if a tissue-engineering alternative were to be developed.

Chapter 3 tests the efficacy of two well-known biomaterials to regenerate the load-bearing and multi-faceted mandibular condylar cartilage: poly (glycerol sebacate) (PGS) and gelatin sponges. Magnesium ions and tri-magnesium phosphate were also incorporated into the scaffolds to see if osteoinduction would occur. The results of the *in vivo* study highlights the benefits of PGS in cartilage regeneration applications. After 3 months, there was cellular, collagen, and GAG presence within the osteochondral defects. Magnesium ions were also soaked into the material prior to implantation. However, there was no observed bone regeneration. The most likely explanation is the leeching of ions from the scaffolds once introduced into the surgical area: the blood flow and absorbance of the material could diffuse the ions to other areas besides the defect. Gelatin scaffolds also showed promise with cartilage presence in the defect after the 3 month time point. The material also had safranin O and collagen II positive stains. As with the PGS scaffold, however, there was no observed bone regeneration with trimagnesium phosphate (TMP). Remaining parts of the scaffold at 3 months could be explained by TMP slowing down the enzymatic degradation process of the construct. The lack of degradation could correlate to slowed release of magnesium ions in the area; possibly slow enough to not see any osteogenic benefits, such as this case. Overall, both materials could be viable for regenerative application of the

cartilage. In addition, the choice of the caprine animal model provides its own advantages, over the gold standard porcine model, for TMJ regenerative models. The accessibility of the TMJ in the Spanish Boer goat provides consistency and accuracy for possible operational procedures in the joint.

The final chapter evaluates gelatin-based hydrogels *in vitro* as a material to regenerate the mandibular condylar cartilage and subchondral bone. Gelatin was chosen based on the cartilage regeneration *in vivo* from the previous chapter, and its characteristic of being able to be used in a variety of formulations as a biomaterial. The application that was focused on, for this chapter, the use of gelatin methacrylate (GELMA) in hydrogels. In this form, this material has the benefit of being monolithically casted into different shapes in the presence of UV light when functionalized. A combination of this hydrogel (PGH) was also studied. First, BMSCs were seeded into the two different scaffolds to observe the potential for each material to host stem cell differentiation towards bone or cartilage, when cultured in osteogenic and chondrogenic media, respectively. PGH inhibited differentiation of the stem cells towards osteoblasts, but both GEL and PGH allowed for chondrocyte differentiation.

Next, primary bone and cartilage cells were seeded into the GEL and PGH scaffolds. GAG quantification and the GAG/ DNA ratio showed chondrogenesis for costal chondrocytes seeded in GEL hydrogels. The same was seen in PGH hydrogels seeded with costal chondrocytes, but not when seeded with mandibular condylar cartilage cells. This could be attributed to the material properties affecting the attachment or signaling of the cells, preventing the deposition of GAG within the construct. However, with the opposite seen in costal chondrocytes, this could be due to the cell lineage rather than the material. The mechanical properties of the MCC cells seeded in GEL scaffold were also similar to the measured properties of the native MCC compressive

properties from the second chapter. Overall, the PGH hydrogels with any cell type appeared to have lower compressive properties than the GEL counterparts. However, the material's ability to control cell phenotype cannot be ignored. Even though GEL supported chondrogenesis and achieved mechanical properties similar to the native condylar cartilage, the PGH hydrogels inhibited hypertrophy. Modification of the components of the PGH hydrogel could target a desirable balance between recapitulating the compressive properties of the cartilage, and maintaining different cell populations that match the MCC. From the results of the aforementioned studies, this could be achieved with a combination of the materials. Future studies would be to study cell migration into acellular PGH and GEL hydrogels *in vivo*, as these findings have demonstrated the efficacy of using these biomaterials based on their interactions with the native cells in the joint. Regardless, the use of hydrogels towards mandibular condylar cartilage regeneration shows promise and could even be used for other articular cartilage applications, besides the TMJ, in the future.

Bibliography

Allen, K. D., & Athanasiou, K. A. (2006). Viscoelastic characterization of the porcine temporomandibular joint disc under unconfined compression. *J Biomech, 39*(2), 312-322. doi: 10.1016/j.jbiomech.2004.11.012

Almarza, A. J., & Athanasiou, K. A. (2004). Design characteristics for the tissue engineering of cartilaginous tissues. *Ann Biomed Eng, 32*(1), 2-17.

Almarza, A. J., Bean, A. C., Baggett, L. S., & Athanasiou, K. A. (2006). Biochemical analysis of the porcine temporomandibular joint disc. *Br J Oral Maxillofac Surg, 44*(2), 124-128. doi: 10.1016/j.bjoms.2005.05.002

Almarza, A. J., Brown, B. N., Arzi, B., Angelo, D. F., Chung, W., Badylak, S. F., & Detamore, M. (2018). Preclinical Animal Models for Temporomandibular Joint Tissue Engineering. *Tissue Engineering Part B-Reviews, 24*(3), 171-178.

Almarza, A. J., Hagandora, C. K., & Henderson, S. E. (2011). Animal models of temporomandibular joint disorders: implications for tissue engineering approaches. *Ann Biomed Eng, 39*(10), 2479-2490. doi: 10.1007/s10439-011-0364-8

Berglund, I. S., Brar, H. S., Dolgova, N., Acharya, A. P., Keselowsky, B. G., Sarntinoranont, M., & Manuel, M. V. (2012). Synthesis and characterization of Mg-Ca-Sr alloys for biodegradable orthopedic implant applications. *J Biomed Mater Res B Appl Biomater, 100*(6), 1524-1534. doi: 10.1002/jbm.b.32721

Bondarenko, A., Angrisani, N., Meyer-Lindenberg, A., Seitz, J. M., Waizy, H., & Reifenrath, J. (2014). Magnesium-based bone implants: immunohistochemical analysis of peri-implant osteogenesis by evaluation of osteopontin and osteocalcin expression. *J Biomed Mater Res A, 102*(5), 1449-1457. doi: 10.1002/jbm.a.34828

Chaya, A., Yoshizawa, S., Verdelis, K., Myers, N., Costello, B. J., Chou, D. T., . . . Sfeir, C. (2015). In vivo study of magnesium plate and screw degradation and bone fracture healing. *Acta Biomater, 18*, 262-269. doi: 10.1016/j.actbio.2015.02.010

Chaya, A., Yoshizawa, S., Verdelis, K., Noorani, S., Costello, B. J., & Sfeir, C. (2015). Fracture healing using degradable magnesium fixation plates and screws. *J Oral Maxillofac Surg, 73*(2), 295-305. doi: 10.1016/j.joms.2014.09.007

Chen, D., He, Y., Tao, H., Zhang, Y., Jiang, Y., Zhang, X., & Zhang, S. (2011). Biocompatibility of magnesium-zinc alloy in biodegradable orthopedic implants. *Int J Mol Med, 28*(3), 343-348. doi: 10.3892/ijmm.2011.707

Chen, S., Guan, S., Li, W., Wang, H., Chen, J., Wang, Y., & Wang, H. (2012). In vivo degradation and bone response of a composite coating on Mg-Zn-Ca alloy prepared by microarc oxidation and electrochemical deposition. *J Biomed Mater Res B Appl Biomater, 100*(2), 533-543. doi: 10.1002/jbm.b.31982

Cheng, M. Q., Wahafu, T. E. H. J., Jiang, G. F., Liu, W., Qiao, Y. Q., Peng, X. C., . . . Liu, X. Y. (2016). A novel open-porous magnesium scaffold with controllable microstructures and properties for bone regeneration. *Sci Rep, 6*. doi: Artn 24134

Cheng, P., Han, P., Zhao, C., Zhang, S., Wu, H., Ni, J., . . . Chai, Y. (2016). High-purity magnesium interference screws promote fibrocartilaginous entheses regeneration in the anterior cruciate ligament reconstruction rabbit model via accumulation of BMP-2 and VEGF. *Biomaterials, 81*, 14-26. doi: 10.1016/j.biomaterials.2015.12.005

Cheung, J. O. P., Grant, M. E., Jones, C. J. P., Hoyland, J. A., Freemont, A. J., & Hillarby, M. C. (2003). Apoptosis of terminal hypertrophic chondrocytes in an in vitro model of endochondral ossification. *Journal of Pathology, 201*(3), 496-503.

Chin, A. R., Gao, J., Wang, Y. D., Taboas, J. M., & Almarza, A. J. (2018). Regenerative Potential of Various Soft Polymeric Scaffolds in the Temporomandibular Joint Condyle. *Journal of Oral and Maxillofacial Surgery, 76*(9), 2019-2026.

Chou, D. T., Hong, D., Saha, P., Ferrero, J., Lee, B., Tan, Z., . . . Kumta, P. N. (2013). In vitro and in vivo corrosion, cytocompatibility and mechanical properties of biodegradable Mg-Y-Ca-Zr alloys as implant materials. *Acta Biomater, 9*(10), 8518-8533. doi: 10.1016/j.actbio.2013.06.025

Commisso, M. S., Calvo-Gallego, J. L., Mayo, J., Tanaka, E., & Martinez-Reina, J. (2016). Quasi-Linear Viscoelastic Model of the Articular Disc of the Temporomandibular Joint. *Experimental Mechanics, 56*(7), 1169-1177.

Conrad, B., Han, L. H., & Yang, F. (2018). Gelatin-Based Microribbon Hydrogels Accelerate Cartilage Formation by Mesenchymal Stem Cells in Three Dimensions. *Tissue Engineering Part A, 24*(21-22), 1631-1640.

Cordero, J., Munuera, L., & Folgueira, M. D. (1994). Influence of metal implants on infection. An experimental study in rabbits. *J Bone Joint Surg Br, 76*(5), 717-720.

Detamore, M. S., Orfanos, J. G., Almarza, A. J., French, M. M., Wong, M. E., & Athanasiou, K. A. (2005). Quantitative analysis and comparative regional investigation of the extracellular matrix of the porcine temporomandibular joint disc. *Matrix Biol, 24*(1), 45-57. doi: 10.1016/j.matbio.2004.11.006

Dou, Y., Li, N., Zheng, Y., & Ge, Z. (2014). Effects of fluctuant magnesium concentration on phenotype of the primary chondrocytes. *J Biomed Mater Res A, 102*(12), 4455-4463. doi: 10.1002/jbm.a.35113

Erdmann, N., Bondarenko, A., Hewicker-Trautwein, M., Angrisani, N., Reifenrath, J., Lucas, A., & Meyer-Lindenberg, A. (2010). Evaluation of the soft tissue biocompatibility of MgCa0.8 and surgical steel 316L in vivo: a comparative study in rabbits. *Biomed Eng Online, 9*. doi: Artn 63

Ezechieli, M., Diekmann, J., Weizbauer, A., Becher, C., Willbold, E., Helmecke, P., . . . Windhagen, H. (2014). Biodegradation of a magnesium alloy implant in the intercondylar femoral notch showed an appropriate response to the synovial membrane in a rabbit model in vivo. *J Biomater Appl, 29*(2), 291-302. doi: 10.1177/0885328214523322

Feyerabend, F., Witte, F., Kammal, M., & Willumeit, R. (2006). Unphysiologically high magnesium concentrations support chondrocyte proliferation and redifferentiation. *Tissue Eng, 12*(12), 3545-3556. doi: 10.1089/ten.2006.12.3545

Frost, H. M. (1994). Wolff's Law and bone's structural adaptations to mechanical usage: an overview for clinicians. *Angle Orthod, 64*(3), 175-188. doi: 10.1043/0003-3219(1994)064<0175:WLABSA>2.0.CO;2

Galli, S., Naito, Y., Karlsson, J., He, W., Miyamoto, I., Xue, Y., Andersson, M., Mustafa, K., Wennerberg, A., Jimbo, R. (2014). Local release of magnesium from mesoporous TiO2 coatings stimulates the peri-implant expression of osteogenic markers and improves osteoconductivity in vivo. *Acta Biomater, 10*(12), 5193-5201.

Gao, J., Ensley, A. E., Nerem, R. M., & Wang, Y. (2007). Poly(glycerol sebacate) supports the proliferation and phenotypic protein expression of primary baboon vascular cells. *J Biomed Mater Res A, 83*(4), 1070-1075. doi: 10.1002/jbm.a.31434

Gu, X. N., Xie, X.H., Li, N., Zheng, Y.F., Qin, L. (July 2012). In vitro and in vivo studies on a Mg-Sr binary alloy system developed as a new kind of biodegradable metal. *Acta Biomater, 8*(6), 2360-2374.

Gu, X. N., Zheng, Y. F., Cheng, Y., Zhong, S. P., & Xi, T. F. (2009). In vitro corrosion and biocompatibility of binary magnesium alloys. *Biomaterials, 30*(4), 484-498. doi: 10.1016/j.biomaterials.2008.10.021

Guan, X. M., Xiong, M. P., Zeng, F. Y., Xu, B., Yang, L. D., Guo, H., . . . Yuan, G. Y. (2014). Enhancement of Osteogenesis and Biodegradation Control by Brushite Coating on Mg-Nd-Zn-Zr Alloy for Mandibular Bone Repair. *Acs Applied Materials & Interfaces, 6*(23), 21525-21533. doi: 10.1021/am506543a

Hagandora, C. K., Chase, T. W., & Almarza, A. J. (2011). A comparison of the mechanical properties of the goat temporomandibular joint disc to the mandibular condylar cartilage in unconfined compression. *J Dent Biomech, 2011*, 212385. doi: 10.4061/2011/212385

Hagandora, C. K., Chase, T. W., Almarza, A. J. (2011). A Comparison of the Mechanical Properties of the Goat Temporomandibular Joint Disc to the Mandibular Condylar Cartilage in Unconfined Compression. *J Dent Biomech, 212385*.

Hagandora, C. K., Tudares, M. A., & Almarza, A. J. (2012). The effect of magnesium ion concentration on the fibrocartilage regeneration potential of goat costal chondrocytes. *Ann Biomed Eng, 40*(3), 688-696. doi: 10.1007/s10439-011-0433-z

Han, J., Wan, P., Sun, Y., Liu, Z., Fan, X., Tan, L., Yang, K. (March 2016). Fabrication and Evaluation of a Bioactive Sr-Ca-P Contained Micro-Arc Oxidation Coating on Magnesium Strontium Alloy for Bone Repair Application. *Journal of Materials Science and Technology, Volume 32*(3), Pages 233-244.

Han, P., Cheng, P., Zhang, S., Zhao, C., Ni, J., Zhang, Y., . . . Chai, Y. (2015). In vitro and in vivo studies on the degradation of high-purity Mg (99.99wt.%) screw with femoral intracondylar fractured rabbit model. *Biomaterials, 64*, 57-69. doi: 10.1016/j.biomaterials.2015.06.031

Henderson, S. E., Verdelis, K., Maiti, S., Pal, S., Chung, W. L., Chou, D. T., . . . Almarza, A. J. (2014). Magnesium alloys as a biomaterial for degradable craniofacial screws. *Acta Biomater, 10*(5), 2323-2332. doi: 10.1016/j.actbio.2013.12.040

Hofstetter, J., Martinelli, E., Pogatscher, S., Schmutz, P., Povoden-Karadeniz, E., Weinberg, A. M., . . . Loffler, J. F. (2015). Influence of trace impurities on the in vitro and in vivo degradation of biodegradable Mg-5Zn-0.3Ca alloys. *Acta Biomater, 23*, 347-353. doi: 10.1016/j.actbio.2015.05.004

Hong, D., Saha, P., Chou, D. T., Lee, B., Collins, B. E., Tan, Z., . . . Kumta, P. N. (2013). In vitro degradation and cytotoxicity response of Mg-4% Zn-0.5% Zr (ZK40) alloy as a potential biodegradable material. *Acta Biomater, 9*(10), 8534-8547. doi: 10.1016/j.actbio.2013.07.001

Hu, T., Xu, H., Wang, C., Qin, H., & An, Z. (2018). Magnesium enhances the chondrogenic differentiation of mesenchymal stem cells by inhibiting activated macrophage-induced inflammation. *Sci Rep, 8*(1), 3406. doi: 10.1038/s41598-018-21783-2

Huan, Z. G., Leeflang, M. A., Zhou, J., Fratila-Apachitei, L. E., & Duszczyk, J. (2010). In vitro degradation behavior and cytocompatibility of Mg-Zn-Zr alloys. *J Mater Sci Mater Med, 21*(9), 2623-2635. doi: 10.1007/s10856-010-4111-8

Janning, C., Willbold, E., Vogt, C., Nellesen, J., Meyer-Lindenberg, A., Windhagen, H., . . . Witte, F. (2010). Magnesium hydroxide temporarily enhancing osteoblast activity and decreasing the osteoclast number in peri-implant bone remodelling. *Acta Biomater, 6*(5), 1861-1868. doi: 10.1016/j.actbio.2009.12.037

Kim, K. W., Wong, M. E., Helfrick, J. F., Thomas, J. B., & Athanasiou, K. A. (2003). Biomechanical tissue characterization of the superior joint space of the porcine temporomandibular joint. *Ann Biomed Eng, 31*(8), 924-930. doi: 10.1114/1.1591190

Lamela, M. J., Fernandez, P., Ramos, A., Fernandez-Canteli, A., & Tanaka, E. (2013). Dynamic compressive properties of articular cartilages in the porcine temporomandibular joint. *Journal of the Mechanical Behavior of Biomedical Materials, 23*, 62-70.

Lamela, M. J., Prado, Y., Fernandez, P., Fernandez-Canteli, A., & Tanaka, E. (2011). Non-linear Viscoelastic Model for Behaviour Characterization of Temporomandibular Joint Discs. *Experimental Mechanics, 51*(8), 1435-1440.

Lempriere, B. M. (1968). Poissons Ratio in Orthotropic Materials. *Aiaa Journal, 6*(11), 2226-+.

Li, X. M., Chen, S. W., Li, J. C., Wang, X. L., Zhang, J., Kawazoe, N., & Chen, G. P. (2016). 3D Culture of Chondrocytes in Gelatin Hydrogels with Different Stiffness. *Polymers, 8*(8).

Li, Y., Wen, C., Mushahary, D., Sravanthi, R., Harishankar, N., Pande, G., Hodgson, P. (2012). Mg-Zr-Sr alloys as biodegradable implant materials. *Acta Biomater, 8*(8), 3177-3188.

Li, Z., Gu, X., Lou, S., & Zheng, Y. (2008). The development of binary Mg-Ca alloys for use as biodegradable materials within bone. *Biomaterials, 29*(10), 1329-1344. doi: 10.1016/j.biomaterials.2007.12.021

Liao, Y., Xu, Q., Zhang, J., Niu, J., Yuan, G., Jiang, Y., . . . Wang, X. (2015). Cellular response of chondrocytes to magnesium alloys for orthopedic applications. *Int J Mol Med, 36*(1), 73-82. doi: 10.3892/ijmm.2015.2211

Liu, C., He, P., Wan, P., Li, M., Wang, K., Tan, L., . . . Yang, K. (2015). The in vitro biocompatibility and macrophage phagocytosis of Mg17Al12 phase in Mg-Al-Zn alloys. *J Biomed Mater Res A, 103*(7), 2405-2415. doi: 10.1002/jbm.a.35374

Mow, V. C., Kuei, S. C., Lai, W. M., & Armstrong, C. G. (1980). Biphasic Creep and Stress-Relaxation of Articular-Cartilage in Compression - Theory and Experiments. *Journal of Biomechanical Engineering-Transactions of the Asme, 102*(1), 73-84.

Nakano, T., & Scott, P. G. (1989a). Proteoglycans of the articular disc of the bovine temporomandibular joint. I. High molecular weight chondroitin sulphate proteoglycan. *Matrix, 9*(4), 277-283.

Nakano, T., & Scott, P. G. (1989b). A quantitative chemical study of glycosaminoglycans in the articular disc of the bovine temporomandibular joint. *Arch Oral Biol, 34*(9), 749-757. doi: 10.1016/0003-9969(89)90082-4

Nichol, J. W., Koshy, S. T., Bae, H., Hwang, C. M., Yamanlar, S., & Khademhosseini, A. (2010). Cell-laden microengineered gelatin methacrylate hydrogels. *Biomaterials, 31*(21), 5536-5544. doi: 10.1016/j.biomaterials.2010.03.064

NIH. (2016). Magnesium: Fact Sheet for Consumers. *NIH Office of Dietary Supplements*.

Park, K. S., Kim, B. J., Lih, E., Park, W., Lee, S. H., Joung, Y. K., & Han, D. K. (2018). Versatile effects of magnesium hydroxide nanoparticles in PLGA scaffold-mediated chondrogenesis. *Acta Biomater, 73*, 204-216. doi: 10.1016/j.actbio.2018.04.022

Peng, S., Liu, X. S., Wang, T., Li, Z., Zhou, G., Luk, K. D., . . . Lu, W. W. (2010). In vivo anabolic effect of strontium on trabecular bone was associated with increased osteoblastogenesis of bone marrow stromal cells. *J Orthop Res, 28*(9), 1208-1214. doi: 10.1002/jor.21127

Pichler, K., Kraus, T., Martinelli, E., Sadoghi, P., Musumeci, G., Uggowitzer, P. J., & Weinberg, A. M. (2014). Cellular reactions to biodegradable magnesium alloys on human growth plate chondrocytes and osteoblasts. *Int Orthop, 38*(4), 881-889. doi: 10.1007/s00264-013-2163-3

Rad, E. B., Mostofi, S., Katschnig, M., Schmutz, P., Pawelkiewicz, M., Willumeit-Romer, R., . . . Weinberg, A. (2017). Differential apoptotic response of MC3T3-E1 pre-osteoblasts to biodegradable magnesium alloys in an in vitro direct culture model. *Journal of Materials Science-Materials in Medicine, 28*(10). doi: Artn 155

Reifenrath, J., Marten, A. K., Angrisani, N., Eifler, R., & Weizbauer, A. (2015). In vitro and in vivo corrosion of the novel magnesium alloy Mg-La-Nd-Zr: influence of the measurement technique and in vivo implant location. *Biomed Mater, 10*(4), 045021. doi: 10.1088/1748-6041/10/4/045021

Sartori, M., Pagani, S., Ferrari, A., Costa, V., Carina, V., Figallo, E., . . . Giavaresi, G. (2017). A new bi-layered scaffold for osteochondral tissue regeneration: In vitro and in vivo preclinical investigations. *Materials Science & Engineering C-Materials for Biological Applications, 70*, 101-111. doi: 10.1016/j.msec.2016.08.027

Schaller, B., Saulacic, N., Imwinkelried, T., Beck, S., Liu, E. W., Gralla, J., . . . Iizuka, T. (2016). In vivo degradation of magnesium plate/screw osteosynthesis implant systems: Soft and hard tissue response in a calvarial model in miniature pigs. *J Craniomaxillofac Surg, 44*(3), 309-317. doi: 10.1016/j.jcms.2015.12.009

Shen, T. a., Dai, Y.a, Li, X.a, Xu, S.b, Gou, Z.c, Gao, C.a,d. (June 2018). Regeneration of the Osteochondral Defect by a Wollastonite and Macroporous Fibrin Biphasic Scaffold(*ACS Biomaterials Science and Engineering, 4*(6), 1942-1953.

Singh, M., & Detamore, M. S. (2009). Stress Relaxation Behavior of Mandibular Condylar Cartilage Under High-Strain Compression. *Journal of Biomechanical Engineering-Transactions of the Asme, 131*(6). doi: Artn 061008

Song, X. Z., Chang, L., Wang, J., Zhu, S. J., Wang, L. G., Feng, K., . . . Guan, S. K. (2018). Investigation on the in vitro cytocompatibility of Mg-Zn-Y-Nd-Zr alloys as degradable orthopaedic implant materials. *Journal of Materials Science-Materials in Medicine, 29*(4). doi: ARTN 44

Sun, J., Wang, J., Jiang, H., Chen, M., Bi, Y., & Liu, D. (2013). In vivo comparative property study of the bioactivity of coated Mg-3Zn-0.8Zr alloy. *Mater Sci Eng C Mater Biol Appl, 33*(6), 3263-3272. doi: 10.1016/j.msec.2013.04.006

Tamimi, F., Le Nihouannen, D., Bassett, D. C., Ibasco, S., Gbureck, U., Knowles, J., . . . Barralet, J. E. (2011). Biocompatibility of magnesium phosphate minerals and their stability under physiological conditions. *Acta Biomater, 7*(6), 2678-2685. doi: 10.1016/j.actbio.2011.02.007

Tarafder, S., Davies, N.M., Bandyopadhyay, A., Bose, S. (December 2013). 3D printed tricalcium phosphate bone tissue engineering scaffolds: Effect of SrO and MgO doping on in vivo osteogenesis in a rat distal femoral defect model. *Biomaterials Science, 1*(12), 1250-1259.

Tie, D., Guan, R. G., Liu, H. N., Cipriano, A., Liu, Y. L., Wang, Q., . . . Hort, N. (2016). An in vivo study on the metabolism and osteogenic activity of bioabsorbable Mg-1Sr alloy. *Acta Biomater, 29*, 455-467. doi: 10.1016/j.actbio.2015.11.014

Waizy, H., Diekmann, J., Weizbauer, A., Reifenrath, J., Bartsch, I., Neubert, V., . . . Windhagen, H. (2014). In vivo study of a biodegradable orthopedic screw (MgYREZr-alloy) in a rabbit model for up to 12 months. *J Biomater Appl, 28*(5), 667-675. doi: 10.1177/0885328212472215

Wang, H., Guan, S., Wang, Y., Liu, H., Wang, H., Wang, L., . . . Chen, K. (2011). In vivo degradation behavior of Ca-deficient hydroxyapatite coated Mg-Zn-Ca alloy for bone implant application. *Colloids Surf B Biointerfaces, 88*(1), 254-259. doi: 10.1016/j.colsurfb.2011.06.040

Wang, Y., Ouyang, Y., Pang, X., Mao, L., Yuan, G., Jiang, Y., & He, Y. (2012). Effects of degradable MG-ND-ZN-ZR alloy on osteoblastic cell function. *Int J Immunopathol Pharmacol, 25*(3), 597-606.

Wu, F., Wei, J., Guo, H., Chen, F., Hong, H., & Liu, C. (2008). Self-setting bioactive calcium-magnesium phosphate cement with high strength and degradability for bone regeneration. *Acta Biomater, 4*(6), 1873-1884. doi: 10.1016/j.actbio.2008.06.020

Xia, Y., Zhang, B., Wang, Y., Qian, M., Geng, L. (May 2012). In-vitro cytotoxicity and in-vivo biocompatibility of as-extruded Mg-4.0Zn-0.2Ca alloy. *Materials Science and Engineering C, 32*(4), 665-669.

Yang, J. X., Cui, F.Z., Lee, I.-S., Zhang, Y., Yin, Q.S., Xia, H., Yang, S.X. (2012). In vivo biocompatibility and degradation behavior of Mg alloy coated by calcium phosphate in a rabbit model. *J Biomater Appl, 27*(2), 153-164.

Zeng, D., Xia, L., Zhang, W., Huang, H., Wei, B., Huang, Q., Wei, J., Liu, C., Jiang, X. (April 2012). Maxillary sinus floor elevation using a tissue-engineered bone with calcium-magnesium phosphate cement and bone marrow stromal cells in rabbits. *Tissue Engineering - Part A, 18*(7-8), 870-881.

Zhang, E., Xu, L., Yu, G., Pan, F., Yang, K. (September 2009). In vivo evaluation of biodegradable magnesium alloy bone implant in the first 6 months implantation. *J Biomed Mater Res A, 90*(3), 882-893.

Zhang, S., Zhang, X., Zhao, C., Li, J., Song, Y., Xie, C., Tao, H., Zhang, Y., He, Y., Jiang, Y., Bian, Y. (2010). Research on an Mg-Zn alloy as a degradable biomaterial. *Acta Biomater, 6*(2), 626-640.

Zhao, X., Liu, S., Yildirimer, L., Zhao, H., Ding, R. H., Wang, H. N., . . . Weitz, D. (2016). Injectable Stem Cell-Laden Photocrosslinkable Microspheres Fabricated Using Microfluidics for Rapid Generation of Osteogenic Tissue Constructs. *Advanced Functional Materials, 26*(17), 2809-2819.